POLITECNICO DI MILANO
DEPARTMENT OF ENERGY
DOCTORAL PROGRAM IN ENERGY AND NUCLEAR SCIENCE AND TECHNOLOGY

DEVELOPMENT OF ADVANCED SIMULATION TOOLS FOR CIRCULATING-FUEL NUCLEAR REACTORS

Doctoral Dissertation of:
Manuele Aufiero

Supervisors:
Prof. Antonio Cammi
Prof. Lelio Luzzi

Tutor:
Prof. Lelio Luzzi

The Chair of the Doctoral Program:
Prof. Carlo Enrico Bottani

26^{th} Cycle

February 2014 – Milano, Italy

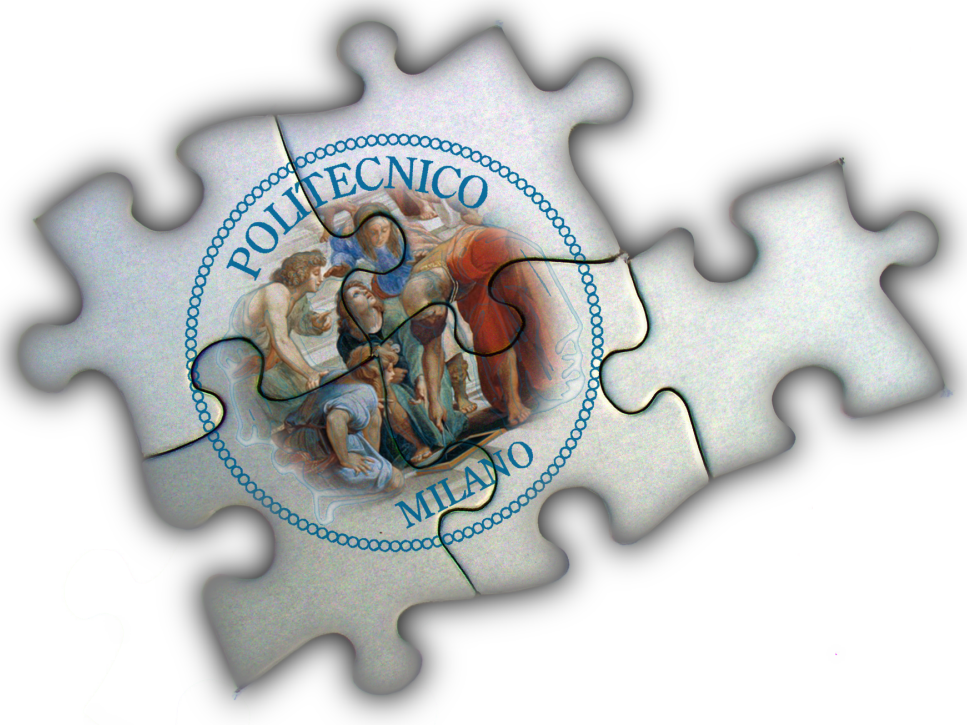

Page 2, *La Scuola di Atene*, Raffaello Sanzio.
Page 17, *I gasometri*, Bovisa, Milano.
Page 47, *Chiamata del due "alla Colombo" (con carico giocato in prima mano)*, M. Aufiero and A. Sartori vs. S. Lorenzi et al., Grande Capannone, Polimi Bovisa.
Page 67, *Les Boules*, Grenoble.
Page 97, *Regenstiefel*, PSI, Villigen.

Acknowledgements

THE thesis has been carried out in the framework of a collaboration between Politecnico di Milano, the Laboratoire de Physique Subatomique et de Cosmologie (LPSC) CNRS–Grenoble (France), INOPRO (France), the Paul Scherrer Institut (PSI, Switzerland) and other institutions participating to the Euratom FP7 EVOL Project. Active collaborations with foreign institutions have been supported by Politecnico di Milano via the PhD grant "International Mobility 2012/2013".

During the thesis, I spent two research periods at LPSC/CNRS Grenoble (February – June, 2013) and at the Paul Scherrer Institut (August – October, 2013).

The work has been supported by CINECA supercomputing center under ISCRA Project MPMCF – *Multi-Physics Modelling of Circulating-Fuel Nuclear Reactors*, by Regione Lombardia and CILEA supercomputing center under LISA Project CFMC – *Simulazioni Monte Carlo per reattori a sali fusi*, and by an Amazon Web Services (AWS) in Education grant award.

The help from the SERPENT developers team (VTT, Technical Research Centre of Finland) has been invaluable for the development and extension of some of the tools presented in this thesis.

Abstract

MOLTEN Salt Reactors (MSRs) are characterized by a unique distinguishing feature: the presence of a liquid nuclear fuel. This peculiarity may lead to intrinsic improvements in the fuel cycle closure and reactor safety enhancement. On the other hand, it represents one of the most challenging aspects for reactor design, analysis and operation. The context of the PhD thesis is the development and assessment of advanced modeling and simulation tools for circulating-fuel nuclear reactors. The Molten Salt Fast Reactor (MSFR) is the reference circulating-fuel system selected by the Generation-VI International Forum. This reactor concept was mainly developed in the frame of the EURATOM FP7 EVOL Project, and it is adopted as the reference case study for the tools developed in this thesis.

In the first part of the thesis, an extension of the SERPENT-2 Monte Carlo code to study MSR fuel burn-up is presented. The code is employed to analyse the MSFR fuel cycle and core material evolution. The extension allows for continuous reprocessing via explicit introduction of decay and transmutation terms in the system of burn-up equations. The code features also a reactivity control that allows keeping the multiplication factor close to 1 during the whole simulation, for a correct estimation of the main breeding parameters.

The second part of the thesis is focused on multiphysics modelling. The open-source C++ library Open-FOAM is adopted to develop a coupled neutronics/thermal-hydraulics solver for the steady-state and transient analysis of the MSFR. Namely, the equations involved in the multiphysics solution are the time-dependent neutron diffusion, the balance equations for delayed neutron and decay heat precursors, and the incompressible Reynolds-Averaged Navier-Stokes equations for the solution of the turbulent fluid flow. The modeling efforts are focused on the implementation of coupling techniques, and the adoption of strategies for the reduction of computational requirements.

The effective delayed neutron fraction is an important reactor kinetics parameter. In circulating-fuel systems, the motion of delayed neutron precursors prevents the adoption of commonly available neutron transport codes. The third part of the thesis is focused on the calculation of the effective delayed neutron fraction: three methods are presented, which involve a correct importance weighting of the delayed neutron source, in case of fuel motion. The three approaches are based on analytical, deterministic and Monte Carlo methods, and are adopted to study the effective delayed neutron fraction in the MSFR, in different operating conditions.

Contents

Acknowledgements **3**

Abstract **5**

Introduction **9**
Objectives and outline of the thesis 10
The Molten Salt Fast Reactor 12
OpenFOAM 13

1 Fuel burn-up and core material evolution **17**
1.1 Introduction 18
1.2 On-line fuel reprocessing 20
1.3 Reactivity control and equilibrium search 23
1.4 MSFR fuel isotopic evolution 27
1.5 Helium production and tungsten depletion in structural components 39
1.6 Concluding remarks 43

2 Multiphysics modelling **47**
2.1 Introduction 48
2.2 Modelling approach 49
2.3 Numerical results 59
2.4 Concluding remarks 64

3 Effective delayed neutron fraction **67**
3.1 Introduction 67
3.2 Methods 70
3.3 Numerical results 82
3.4 Concluding remarks 89

Conclusions **93**

A Appendix **97**
A.1 Comparison of neutronic results within the EVOL Project 98
A.2 Adjoint-weighted kinetics parameters 100
A.3 Adjoint-weighted k_{eff} sensitivity coefficients 107
A.4 Neutron transport tools for multiphysics applications 111

List of Figures **121**

List of Tables **124**

References **127**

Ringraziamenti **133**

It is belief of fluid fuel enthusiasts that in the **very long run** *the simplification in fuel cycle and, more important, the better neutron economy made possible by the use of fluid fuels will outweigh the difficult handling problems and ultimately weight the balance of reactor development towards these systems. [...]*
It is my hope that the results described here will be helpful to all who are interested in fluid fuel systems, and that, by disseminating this information, new ideas and new approaches will be generated to help solve the remaining problems of fluid fuel reactors.

Alvin Weinberg
"Fluid Fuel Reactors" – **June 1958** – Oak Ridge National Laboratory

Introduction

MOLTEN Salt Reactors (MSRs) are characterized by a unique distinguishing feature: the presence of a liquid nuclear fuel. This peculiarity may lead to intrinsic improvements in the fuel cycle closure and reactor safety enhancement. On the other hand, it represents one of the most challenging aspects for reactor design, analysis and operation. The study of the MSR technology has been among the leading research activities of the Oak Ridge National Laboratory (ORNL) during the '50s and '60s, under the laboratory direction of Alvin Weinberg. The research efforts on MSRs for energy production culminated with the operation of the Molten Salt Reactor Experiment (MSRE), which went critical in 1965 and the design of the Molten Salt Breeder Reactor (MSBR) (MacPherson, 1985). Despite the positive experiences, the Molten Salt Reactor Project was closed in the '70s and the MSBR was never built. The MSRE remains the last molten salt reactor ever operated.

Recently, new interest has grown in different countries around the MSR technology, focusing on both thermal- and fast-neutron reactors, for the development of breeder, converter or incinerator systems (Renault and Delpech, 2005; Furukawa *et al.*, 2008; Benes *et al.*, 2008; LeBlanc, 2010; Luzzi *et al.*, 2012). In this context, the adoption of the Molten Salt Reactor concept is envisaged by the Generation IV International Forum (GIF, 2012; Serp *et al.*, 2014) as a promising choice to provide sustainable, safe and proliferation resistant nuclear energy production.

In particular, the Molten Salt Fast Reactor (MSFR, Merle-Lucotte *et al.*, 2011; Brovchenko *et al.*, 2012) has been selected as the reference circulating-fuel reactor in the framework of the GIF-IV, and it is mainly developed in the EURATOM EVOL (Evaluation and Viability Of Liquid fuel fast reactor system) Project. This system features an intermediate-to-fast neutron spectrum and the absence of in-core moderator or structural materials. These characteristics make the MSFR substantially different from the systems on which a small operating and modeling experience was accumulated from the ORNL era on.

The vast majority of simulation tools currently adopted in the nuclear community has been tailored to the specific needs of the second (and third) generation of nuclear reactors. Often, strong assumptions are adopted in the modeling approaches. These simplifications have been developed and justified in the years, thanks to the large operational experience

on Light Water Reactors (LWRs) of the last 50 years. Unfortunately, the presence of a fluid fuel and the adoption of an on-line reprocessing scheme make the commonly adopted tools for neutronics and fuel cycle analysis inadequate for the study of MSRs. Also, among the modeling tools specifically developed in the past for molten salt reactors, most of them are only suitable for graphite-moderated, thermal systems like was the MSRE (Bauman *et al.*, 1971; Křepel *et al.*, 2007).

On the other hand, more accurate modeling approaches are available today, which can offer more general reference solutions to some important problems. These approaches, based for example on the direct coupling between neutron transport and Computational Fluid-Dynamics (CFD) solutions, are not widely employed in the nuclear community apart from specific applications. In the past, nuclear engineering has been one of the most prosperous areas for the development and implementation of innovative computational methods. Today, most of reactor analysis activities, especially in the nuclear industry, are performed by means of modelling tools based on relatively old methods. The reasons for this delay, compared to other engineering fields, were mainly related to the high computational cost of new techniques.

Today, most of the computational restrictions have been progressively overcome, but still the reluctance toward the dismissal of legacy codes, that were validated by years of experience on operating reactors, persists. Unfortunately, in the case of non-moderated MSRs both experience and validated codes are lacking. Moreover, the features of these fast-neutron systems and the related technological challenges call for the adoption of advanced, physics-based simulation techniques to serve as aiding tools in the reactor design and analysis process and to provide reference solutions to simplified modeling approaches.

Objectives and outline of the thesis

This thesis seeks to improve the simulation tools available for the study of innovative circulating-fuel reactors. The employed modelling techniques have been tailored to the specific needs of these reactors, although some of the presented methods can be considered of more general interest. The Molten Salt Fast Reactor is studied in parallel to the process of development and assessment of the different simulation tools. In the analysis of the MSFR, the focus is kept on those aspects that are thought to be more constraining for this technology and are currently studied with a lesser degree of accuracy.

In the first part of the work, the development of a Monte Carlo-based tool for fuel cycle analysis of Molten Salt Reactors is described. In MSRs, the adoption of on-line reprocessing schemes and continuous reactivity control via fuel composition adjustment offers several advantages but prevents the adoption of common fuel burn-up codes. At the same time, the knowledge of the exact core materials composition and related parameters (e.g., decay heat and specific gamma emission) during the reactor evolution is considered of primary importance for safety analysis. Moreover, material isotopic composition is the first essential information required to perform many other reactor analysis steps, also those discussed in the following parts of this work. In Chapter 1, the extension of the Monte Carlo code SERPENT-2 for the burn-up analysis of MSRs is presented, together with the fuel cycle analysis of the MSFR. Some of the results and comparisons obtained within the neutronic benchmark of the EVOL Project (Deliverable EVOL D2.2, 2013) are reported in Section A.1 of the Appendix.

The second part of the work involves the development of a multiphysics modelling tool for MSR transient analysis. A purpose-made solver is developed, adopting the open-source C++ library OpenFOAM. It is applied to catch the interactions between the main physical phenomena governing the MSFR behaviour, through the coupled solution of a set of equations describing the thermal-hydraulics and neutron diffusion in the fuel circuit. The modelling efforts are focused on the implementation of accurate and consistent time-integration and coupling techniques, and the adoption of strategies for the reduction of computational requirements. The main purpose of the proposed OpenFOAM model is to serve as fast-running computational tool in the phase of design optimization of core and fuel loop components. The capability of performing accurate simulations on detailed full-core realistic 3D geometries was not available in previous tools, which are limited to 2D simplified geometries. This feature is shown to be a mandatory requirement for the MSFR analysis and optimization. More in general, the presented tool is designed to investigate the peculiarities of the reactor physics of channel-free circulating-fuel systems, especially in presence of strong thermal feedbacks on neutronics. The OpenFOAM solver is presented in Chapter 2, along with a selected comparison case study against previously available tools. The peculiarities of the dynamic behaviour of graphite-moderated MSRs (e.g., the presence of a positive graphite temperature coefficient) have been the subject of previous extensive investigations (e.g., see Křepel *et al.*, 2007; Nagy *et al.*, 2014) and are not dealt with in the present multiphysics analyses. In the Appendix (Section A.4), possible extensions of the method to Discrete Ordinates and Monte Carlo neutron transport are investigated.

The effective delayed neutron fraction (β_{eff}) is an important reactor kinetics parameter. The contribution of delayed neutrons is of primary importance for the safe control of any nuclear reactor. In circulating-fuel systems, the motion of delayed neutron precursors complicates the calculation of β_{eff} and prevents the adoption of commonly available neutron transport codes. Moreover, in the MSFR and many similar systems, the implementation of the Thorium cycle (with U-233 as fissile), the envisaged incineration of Minor Actinides, and the fuel motion itself, lead to very small β_{eff} values. For these reasons, accurate and reliable reference calculations for the effective delayed neutron fraction are highly desirable. In Chapter 3, three approaches are presented for the calculation of β_{eff} and are applied to the MSFR as test cases. The developed approaches are based on analytical, deterministic and Monte Carlo methods. As known, the effective delayed neutron fraction is highly dependent on the fuel composition. It is shown here that the in-core velocity distribution greatly affects β_{eff} as well. For these reasons, this part turns out to be a natural prosecution of the first two modelling steps presented in this thesis. The Monte Carlo approach makes use of the Iterated Fission Probability method for adjoint weighting. This methodology has been implemented in SERPENT-2 and is briefly reported in Section A.2 of the Appendix.

One of the outcomes of this thesis is the large uncertainty that affects breeding performance estimations of systems operating in an intermediated-to-fast spectrum in the Th/^{233}U fuel cycle. A detailed cross-sections sensitivity/uncertainties analysis would represent an important further step in the study of the MSFR and similar systems. In this direction, a new methodology for the calculation of adjoint-weighted sensitivity coefficients has been implemented in SERPENT-2. The methodology is presented in the Appendix (Section A.3) with a few preliminary verification case studies.

The Molten Salt Fast Reactor

The Molten Salt Fast Reactor (MSFR) is the reference circulating-fuel reactor in the framework of the Generation IV International Forum (GIF, 2012). It has been studied at the Centre National de la Recherche Scientifique (CNRS, Grenoble-France) since 2004 and is presently developed in the FP7 EURATOM EVOL (Evaluation and Viability Of Liquid fuel fast reactor system) Project (EVOL, 2013). The reactor is designed to operate in the Th/^{233}U fuel cycle with a fast-to-intermediate neutron spectrum and a nominal thermal power of 3 GW. It presents a wide flexibility to the initial fissile load and can be started with ^{233}U, enriched ^{235}U/^{238}U and TRansUranics (TRU) elements. The concept features several favourable characteristics with respect to GEN-IV solid-fuelled reactors, as the presence of strong negative void and temperature feedbacks and a low fissile inventory.

Details about the MSFR concept can be found in the references (e.g., Merle-Lucotte *et al.*, 2009, 2011; Brovchenko *et al.*, 2012). System specifications are being optimized within several research activities of the EVOL partners and the reactor design is still evolving. In the following, a brief description of the main general features of the reactor is given[1].

Figure 1 shows a schematic view of the MSFR components (from Brovchenko *et al.*, 2012), the fuel salt being not pictured. The molten salt in the fuel circuit acts both as fuel and coolant. The salt consists of a mixture of ^{7}LiF and ThF_4 at the eutectic point (77.5 – 22.5 mol%) with the other Heavy Metals (HM) fluorides substituting ThF_4. The core of the reactor has a nominal volume of 9 m^3. The fuel salt enters from the bottom and is extracted from the top of the core. The heated mixture flows in sixteen external loops where it exchanges heat and is pumped back to the core. The design of the heat exchangers is still ongoing within the EVOL Project and the adoption of an intermediate loop to separate the radioactivity of the fluid fuel from the energy conversion system is envisaged. The fraction of the fuel salt in the core is approximately 50% and the average nominal in-core temperature is $\sim$700°C. The core shape was originally conceived as a simple cylinder with the diameter equal to the height, mainly from neutron economy optimization. This simple shape has been selected as official geometry for the neutronic benchmark of the EVOL Project and is therefore adopted as the reference configuration for the analysis presented in Chapter 1. Computational Fluid-Dynamics (CFD) analysis of the salt flow in the reactor highlighted that the cylindrical shape leads to unacceptable recirculation close to the radial core wall. A core optimization process led to the proposal of a recirculation-free shape from INOPRO and CNRS (Rouch, 2013; Rouch *et al.*, 2014). This optimized shape is adopted in the multiphysics analysis presented in Chapters 2 and 3.

Above and below the core, nickel-based alloy reflectors are present in order to improve neutron economy. Radially, the core is surrounded by a fertile mixture containing a thorium and lithium fluoride salt, in order to improve the breeding performance of the reactor. The reflector and the fuel salt container structures have to withstand particularly sever conditions from both chemical and irradiation perspectives. The radiation damage is thought to be one of the possible limiting factors for the life of these components, possibly requiring frequent and expensive replacements. A study of the main phenomena involved

[1] Several recent works related to the analysis and design improvement of the MSFR can be found in the *"Special Section: MSR and FHR"* of the Volume 64 (February 2014) of *"Annals of Nuclear Energy"*.

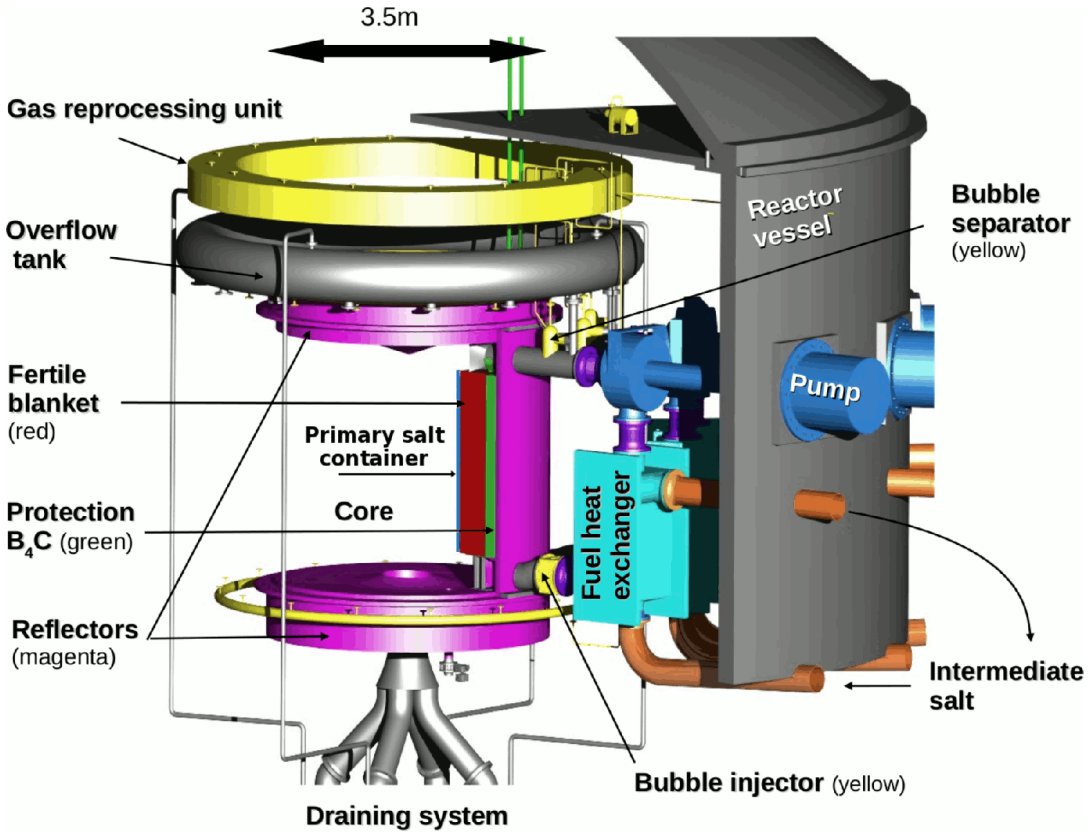

Figure 1: *Schematic representation of the MSFR fuel loop (Brovchenko* et al.*, 2012).*

in radiation-induced damage of the MSFR structural materials is presented in Chapter 1.

Below the active core, a passively actuated valve is designed to discharge the fluid fuel in a criticality-safe drain tank. The fuel salt undergoes two types of treatment: an on-line treatment by neutral gas bubbling in the core, and a remote mini-batch reprocessing on-site. The purpose of these salt treatments is to remove most of the fission products without requiring reactor shut-down. The selected nominal reprocessing rate for soluble fission products involves the extraction of $\sim$40 liters of fuel salt per day. The gaseous treatment is expected to remove the non-soluble fission products with an effective time constant of $\sim$30 seconds. As to the latter assumption, the effective removal rate of metallic fission products will probably be lower. A sensitivity study on the effect of the two extraction parameters is presented in Chapter 1. In Table 1, the main design parameters of the MSFR are listed.

OpenFOAM

The Open-source Field Operation And Manipulation (OpenFOAM, Weller *et al.*, 1998; Jasak *et al.*, 2007) framework is a C++ library providing automatic matrix construction and solution for scalar and vector equations using standard finite-volume approaches based on user-specified differencing and interpolation schemes. The flexibility of design makes this library ideal for modelling complex coupled problems. The framework has been applied extensively for CFD simulations. An attractive feature of the OpenFOAM framework is that the top-level C++ representations of continuum mechanics equations

Table 1: *Nominal design parameters of the MSFR.*

Thermal power	3000 MW
Electrical power	1500 MW
Core inlet temperature	650°C
Core outlet temperature	750°C
Fuel salt composition	(^{233}U-started)
$LiF - ThF_4 - {}^{233}UF_4$	77.5–20–2.5 mol %
Fuel salt composition	(TRU-started)
$LiF - ThF_4 - (TRU)F_3$	77.5–16–6.5 mol %
Soluble FP reprocessing rate	40 liters per day
Non-soluble FP removal time constant	30 s
Fuel salt volume	18 m^3
In-core fuel fraction	50%
Blanket salt composition	(all options)
$LiF - ThF_4$	77.5–22.5 mol %
Fuel salt circulation period	4 s

closely parallel their mathematical descriptions. As an example, the balance equation of the delayed neutron precursors is easily discretized and solved for a single precursor group using the following line of source code:

```
solve
(
    fvm::div(U, c_i)
  - fvm::laplacian(Dt, c_i)
  + fvm::Sp(lambda_i, c_i)
  ==
    beta/k_eff * ((nu_tot & sigma_f) & phi)
);
```

that closely resembles its mathematical formulation:

$$\nabla \left(\mathbf{u} c_i \right) - \nabla \cdot \frac{\nu_T}{Sc_T} \nabla c_i + \lambda_i c_i = \beta_{0,i} \sum_{g=1}^{n} \frac{1}{k_{eff}} \left(\nu \Sigma_f \right)_g \phi_g$$

In this case, phi is a field containing vectors of length n, representing the n energy components of the neutron flux, and the necessary vector and tensor calculus (inner and outer products) is captured through the `&` and `*` C++ operators. In the spirit of this approach, Clifford and Ivanov (2010) extended OpenFOAM to provide a top-level presentation for the implicit solution of multiple coupled variables, based on the block-coupled solver implementation of Clifford and Jasak (2009), which is particularly suited to the solution of the multi-group neutron diffusion equation, and is extensively adopted in the work presented in Chapter 3.

In addition to the ease of implementing the constitutive equations of different physical phenomena, OpenFOAM is provided by different pre-implemented models and solvers

for the simulation of fluid flows. This allowed to focus the development efforts of the thesis work on the implementation and verification of the neutronics and delayed neutron precursors models and on the multiphysics coupling and time integration strategies, as well.

As a further example, the multi-group neutron diffusion equation

$$-\nabla \cdot D_g \nabla \phi_g + \Sigma_{a,g}\phi_g + \sum_{g' \neq g} \Sigma_{s,gg'}\phi_g - \sum_{g' \neq g} \Sigma_{s,g'g}\phi_{g'} = \\ = (1-\beta_0)\,\chi_{p,g} \sum_{g'=1}^{n} \frac{1}{k_{eff}} \left(\nu\Sigma_f\right)_{g'} \phi_{g'} + \sum_{i=1}^{m} \chi_{d,g}\lambda_i c_i$$

is discretized and solved in vector form for all n energy-groups using the following line of source code:

```
solve
(
  - blockFvm::laplacian(D, phi)
  + blockFvm::Sp(sigma_a - sigma_s, phi)
  ==
    (1-beta_tot)/k_eff * ((chi_p * (nu_tot & sigma_f)) & phi)
  + (chi_d * delayedNeutronSource)
);
```

CHAPTER 1

Fuel burn-up and core material evolution

In this Chapter, the extension of the SERPENT-2 code for the burn-up analysis of MSRs is described, along with the fuel cycle analysis of the MSFR. The developed extension of SERPENT-2 directly takes into account the effects of on-line fuel reprocessing on material isotopic evolution via a modification of the algorithm for the construction of the burn-up matrix. The extension was thought as an alternative, Monte Carlo-based tool to the ERANOS-based EQL3D procedure developed at PSI-Switzerland and extended by Carlo Fiorina for the analysis of MSRs. The development was initially started with the Serpent-1 code in the last months of 2011. After the migration to SERPENT-2, further developments led to the capability of continuous reactivity control via feed adjustment, which is designed to resemble the real long-term control strategy of MSFR-like systems. The continuous adjustment allows to accurately estimate reactor breeding performance and fissile production rates. The extension is also featured by an iterative equilibrium search algorithm with convergence acceleration, which is able to find the steady-state reactor composition in a cheap and reliable way. The capabilities of the extended SERPENT-2 are adopted to perform a detailed fuel cycle analysis of the Molten Salt Fast Reactor. A sensitivity study to the reprocessing time constants and the nuclear data libraries adopted in also presented, along with an analysis of some phenomena related to radiation-induced damage in the MSFR structural materials.

The main results presented in this Chapter have been published in: M. Aufiero, A. Cammi, C. Fiorina, J. Leppänen, L. Luzzi, M.E. Ricotti, "An Extended Version of the SERPENT-2 Code to Investigate Fuel Burn-up and Core Material Evolution of the Molten Salt Fast Reactor." Journal of Nuclear Materials 441 (2013) 473–486. The methods implemented have been presented at the 2012 Serpent meeting in Madrid, Spain[1]. The core material evolution of the MSFR has been presented at the 2012 Nuclear Materials Conference in Osaka, Japan.

The obtained results relevant for the MSFR analysis have been extensively compared against those obtained by Mariya Brovchenko and other researcher of the LPSC/CNRS Grenoble, adopting the in-house code REM, also in the framework of the EVOL MSFR neutronic benchmark. SERPENT results can be found in the EVOL report on the official MSFR neutronic benchmark as part of the POLIMI section. Some of these comparisons are reported in the Appendix (Section A.1). Other comparisons between SERPENT and LPSC results are reported and thoroughly discussed in the PhD thesis of Mariya Brovchenko (2013) and in the Deliverable EVOL D2.2 (2013).

[1] See presentation at: **http://montecarlo.vtt.fi/mtg/2012_Madrid/Manuele_Aufiero.pdf**

Table 1.1: *Comparison of recent works dealing with burn-up calculations in MSRs available in recent open literature.*

	Nuttin *et al.* (2005)[a]	Fiorina *et al.* (2013b)[b]	Sheu *et al.* (2013)	Present work
Neutron transport code	MCNP	ERANOS	KENO-VI	SERPENT-2
Neutron transport method	Monte Carlo continuous energy	Deterministic S_n-16	Monte Carlo multi-group (238)	Monte Carlo continuous energy
Burn-up code	REM (in-house code)	ERANOS	ORIGEN-S	SERPENT-2
Solution of the Bateman equations	fourth order Runge-Kutta method	power series approximation of the matrix exponential	power series approximation of the matrix exponential	Chebyshev rational approximation of the matrix exponential
Number of isotopes considered	all the isotopes available in the nuclear data library	167	388	all the isotopes available in the nuclear data library
	short lived isotopes are treated separately	short-cut and simplified decay chains	short lived isotopes are treated separately	all the isotopes are included in the burn-up matrix
Non-soluble FP removal	continuous (non-soluble FP are treated separately)	continuous	batch	continuous
Soluble FP removal	continuous	continuous	batch	continuous
Feed material injection	continuous	batch	batch	continuous
Reactivity control	yes	only guarantees criticality at equilibrium	yes	yes
	continuous adjustment of fissile material injection/extraction rate	–	batch injection of fissile material	continuous adjustment of fissile material injection/extraction rate

[a] For the work of Nuttin *et al.* (2005), the information not available in the paper has been taken from the PhD thesis of Nuttin (2002).
[b] For the work of Fiorina *et al.* (2013b), the information not available in the paper has been taken from the PhD thesis of Fiorina (2013).

1.1 Introduction

THE Molten Salt Fast Reactor offers the possibility to fully benefit from the adoption of a thorium-based closed fuel cycle (Fiorina, 2013). The intermediate-to-fast neutron spectrum adopted allows the effective incineration of transuranium (TRU) isotopes (Merle-Lucotte *et al.*, 2009). Nonetheless, several open issues still exist on different aspects of this innovative system. The adoption of an on-line (continuous) reprocessing scheme offers several advantages but may lead to some problems due to the necessity of handling highly radioactive streams. Moreover, the structural materials have to withstand severe conditions in terms of temperature, chemical environment and neutron flux (Delpech *et al.*, 2010).

The presence of a continuous fuel reprocessing prevents the adoption of commonly available fuel burn-up codes. Few codes were developed specially for this purpose in the past (e.g., Bauman *et al.*, 1971; Nuttin *et al.*, 2005; Fiorina *et al.*, 2013b; Sheu *et al.*, 2013). In Table 1.1, a list of recent works concerning burn-up calculations in MSRs is presented, along with the main features of the employed codes. Some of these codes adopt approximations that may lead to inaccurate fuel evolution predictions or are not fully available. For this reason, a purpose-made extension of the continuous-energy Monte Carlo reactor physics and burn-up code SERPENT-2 has been developed and is proposed in this Chapter.

The extension directly takes into account the effects of on-line fuel reprocessing on

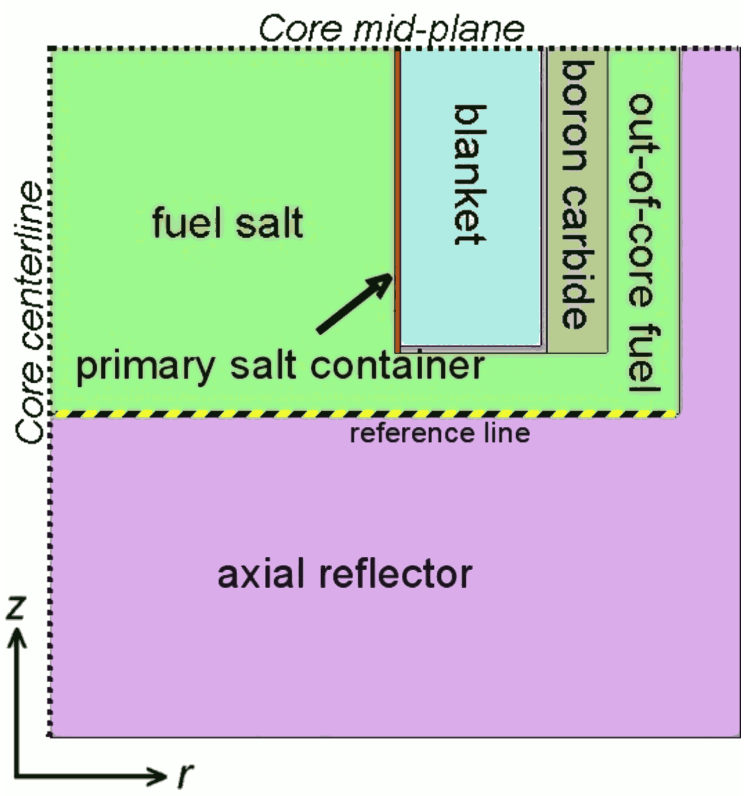

Figure 1.1: *Simplified axial symmetric geometry adopted in the Monte Carlo simulations.*

burn-up calculations and features a reactivity control algorithm. It is here assessed against a dedicated version of the deterministic ERANOS-based EQL3D procedure (Krepel *et al.*, 2009; Fiorina *et al.*, 2013b) and adopted to study the isotopic evolution of MSFR core materials. The work is focused on the study of the breeding performance of the reactor and the analysis of some parameters that are thought to be critical for the deployment of this technology.

The Chapter is organised as follows. In Section 1.2, a detailed description of the methodology adopted and of the extension of the SERPENT-2 code is presented. A comparison with the ERANOS-based EQL3D procedure is also reported for a selected case. In Section 1.3, the implemented reactivity control and equilibrium search methods are described. Finally, the main results related to isotopic evolution of the fuel salt (Section 1.4) and of the nickel-based alloy selected as structural material for the primary salt container and the axial reflectors (Section 1.5) are discussed. A few concluding remarks are drawn in Section 1.6.

A general description of the MSFR has been presented in the Introduction of the thesis. Details about this reactor concept can be found in the references (Merle-Lucotte *et al.*, 2009, 2011; Brovchenko *et al.*, 2012). Here, in Figure 1.1, the simplified axial symmetric geometry selected for the EVOL benchmark and adopted in the present Monte Carlo simulations is shown. Several fuel cycle scenarios have been studied for the MSFR (e.g., see Merle-Lucotte *et al.*, 2009), which adopt different start-up options and feed material compositions. In this Chapter, two cases are investigated: ^{233}U-started and TRU-started options. In the first configuration, the initial fuel salt composition is $LiF - ThF_4 - ^{233}UF_4$

at 77.5 – 20 – 2.5 mol %. In the second configuration, uranium is replaced by TRUs from LWR fuel cycle, with a salt composition of LiF – ThF_4 – $(TRU)F_3$ at 77.5 – 16 – 6.5 mol %. In both cases, the main feed material is composed only by thorium and the criticality of the system in ensured by extracting (or injecting) uranium from the fuel.

1.2 On-line fuel reprocessing

This Section presents the main features of the extension of the SERPENT-2 code (version 2.1.7), and its assessment against the ERANOS-based EQL3D procedure, performed through a fuel isotopic evolution case study (MSFR, TRU-started option).

1.2.1 SERPENT-2 extension for on-line fuel reprocessing

Equation (1.1) describes the rate of change of the concentration of a generic nuclide due to neutron induced reactions and decay processes:

$$\frac{dN_i}{dt} = \sum_j N_j \, \phi \cdot \sigma_{j \to i} - \sum_j N_i \, \phi \cdot \sigma_{i \to j} + \sum_j N_j \lambda_j b_{j \to i} - N_i \lambda_i \tag{1.1}$$

where N_i is the atomic density of the generic nuclide i, ϕ is the neutron flux, $\sigma_{j \to i}$ is the microscopic one-group transmutation cross-section of nuclide j to nuclide i, λ_i is the decay constant of the nuclide i, and $b_{j \to i}$ is the branching ratio from nuclide j to nuclide i.

On-line fuel reprocessing can be explicitly introduced in the system of equations by adding effective decay and transmutation terms for the different nuclides. In this way, the modified system can be solved adopting efficient techniques (Pusa and Leppänen, 2010; Isotalo and Aarnio, 2011a). In the present work, the Chebyshev Rational Approximation Method (CRAM) (Pusa, 2011) available in SERPENT is adopted for the solution of the matrix exponential derived from the system of burn-up equations.

The primary scope of on-line reprocessing in MSRs is the extraction of fission products (FPs) produced during the operation of the reactor. The general behaviour of the reactor and its performance are influenced by the concentration of fission products that act as neutron poisons. In the present work, due to the unavailability of a detailed characterization of the fuel reprocessing plant, a simplified treatment for the FPs removal is adopted (Mathieu, 2005). Elements that are not soluble in the molten salt mixture (i.e., gaseous and metallic species) are continuously extracted through gas bubbling. Other fission products are removed by reprocessing small amount of salt every day. In nominal conditions, the effective removal time constant adopted for the elements removed by gas bubbling is 30 s. The effective soluble fission products removal cycle lasts 450 days(Merle-Lucotte *et al.*, 2009). This value, similar to those found in other works concerning non-moderated MSRs (e.g., Ignatiev *et al.*, 2003), is equivalent to an effective reprocessing of 40 liters per day. Figure 1.2 shows the soluble and insoluble element groups involved in the fuel cycle calculations.

During fuel isotopic evolution calculations, the total molar fraction of Heavy Metal (HM) fluorides is kept constant at 22.5%. For this purpose, fissioned isotopes are replaced with the HM feed material (e.g., thorium). This is achieved, in the extended SERPENT-2 version, by modifying the burn-up equations of the isotopes present in the feed vector,

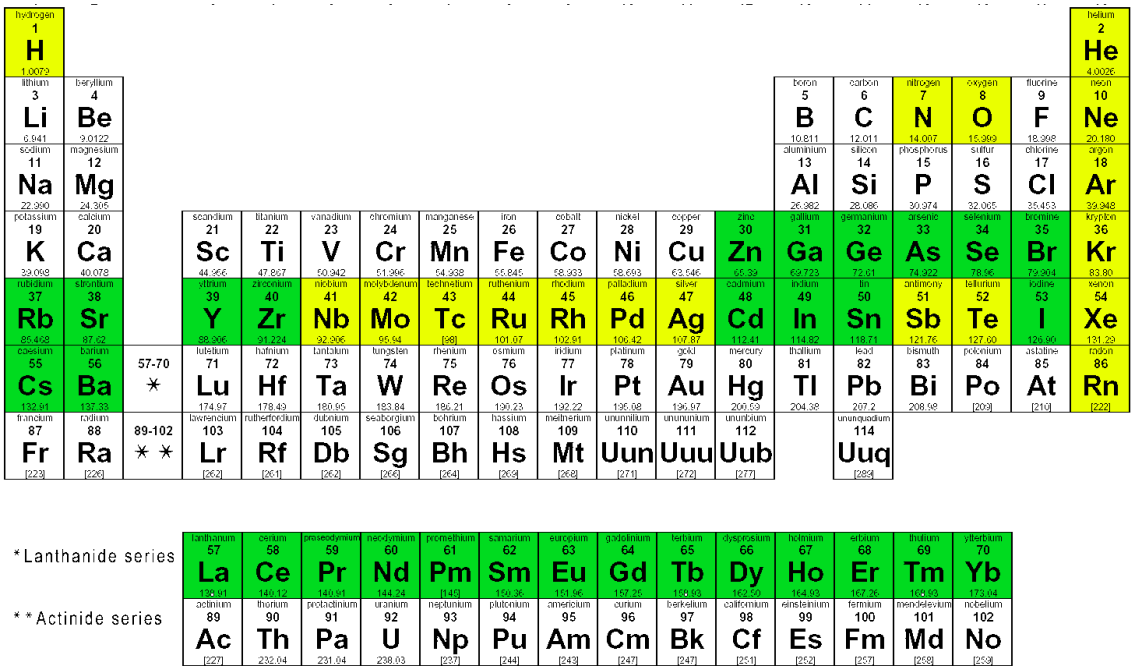

Figure 1.2: *Soluble (green) and insoluble (yellow) elements involved in the fuel cycle calculations.*

adding the following additional term to the Right-Hand Side (RHS) of Equation 1.1:

$$c_i \sum_{k=HM} N_k \, \phi \cdot \sigma_{k,f} \tag{1.2}$$

where $\sigma_{k,f}$ is the one-group fission cross-section of the HM nuclide k and c_i is the atomic fraction of the isotope i in the feed vector. In case of single isotope in the feed material (e.g., ^{232}Th), Equation 1.1 becomes:

$$\frac{dN_i}{dt} = \sum_j N_j \, \phi \cdot \sigma_{j \to i} - \sum_j N_i \, \phi \cdot \sigma_{i \to j} + \sum_j N_j \lambda_j b_{j \to i} + \sum_{k=HM} N_k \, \phi \cdot \sigma_{k,f} - N_i \lambda_i$$

As fission products are generated, lithium is progressively removed[2]. In this case, Equation 1.1 becomes:

$$\begin{aligned} \frac{dN_{Li}}{dt} &= \sum_j N_j \, \phi \cdot \sigma_{j \to Li} - \sum_j N_{Li} \, \phi \cdot \sigma_{Li \to j} + \\ &+ \sum_j N_j \lambda_j b_{j \to Li} - \sum_{k=HM} N_j \, \phi \cdot \sigma_{k,f} \cdot \left(\sum_{l=FP} FY_{k \to l} \right) \end{aligned} \tag{1.3}$$

where $FY_{k \to l}$ is the fission yield for the production of the FP l from a fission of the HM k and $\left(\sum_{l=FP} FY_{k \to l} \right)$ is approximately 2 in most cases.

The removal of fission products is achieved by adding an explicit decay term to the burn-up equations. For the generic fission product l, we can add to the RHS of Equation

[2] This operating strategy has been selected for the EVOL benchmark, in order to keep the evolving salt mixture close to the eutectic point. Of course, other strategies are possibles.

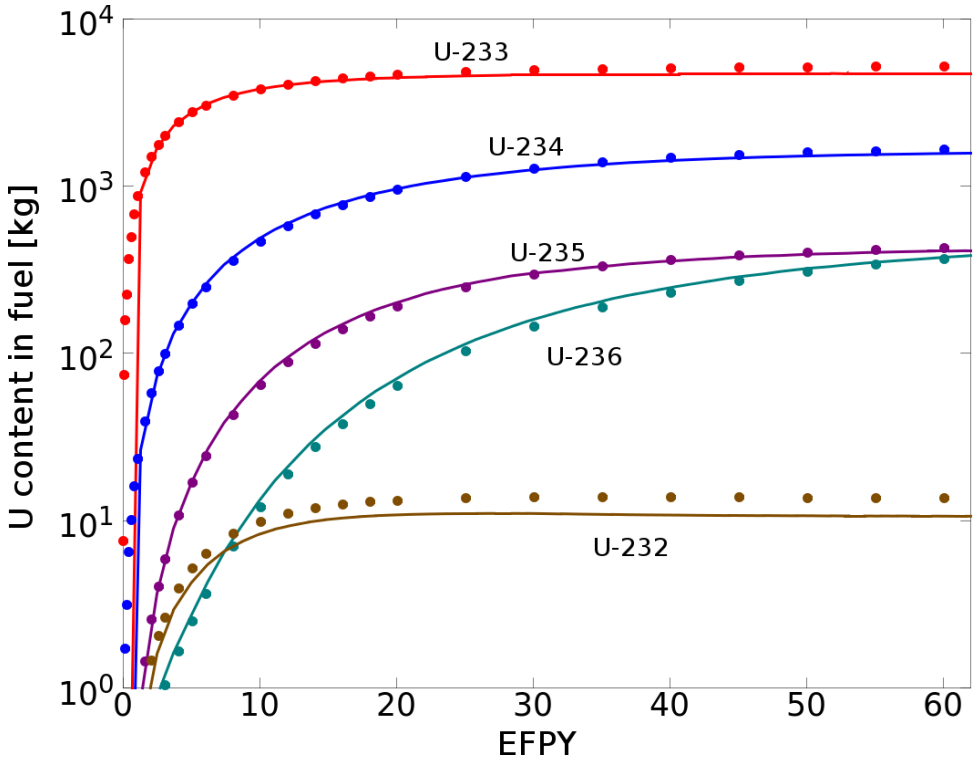

Figure 1.3: *Content of uranium isotopes in the fuel salt (TRU-started MSFR case study). Solid lines: EQL3D/ERANOS; dots: extended SERPENT-2.*

1.1:

$$- N_l \lambda_{l,repro} \tag{1.4}$$

where $\lambda_{l,repro}$ is the effective removal time constant of the particular chemical specie. As stated before, the atomic density of lithium is consequently increased. The following additional term is added to the RHS of Equation 1.3

$$\sum_{l=FP} N_l \lambda_{l,repro} \tag{1.5}$$

1.2.2 Assessment against the ERANOS-based EQL3D procedure

The standard SERPENT-2 code results has been assessed against several other codes and experiments by the VTT developers team (SERPENT, 2011). A verification of the extended version of SERPENT-2 is presented in this Section, through a comparison with the ERANOS-based EQL3D procedure (Krepel *et al.*, 2009; Fiorina *et al.*, 2013b).

The code-to-code comparison has been performed with a fuel isotopic evolution case study, based on the MSFR TRU-started option (Merle-Lucotte *et al.*, 2009). In this option, the initial fissile material is composed by transuranic isotopes from LWR fuel cycle. The comparison is made on a simulation in which only ^{232}Th is injected in the fuel salt as feed material. The effective removal time constant for the insoluble fission products has been set to 30 s. The effective reprocessing rate adopted for the soluble fission products is 5 liters per day. The JEFF-3.1 library (Koning *et al.*, 2006) was adopted for both codes.

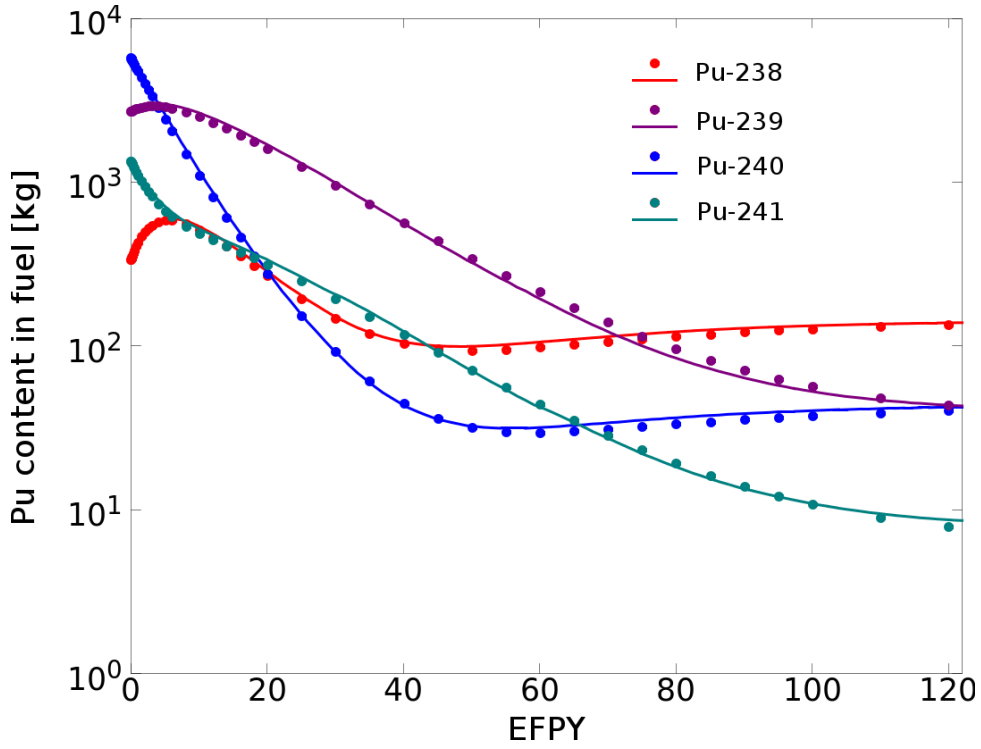

Figure 1.4: *Content of plutonium isotopes in the fuel salt (TRU-started MSFR case study). Solid lines: EQL3D/ERANOS; dots: extended SERPENT-2.*

Figures 1.3 and 1.4 show the uranium and plutonium content over the reactor operation time, as predicted by the two codes. Solid lines represent the results from the ERANOS-based EQL3D procedure, dots represent results from the extended version of SERPENT-2. Table 1.2 shows the mass content of the major uranium and plutonium isotopes after 100 years as predicted by the two codes. The results of the two simulations are in a good agreement, considering the differences between the two codes, in the solution of both the neutron transport and the burn-up equations. However, a significant difference in the ^{232}U equilibrium concentration can be appreciated. Even if the total amount of this is isotope in the fuel salt is limited to few kg, a precise estimation of its concentration is desirable. In fact, the ^{232}U decay chain includes strong-gamma emitters that cause concerns in the handling of fuel salt (see Section 1.4). The reason of this difference is related to the coarse energy discretization employed in the ERANOS calculations. Indeed, the 33 energy groups adopted are not enough to precisely describe the neutron flux at the high energies at which the $(n, 2n)$ threshold reactions responsible of the ^{232}U production occur.

1.3 Reactivity control and equilibrium search

1.3.1 Reactivity control algorithm in SERPENT-2

In circulating fuel reactors, long term reactivity swing can be managed by direct insertion (or removal) of fissile material. This allows for better breeding performance, compared to the adoption of control rods or burnable absorbers. Moreover, it reduces the potential risks

Table 1.2: *Mass content in the fuel salt after 100 years for plutonium isotopes. Comparison between the extended version of SERPENT-2 and EQL3D/ERANOS.*

Isotope	Mass content $[kg]$		Rel. diff. $[\%]$
	SERPENT-2	ERANOS	
U-232	13.6	10.4	30.8
U-233	5223	4700	11.1
U-234	1739	1630	6.9
U-235	455	428	6.3
U-236	486	474	2.5
Pu-238	126	133	-5.3
Pu-239	37.3	40.2	-7.2
Pu-240	56.4	52.8	6.8
Pu-241	10.7	10.9	-1.9

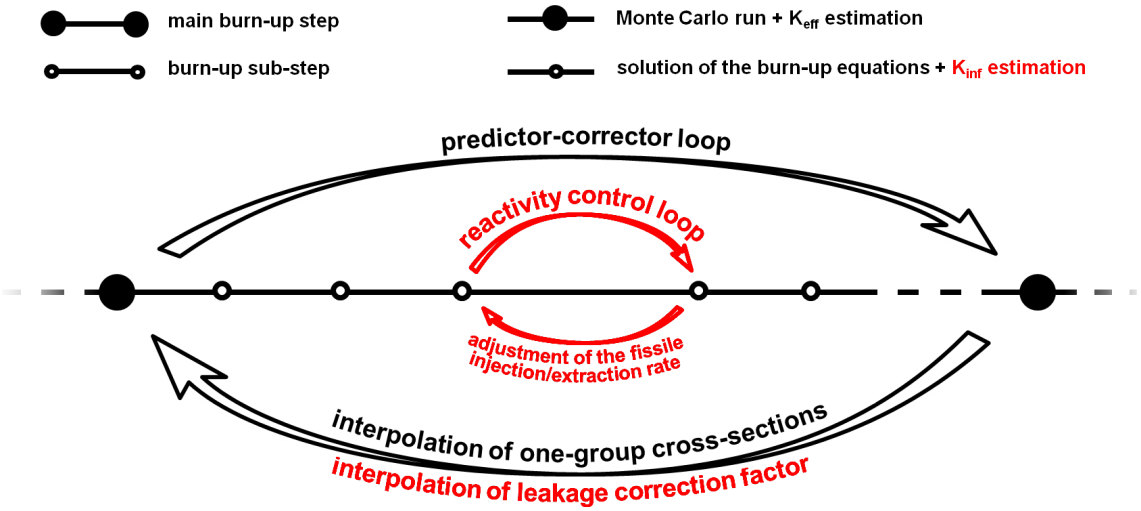

Figure 1.5: *Simplified scheme of the reactivity control algorithm implemented in the extended SERPENT-2 version. Newly implemented features are marked in red.*

for reactivity initiated accidents. The main reactor breeding parameters (i.e., conversion ratio, doubling time and instantaneous fissile material production/consumption rate) can be correctly estimated only if the proper composition, which leads to system criticality, is adopted. For this purpose, the developed extension of the SERPENT-2 code features a reactivity control that allows to keep the effective multiplication factor close to 1 during the whole simulation. This is performed by continuously adjusting the fissile-to-fertile ratio in the feed material.

Figure 1.5 shows a simplified scheme of the reactivity control algorithm implemented. The predictor-corrector and sub-steps methods available in SERPENT-2 allow efficient burn-up calculations thanks to the finer time discretization, with respect to common depletion schemes, with negligible slowdown of the simulations (Isotalo and Aarnio, 2011b). The one-group transmutation cross-sections of each nuclide are calculated at each main burn-up step through Monte Carlo runs. This operation greatly dominates the cpu-time requirements in most cases. The main burn-up steps are subdivided in several (e.g., 50 in the present work) sub-steps, in which the system of burn-up equations is actually solved. At

each sub-step, the one-group cross sections and neutron flux are interpolated between the two closest Monte Carlo runs. The implementation of reactivity control in the SERPENT-2 depletion algorithm is briefly explained in the following.

At each sub-step, the one-group microscopic cross-sections, along with the atomic densities provided by the solution of the system of burn-up equations, are adopted to calculate the infinite multiplication factor k_{inf} in the fuel material. In order to correctly estimate the reactivity of the system, a correction for the leakage term is needed. At each Monte Carlo run performed for neutron spectrum calculation and one-group cross-section collapse, the effective multiplication factor k_{eff} is also estimated. At this point, both k_{eff} and k_{inf} are known. A leakage correction factor can thus be calculated at each Monte Carlo run. If this correction factor is interpolated at each sub-step between the two closest calculations (as it is done for one-group cross-sections), an accurate estimate of the effective multiplication factor is available during the whole simulation.

Once the k_{eff} is known, the fissile material injection/extraction rate can be adjusted at each sub-step to keep the system critical. A direct relationship between the fissile material injection rate and the reactivity is not easily obtainable under general hypotheses. In the present work, the secant method is iteratively adopted inside the sub-step to modify the injection rate, until the target effective multiplication factor ($k_{eff,tgt}$) is reached within a desired tolerance (ε).

The extended version of the SERPENT-2 depletion calculation algorithm adopted in the present work is presented in the following, and sketched in Figure 1.5.

(1) For each burn-up step

- **(2)** Estimate one-group cross-sections and k_{eff} through a Monte Carlo run with the initial material composition (predictor step)
- **(3)** Calculate the leakage correction factor
- **(4)** For each sub-step
  - **(5)** Interpolate the one-group cross-sections and the leakage correction factor between the two closest Monte Carlo runs
  - **(6)** Solve the system of burn-up equations and calculate the isotopic composition at the end of the sub-step
  - **(7)** Estimate k_{eff} through one-group cross-sections and the leakage correction factor
  - **(8)** If $|k_{eff} - k_{eff,tgt}| > \varepsilon$
    - **(9)** Adjust the fissile material injection/extraction rate and repeat steps **(6)** to **(8)**
- **(10)** Run a Monte Carlo simulation with the final material composition (corrector step) and repeat steps **(2)** to **(9)**
- **(11)** Use the final composition as initial composition for the next burn-up step

The implemented reactivity control algorithm makes use of quantities that are already calculated in SERPENT by default (i.e., k_{eff} and one-group cross-sections), requiring little additional computational effort. Due to the iterative criticality search at each sub-step, the solution of the system of burn-up equations is performed several times (few

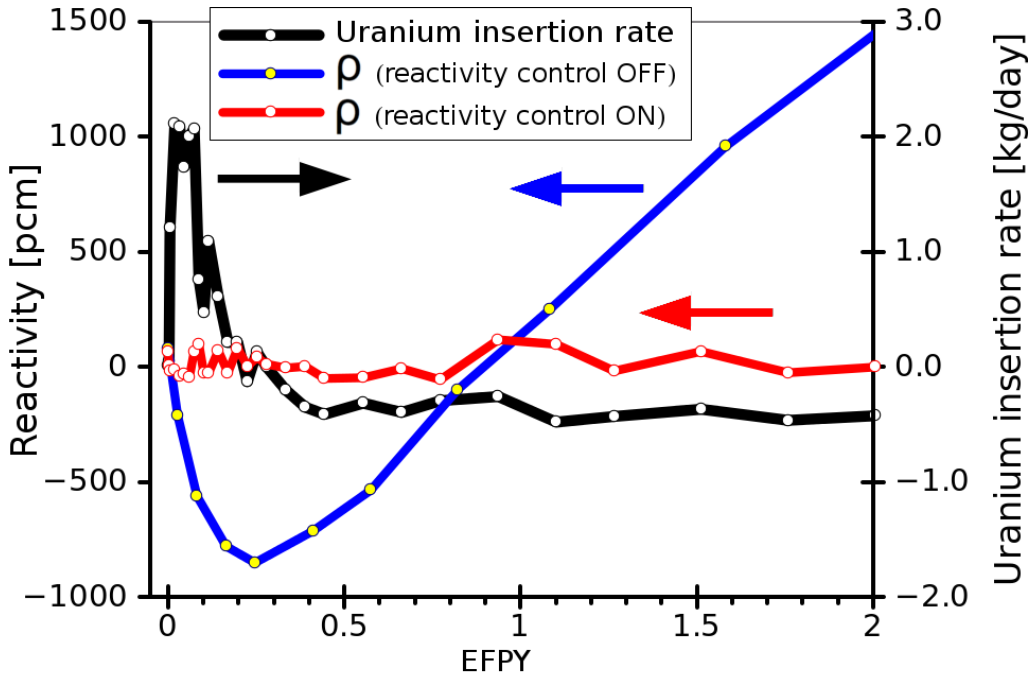

Figure 1.6: *Reactivity and uranium insertion rate (TRU-started MSFR).*

hundreds) per burn-up step. Thanks to the adoption of the CRAM method available in SERPENT, the relative increase in the total calculation time due to the reactivity control is in the order of few percent in most cases.

In order to assess the capabilities of the implemented algorithm, the TRU-started scenario has been simulated with and without the reactivity control. Figure 1.6 shows the predicted reactivity for the two cases, along with the ^{233}U insertion rate required to keep the system close to criticality. In the simulation performed without the adoption of the control algorithm (blue line), the reactivity of the system reaches a value of approximately -800 pcm after 3 months (^{233}Pa build-up) and then rises to 1500 pcm after two years of operation. The adoption of the control algorithm (red line) leads to a simulation in which the reactivity is kept in a relatively narrow interval close to zero (approximately $\pm$ 100 pcm).

1.3.2 Accelerated equilibrium search

The equilibrium composition of a breeder reactor, which might be reached after several tens of years of operation, is often studied as an indicator of the reactor behaviour (Salvatores *et al.*, 2009). The equilibrium state is independent of the initial fuel composition and is influenced only by the feed vector and, in MSRs, by the reprocessing rates (Merle-Lucotte *et al.*, 2011). For this purpose, the developed burn-up procedure is featured also by an iterative equilibrium search algorithm. Adopting an initial guess composition, a first Monte Carlo run is performed and the equilibrium parameters (i.e., the isotopic vector composition and the fissile-to-fertile ratio in the feed material) are calculated from the burn-up matrix. Then, a new transport cycle is run and the process is repeated adopting the effective transmutation cross-sections computed for the updated composition. The adopted equilibrium search algorithm is briefly sketched in Figure 1.7.

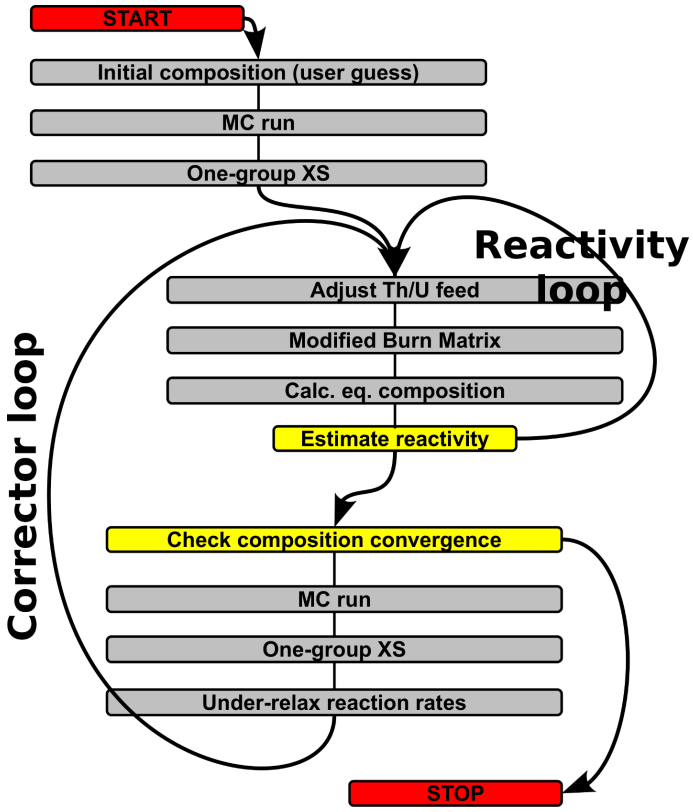

Figure 1.7: *Algorithm for the equilibrium search.*

The convergence of this scheme is, in general, unstable. Instabilities become more relevant in case of moderated reactors in which self-shielding effects are more effective. For this reason, under-relaxation techniques are adopted, which allow to reach an accurate equilibrium state in few iterations.

In Figure 1.8, results of a convergence test of the equilibrium search algorithm is shown, for the effective multiplication factor (black line) and the atomic density of ^{233}Pa and ^{238}Pu (blue and red lines, respectively). The test is relative to a ^{233}U-started MSFR case with nominal reprocessing parameters. Stable convergence is reached within a few iterations.

The algorithm is designed to minimize transport cycles, which represents most of the computational efforts and results to be computationally competitive (from a cpu-time point of view) even with traditionally fast-running codes, based on less accurate deterministic transport, and not featuring any accelerated equilibrium search technique.

1.4 MSFR fuel isotopic evolution

In this Section, the extended version of SERPENT-2 is employed to study the MSFR fuel isotopic evolution. Results from a fuel cycle analysis are presented, along with a sensitivity study on the reprocessing time constants and the investigation of some parameters relevant for reprocessing operations (i.e., decay heat, high energy gamma activity and neutron emission in the fuel salt). A sensitivity study on the adopted nuclear data library is also presented, as result of a comparison between calculations performed adopt-

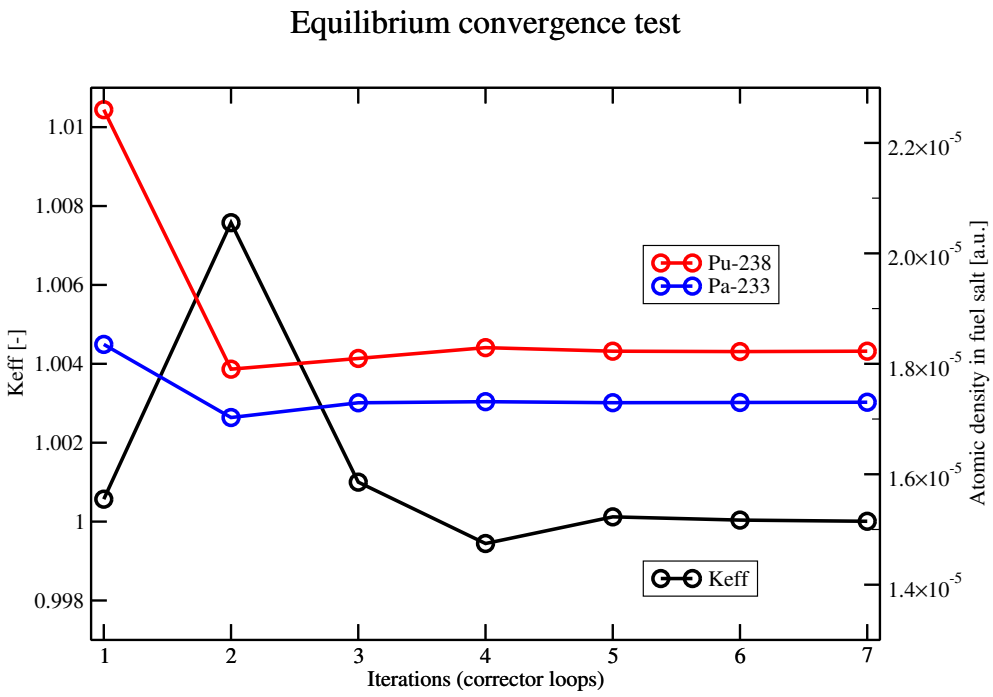

Figure 1.8: *Equilibrium search from ^{233}U-started MSFR. Convergence test.*

ing JEFF-3.1 (Koning *et al.*, 2006) and ENDF/B-VII (Chadwick *et al.*, 2006) data. At the end of this Section, the radiotoxicity generation for the MSFR equilibrium composition in nominal conditions is shortly discussed.

1.4.1 Transient analysis

As briefly pointed out in the previous section, reactivity in MSRs can be controlled by insertion/removal of fissile material in the fuel salt.

Figure 1.9 shows the cumulative mass of ^{233}U that can be extracted from the system for the ^{233}U-started case study, as predicted by SERPENT-2 adopting the JEFF-3.1 library. The red line represents the net amount of fissile material that is extracted from the fuel, while keeping the reactivity close to zero. Without considering the blanket salt, the reactor appears to behave closely to an iso-breeder system, producing slightly more than the fissile material it consumes. The blue line represents the cumulative production of ^{233}U in the blanket salt. The presence of the external blanket greatly increases the excess production of uranium. In black, the sum of the curves is presented. It can be observed that the system reaches a net production of 5 tons of ^{233}U in about 40 years. This is approximately the fissile quantity required to start a new MSFR. Hence, the system shows a first doubling time of about 40 years.

For a given quantity of fissile material required to start-up a new reactor, "first doubling time" is referred to as the minimum time period needed to extract this quantity after the initial start-up of the reactor. This quantity depends on the initial fuel composition. On the other hand, "Equilibrium doubling time" is referred to as the time period needed to

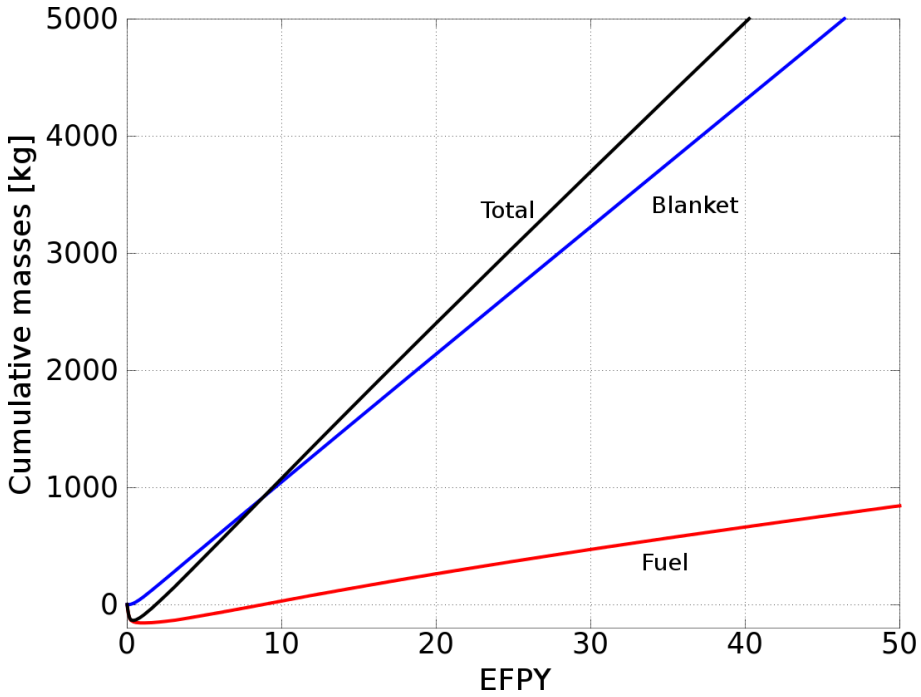

Figure 1.9: *Cumulative uranium production from fuel and blanket in the first 50 years of operation (^{233}U-started MSFR case study).*

produce the required quantity of fissile material, at the extraction rate characteristic of the equilibrium state of the reactor. For a given reactor configuration, this quantity does not depend on the particular initial fuel composition but only on the feed material employed and the reprocessing time constants adopted. For the purpose of the present work, the fissile material considered is ^{233}U and the required quantity is about 5 tons.

Details of the first 5 years for the same case study are presented in Figure 1.10. Even if the system shows globally good breeding performance, in the first months, the insertion of about 150 kg of ^{233}U is required to keep the system critical. This is mainly due to the build-up of ^{233}Pa that acts as neutron absorber and decays to ^{233}U with a time constant of about 27 days.

Table 1.3 shows the yearly extraction rates from the fuel and blanket salts for the ^{233}U-

Table 1.3: *Uranium production after 100 years of operation – JEFF-3.1 library (^{233}U-started MSFR case study).*

	Yearly extraction of ^{233}U $[kg]$	
	Fuel	Blanket
	21	113
	Composition of the extracted uranium $[\%]$	
	Fuel	Blanket
U-232	0.17	0.05
U-233	66.85	99.00
U-234	21.54	0.93
U-235	5.65	0.02
U-236	5.79	-

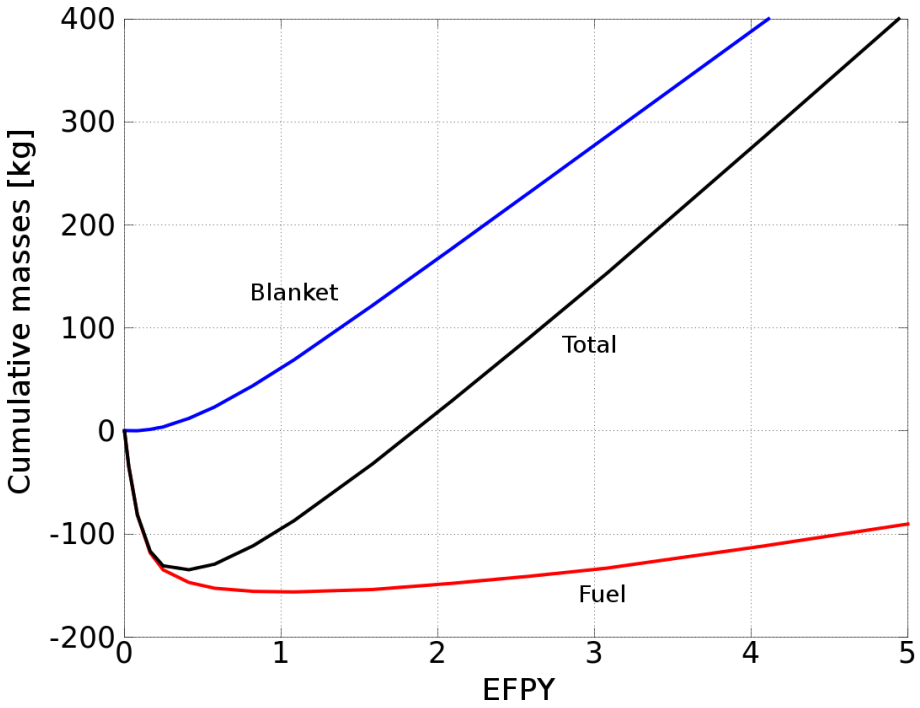

Figure 1.10: *Cumulative uranium production from fuel and blanket in the first 5 years of operation (^{233}U-started MSFR case study).*

started MSFR case study after 100 years (JEFF-3.1 library). The isotopic quality of the uranium extracted from fuel and blanket salt is significantly different. The contamination from ^{232}U in the two isotopic vectors is of relevant importance due to the strong-gamma emitters in its decay chain. The relative content of ^{232}U for the fuel and blanket is about 1700 and 500 at. ppm, respectively. These values are comparable to those found in other thorium-based reactors (Fiorina *et al.*, 2013a).

1.4.2 Equilibrium calculations

In the following, the effect of reprocessing rates on some important parameters is studied for the equilibrium state. First of all, the Conversion Ratio (CR) is analysed as index of the breeding capability of the system. The CR is strongly related to the reprocessing rate. If FPs are removed slowly from the core, neutron economy is worsened by the increased neutron capture rate.

Figure 1.11 shows the dependence of the CR on the effective reprocessing rate for the soluble fission products removal. For this analysis the conversion ratio has been computed as follows:

$$CR \simeq \frac{r_{capt,Th_{232}} - r_{capt,Pa_{233}}}{r_{abs,U_{233}}} \tag{1.6}$$

where, $r_{capt,Th_{232}}$ is the neutron capture rate from ^{232}Th, $r_{capt,Pa_{233}}$ is the neutron capture rate from ^{233}Pa and $r_{abs,U_{233}}$ is the neutron absorption rate from ^{233}U. This definition of CR gives accurate results at equilibrium compositions and greatly simplifies the calculations. The reactor shows a relatively high conversion ratio near nominal conditions (40 liters reprocessed per day). If the reprocessing rate is lowered, the breeding capabilities are reduced until the iso-breeder condition is reached for a reprocessed fuel salt

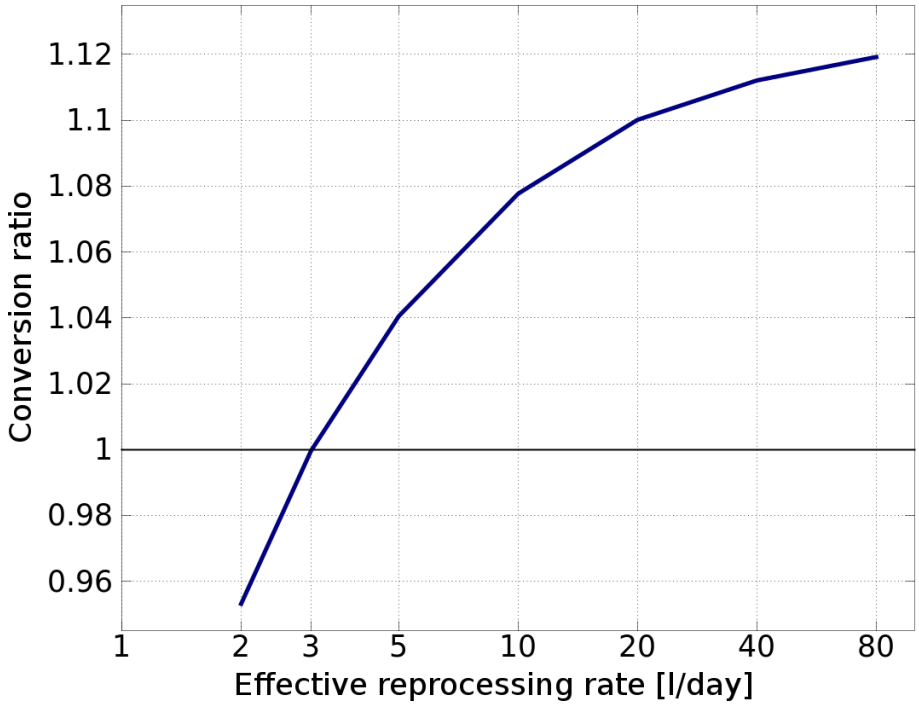

Figure 1.11: *Conversion ratio at equilibrium as function of the daily fuel salt reprocessed amount (JEFF-3.1 library).*

amount of about 3 liters per day (equivalent to an effective soluble FP removal cycle of $\sim$16 years). This value is much lower with respect to values typical for graphite-moderated MSRs[3]. This can be ascribed mainly to the intermediate-to-fast neutron spectrum of this reactor, which reduces the neutron capture rate of ^{233}Pa and fission products.

Figure 1.12 shows the molar concentration of trifluorides in the fuel salt as function of the reprocessing rate. At nominal condition, the total trifluorides concentration is approximately 0.5 mol %. For lower reprocessing rates, the equilibrium concentration of trivalent elements grows and solubility issues may become relevant. The black line represents the total molar concentration of trifluorides. Red lines show the solubility limits at 600°C and 800°C, measured by Barton *et al.* (1970). According to the lower temperature of the fuel salt in the reactor, solubility can entail a lower limit to the reprocessing rate adopted. Taking 600°C as possible lowest temperature in the primary circuit (650°C is the average core inlet temperature in nominal conditions), the minimum reprocessing rate required is about 7 liters per days. The MSFR reveals to be a flexible reactor that can operate at different reprocessing conditions, according to the necessity to improve the breeding performance or reduce the reprocessing streams.

Non soluble FPs (gaseous and noble metals) are removed quickly from the system by means of gas bubbling with a time constant of few seconds or few tens of seconds (30 seconds in nominal conditions). The impact of this elements on the neutron economy is small, due to the low content in the fuel salt mixture. Nonetheless, the in-core decay heat after shutdown is influenced by the effective removal time constants of the non-soluble fission products.

[3]For example, a removal time cycle of 3 to 5 days for the ^{233}Pa and 30 to 60 days for the rare earth FPs was proposed by Whatley *et al.* (1968) for a graphite-moderated molten salt reactor.

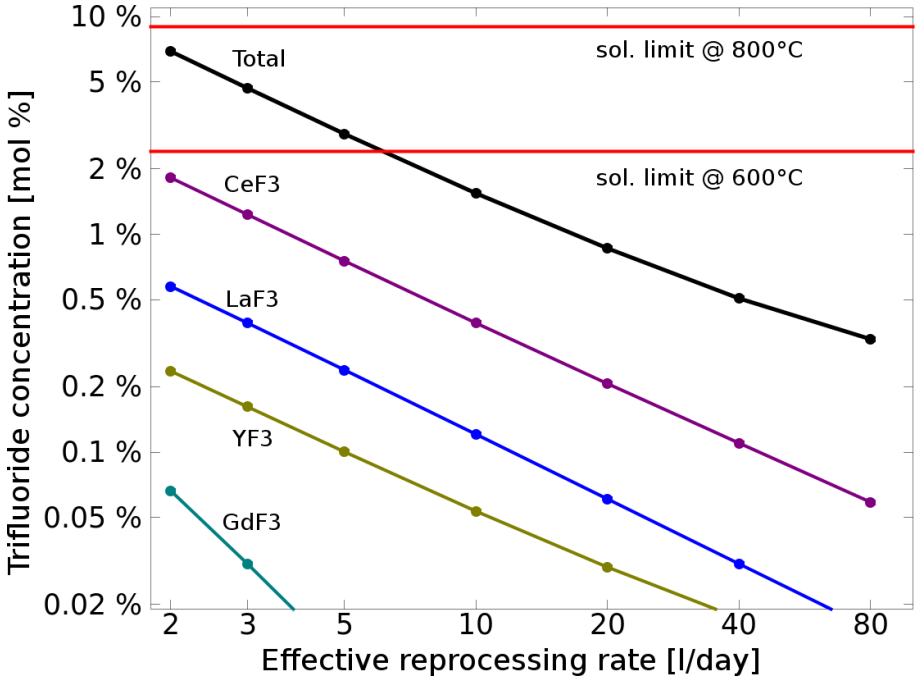

Figure 1.12: *Molar concentration of trifluorides at equilibrium composition for different reprocessing rates.*

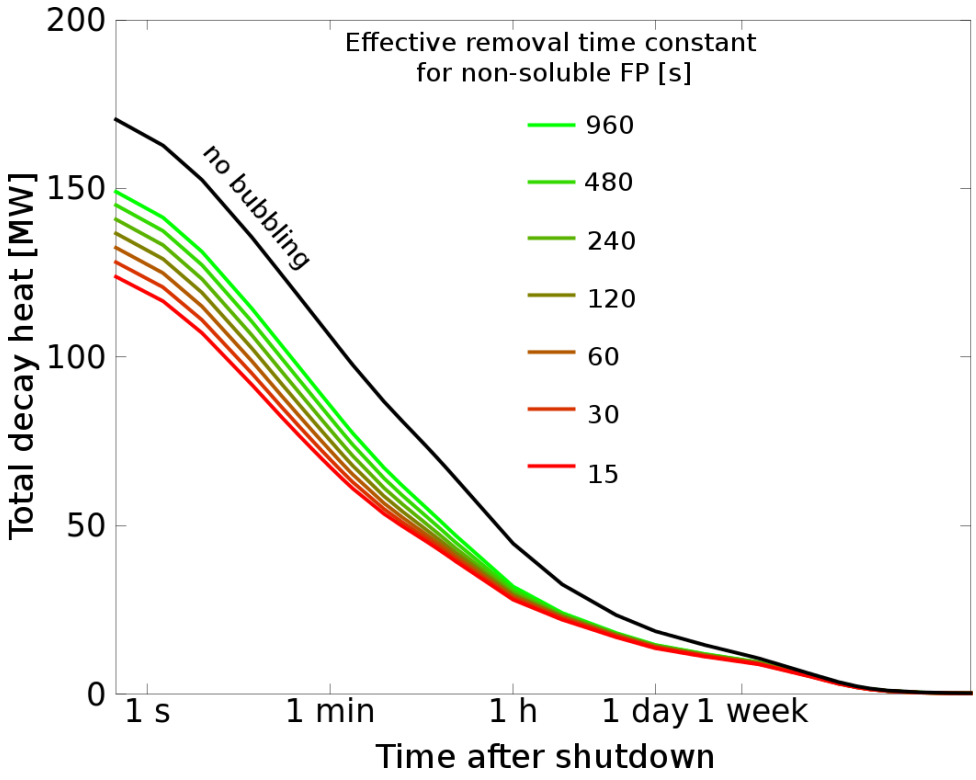

Figure 1.13: *In-core decay heat after reactor shutdown for different effective non soluble FP removal time constants at equilibrium.*

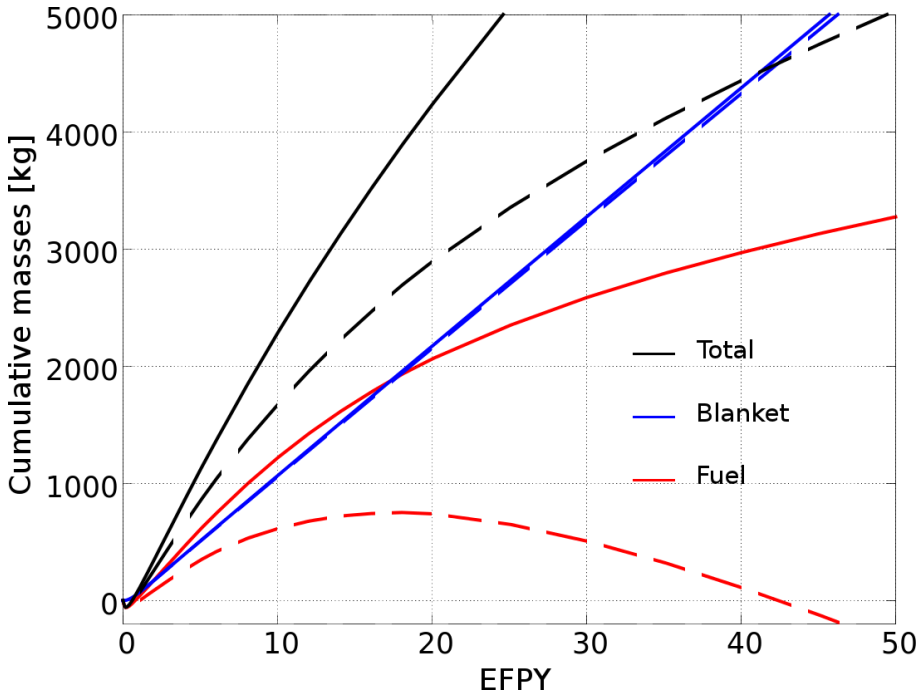

Figure 1.14: *Cumulative uranium production from fuel and blanket: comparison between JEFF-3.1 and ENDF/B-VII results. Solid lines: JEFF-3.1. Dashed lines: ENDF/B-VII (TRU-started case study).*

Figure 1.13 shows the in-core decay heat curves at equilibrium for different effective removal time constants. Gas bubbling is responsible of a reduction of the decay heat at shutdown from about 170 MW (5.67% of the nominal reactor power) to about 130 MW (4.33%) in nominal condition. Increasing bubbling rate can be beneficial in some accidental transient scenarios in which decay heat plays a significant role (e.g., see transient analyses from Brovchenko *et al.*, 2012; Guerrieri *et al.*, 2012).

1.4.3 Nuclear data library sensitivity

In this Section, results from a sensitivity analysis on the adopted nuclear data library are presented. Due to the unavailability of ^{233}U, several starting options have been considered for the MSFR (Merle-Lucotte *et al.*, 2011). Figure 1.14 shows a comparison between JEFF-3.1 and ENDF/B-VII results for what concerns the uranium production in the TRU-started case study. It can be observed that the predictions related to the ^{233}U extraction from the blanket are very similar. On the other hand, the uranium production estimates in the fuel salt are completely different between the two libraries. After about 20 years of operation, according to the ENDF/B-VII results, the fuel salt needs to be fed continuously with ^{233}U in order to keep the system critical (approximately 60 kg per year). On the other hand, JEFF-3.1 results show a breeder behaviour of the system even without the blanket. The uranium production rate from the fuel is increased for the first $\sim$20 years. This leads to a significant reduction of the first doubling time. As a matter of fact, in this case, adopting the JEFF-3.1 library, the net production of 5 tons of ^{233}U is reached in about 25 years (to be compared to about 40 years for the ^{233}U-started case study).

Table 1.4 shows the doubling time estimates obtained with the two evaluated nuclear data libraries. The results show a discrepancy of more than 100% in most cases. In

Table 1.4: *Doubling time: comparison between JEFF-3.1 and ENDF/B-VII results.*

First doubling time [years] (TRU-started)			
Reproc. rate	JEFF-3.1	ENDF/B-VII	Diff. [%]
20 [l/day]	27.8	68.3	+145
40 [l/day]	25.2	51.2	+103
80 [l/day]	23.9	45.0	+87
Equilibrium doubling time [years]			
Reproc. rate	JEFF-3.1	ENDF/B-VII	Diff. [%]
20 [l/day]	46.3	171	+270
40 [l/day]	40.9	119	+190
80 [l/day]	38.7	102	+165

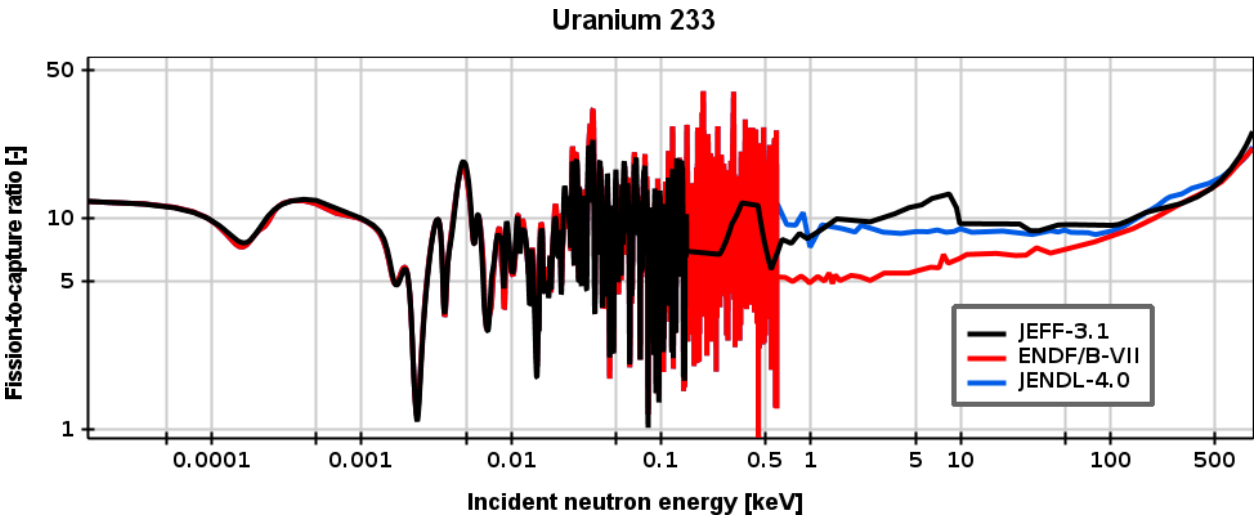

Figure 1.15: *Fission-to-capture ratio of ^{233}U as function of the incident neutron energy.*

nominal reprocessing conditions (40 liters reprocessed per day), the equilibrium doubling time is increased of about three times, from about 40 years (JEFF-3.1) to approximately 120 years (ENDF/B-VII).

A preliminary analysis of the cross-section data showed that the main reason of this huge discrepancy lies in the uncertainty on the ^{233}U capture cross-section. Figure 1.15 represents the fission-to-capture ratio as function of the incident neutron energy for JEFF-3.1 and ENDF/B-VII evaluated nuclear data libraries. The JENDL-4.0 library (Shibata *et al.*, 2011) is included for comparison. It can be noticed that, even if there is a good agreement at thermal energies, in the range between 1 keV and 100 keV, data present sizeable differences, up to a factor two.

Figure 1.16 shows the conversion ratio calculated at the equilibrium composition, adopting the JEFF-3.1 and ENDF/B-VII libraries. It can be observed that big differences are present, as in the case of doubling time estimates. Clearly, the dependence of the CR on the reprocessing rate is the same for the two libraries. Nonetheless, the uncertainty in nuclear data appears to be an open issue for the deployment of the MSFR technology and similar systems. A more detailed sensitivity analysis to the cross-sections for the main reactor parameters appears desirable. In this direction, an ongoing research activity is devoted to the development of a Monte Carlo-based analysis. The implementation

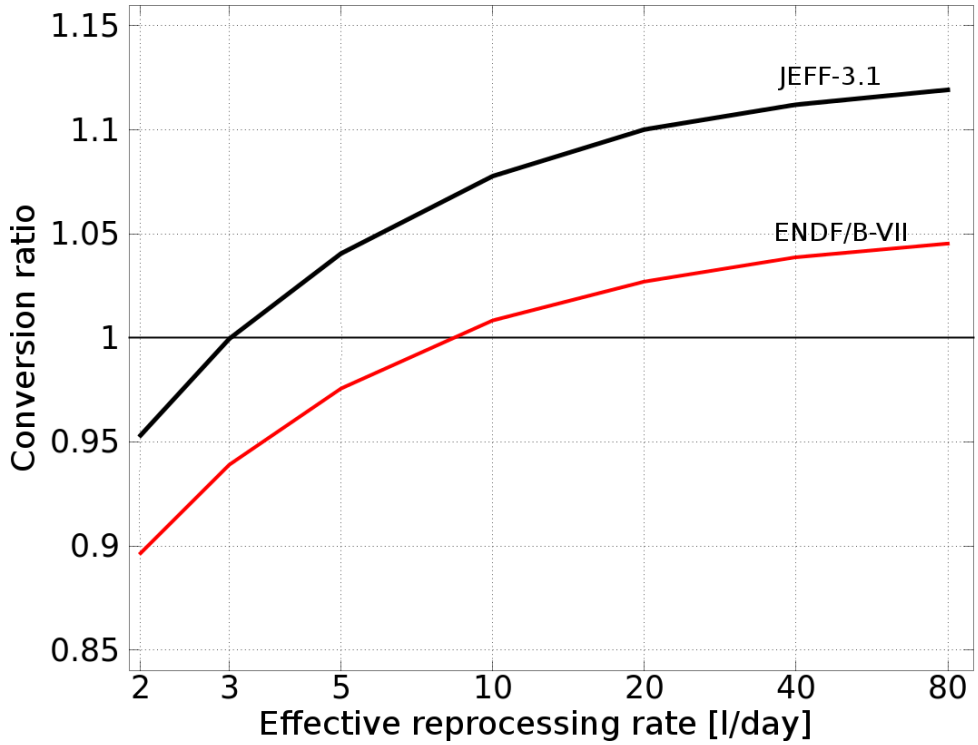

Figure 1.16: *Conversion ratio at equilibrium as function of the daily fuel salt reprocessed amount: comparison between JEFF-3.1 and ENDF/B-VII.*

in SERPENT-2 of a k_{eff} sensitivity calculation technique is described in the Appendix (Section A.3), along with a few preliminary verification cases.

In any case, additional ^{233}U capture cross-section measurements in the 1 to 100 keV energy range are desirable.

1.4.4 Handling of fuel salt

The adoption of a molten salt as fuel avoids the problematic fuel fabrication in presence of strongly radioactive elements, common in closed fuel cycles implementation based on solid-fuelled fast reactors. On the other hand, it implies the adoption of continuous reprocessing by means of pyrochemical techniques (Delpech *et al.*, 2009b). In this context, decay of fission products plays a major role in determining the feasibility of a given reprocessing scheme and the associated requirements (e.g., cooling, shielding, remote handling, etc.). The extended version of SERPENT-2 allows to take into account all the isotopes present in the cross-section and decay nuclear data libraries adopted. In the following, curves relative to decay heat, high energy gamma and neutron emission are shown. Results are expressed per liter of fuel salt.

Figure 1.17 shows the decay heat curve of fuel salt extracted from the reactor as function of the cooling time. The red line is relative to nominal conditions. The black line indicates the results of a simulation without removal of non soluble FPs by gas bubbling. In this case, the specific decay heat is greater than 1 kW per liter, one day after the extraction, while, in nominal conditions, it is approximately 0.8 kW per liter. In both cases, the decay power remains in the order of few hundreds of Watt per liter in the first

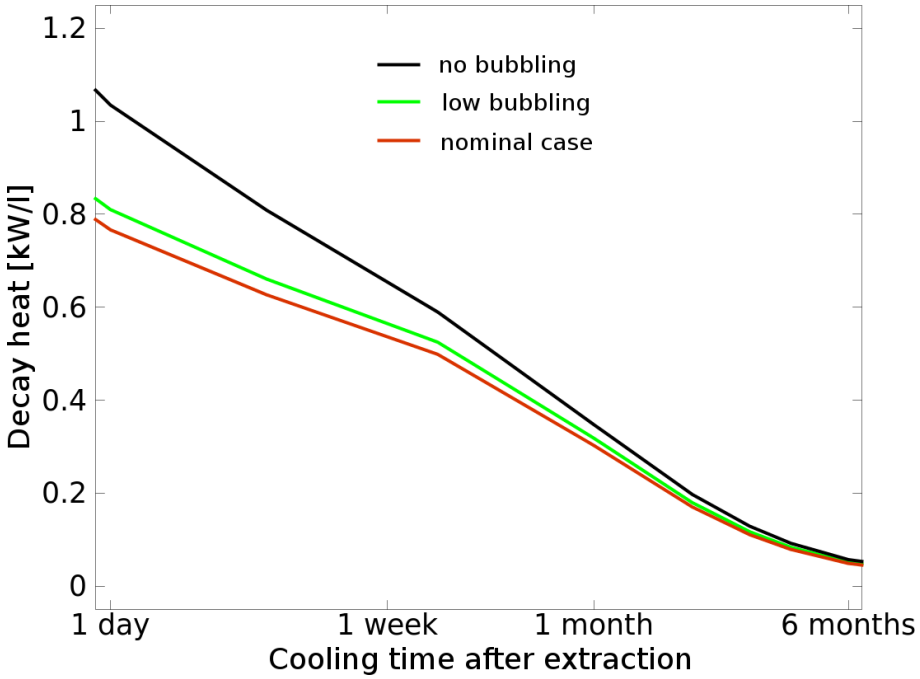

Figure 1.17: *Specific decay heat in the fuel salt after extraction.*

month. These values call for the adoption of active heat removal system in the reprocessing scheme, considering that, in nominal condition, about 40 liters are reprocessed per day and cooling times greater than few weeks or months lead to a significant increase of the total (in core + out of core) salt amount. Non soluble FP removal reduces the total energy released in the reprocessing streams of about 20%.

Figure 1.18 shows the specific emission of high energy gamma in the fuel salt extracted from the reactor, as function of the cooling time. The emission of photons with very high energy ($\geq$ 3.5 MeV) is quickly reduced after the extraction of the fuel salt and reaches negligible values after about one day. On the other hand, gamma emission in the energy range close to 2 MeV remains high after several weeks of cooling time. The blue line shows the contribution of the ^{208}Tl decay. This isotope, produced within the decay chain of the ^{232}U, is often considered as one of the major problem related to the adoption of the thorium based closed fuel cycle (Dekoussar *et al.*, 2005). Its contribution to high energy gamma emission becomes dominant after few years (the cooling time commonly adopted in most solid-fuelled reactors). The contribution of the fission products is greatly dominant in the first few weeks or months, and thus is very important for the reprocessing phases of the MSFR. Nonetheless, according to the specific reprocessing scheme adopted, ^{232}U may still represent an issue for some reprocessing steps. For a comparative purpose, the gamma emission calculated (Fiorina, 2013) for a fuel assembly of a sodium-cooled reactor (Toshiba-Westinghouse ARR – Advanced Recycling Reactor, Dobson, 2008) after 5 years of cooling time is also shown in Figure 1.18 (yellow dashed line).

Figure 1.19 shows the specific neutron emission rate in the reprocessed fuel salt, after extraction. Although several actinides undergo spontaneous fission, in most cases the relative branching ratio of this process is very low. The results of the simulations show that most of the emitted neutrons are produced by the spontaneous fission of few isotopes with

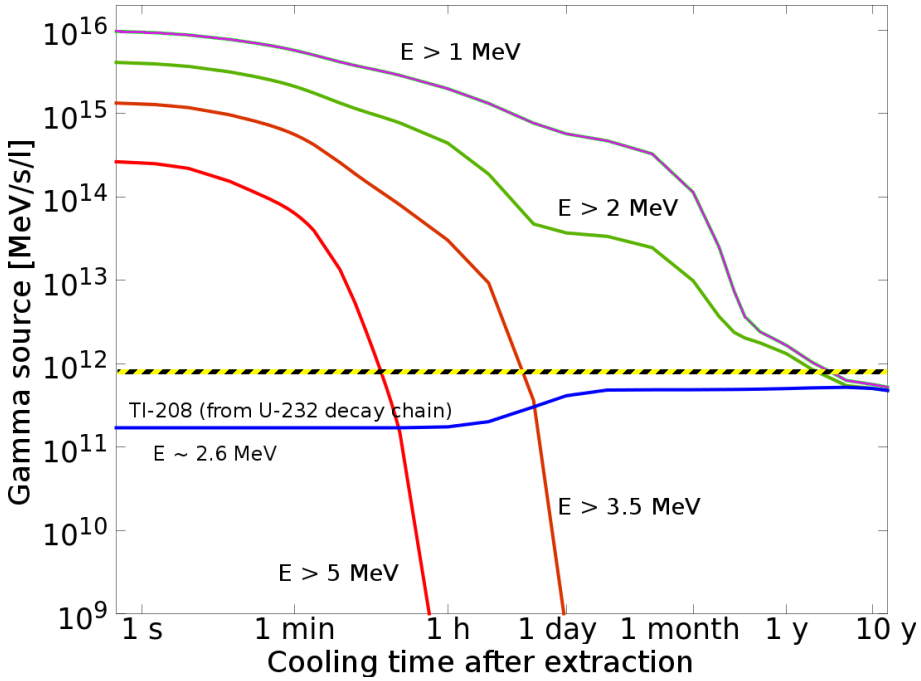

Figure 1.18: *High energy gamma emission in the fuel salt after extraction.*

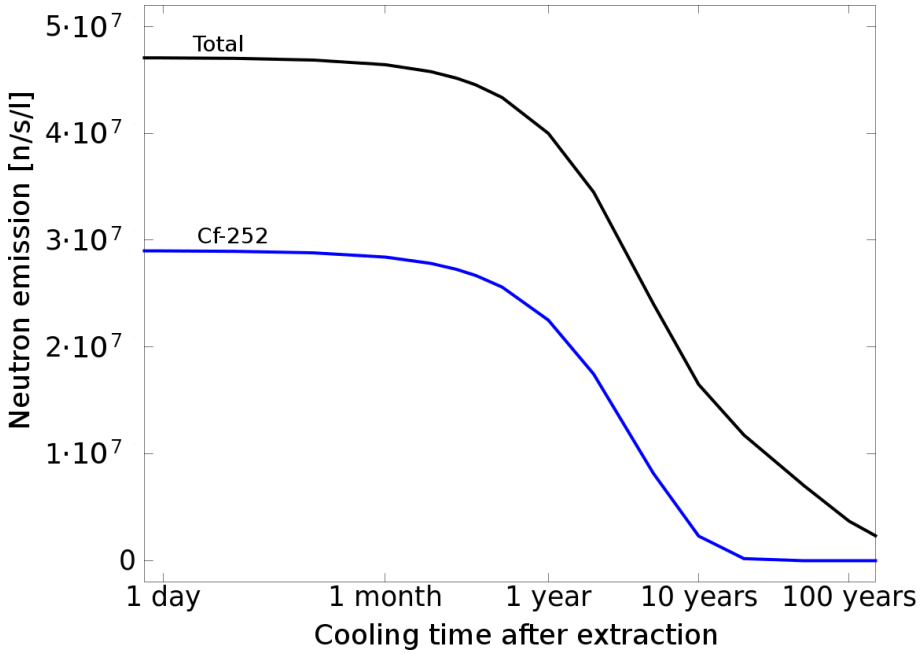

Figure 1.19: *Neutron emission in the fuel salt after extraction.*

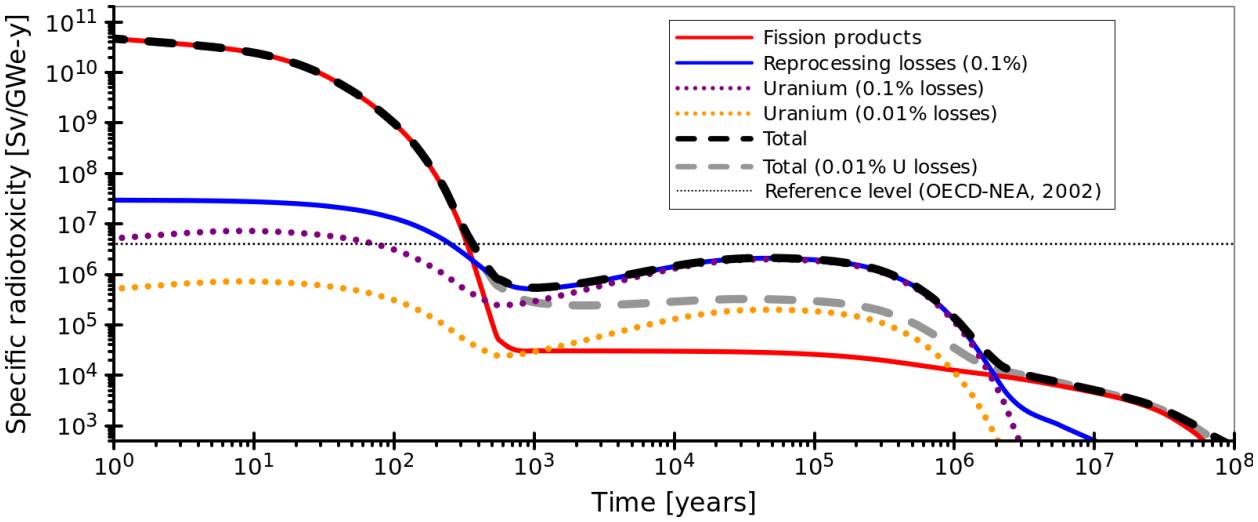

Figure 1.20: *Specific ingestion radiotoxicity generation at equilibrium (nominal conditions).*

relatively high branching ratio. In particular, the blue line represents the neutrons emitted from ^{252}Cf. Even if this isotope is present only in trace in the fuel salt, at equilibrium composition, it is responsible of more than a half of the total neutron emission (in black) for a long period.

As a concluding remark, the emission of photons with energy greater than 2 MeV in the extracted fuel salt (green line in Figure 1.18) is relatively high. Indeed, the results of the simulations show no significant reduction of the gamma and neutrons emission rates in the time range between one and ten days, their level remaining high even after several weeks or months of cooling time.

1.4.5 Radiotoxicity

Figure 1.20 shows the specific radiotoxicity generation of the MSFR at equilibrium composition, operated in nominal reprocessing conditions. The curves are normalized by the electricity production. The MSFR is operated in a closed fuel cycle in which the actinides produced are recycled in the fuel. In this context, the net production of radiotoxicity comes from the fission products, which are continuously extracted, and the reprocessing losses. It can be observed that the total radiotoxicy (black dashed line) is dominated in the first few hundreds years by the contribution of the fission products. In the time interval between one thousand and one million years, radiotoxicity is mainly due to the actinides losses at reprocessing. The reference level ($3.6 \cdot 10^6$ Sv/GW$_e$·y) depicted in the figure represents the radiotoxicity of the natural uranium (and its daughter elements in secular equilibrium) required to fuel a LWR operating in once-through fuel cycle (OECD-NEA, 2002). After the decay of most of the fission products (∼300 years), the radiotoxicity level falls well below the reference line. A comparison of long term radiotoxicity generation between different fast reactors operating with the Th-U closed fuel cycle can be found in (Fiorina *et al.*, 2013b).

The long term radiotoxicity generation of the MSFR is strongly dependent on the reprocessing losses assumed. A value of 0.1% is commonly adopted in fuel cycle studies for solid-fuelled reactors (Salvatores *et al.*, 2009). Despite past experiences and recent

Table 1.5: *Composition of the nickel-based alloy adopted in the SERPENT-2 simulations.*

	Ni	Cr	W	Al
$wt\%$	67.7	7	25	0.3

studies on fuel reprocessing for MSRs, presently, reliable data on the performance of the reprocessing system associated to the MSFR are not available. Consistently with an other work (Fiorina *et al.*, 2013b), the 0.1% value has been adopted for the reprocessing losses of the HM isotopes. It is worth nothing that, adopting suitable reprocessing schemes, the uranium can be extracted before performing the other reprocessing phases (Uhlíř, 2007). In this context, uranium losses might be lower than that assumed for transuranium elements. A simple sensitivity study on the effect of uranium losses has also been preformed. The gray dashed line shows the total radiotoxicity generated under the hypothesis that uranium losses can be lowered to 0.01% adopting a suitable reprocessing scheme.

1.5 Helium production and tungsten depletion in structural components

In this Section, helium production and tungsten transmutation are investigated in the prospect of the evaluation of irradiation induced damage in the MSFR primary salt container and core axial reflectors. These structural components are required to withstand severe conditions from different points of view (Delpech *et al.*, 2009a). The presence of a flowing molten fluoride mixture at high temperature, which constitutes a hard operating environment for most of the commonly adopted alloys, is combined to the presence of an intense neutron flux. A review of material issues with molten fluorides for nuclear applications can be found in (Delpech *et al.*, 2010). For the MSFR, a nickel-based alloy, with high content of chromium and tungsten has been selected as possible structural material candidate (Merle-Lucotte *et al.*, 2009). In the present work, the representative composition of Table 1.5 has been adopted.

The main mechanisms responsible of the helium production in nickel-based structural materials are three (Olander, 1976):

- (n, α) reactions on ^{10}B (boron impurities);
- (n, α) reactions on ^{58}Ni (present in the natural nickel composition);
- (n, α) reactions on ^{59}Ni (produced by neutron irradiation via radiative capture).

While the first reaction can be reduced through the adoption of high purity alloys, the second and third mechanisms are intrinsically related to the presence of nickel. Among these two reactions, the first one is dominant in the first period, because ^{58}Ni is the most abundant isotope of nickel ($\sim$68%) while ^{59}Ni is not present in nature. As ^{59}Ni is progressively produced by neutron capture on ^{58}Ni, the last mechanism of helium production becomes dominant due to the different nuclear reaction cross-sections. (n, α) reactions on ^{58}Ni is a threshold phenomenon that occurs with a low probability only with high energy neutrons. On the other hand, (n, α) reactions on ^{59}Ni occurs for neutron of any energy and presents a much larger cross-sections (see Figure 1.21). The combination of the three above mentioned mechanisms leads to a significant helium production rate in the material zones close to the reactor core.

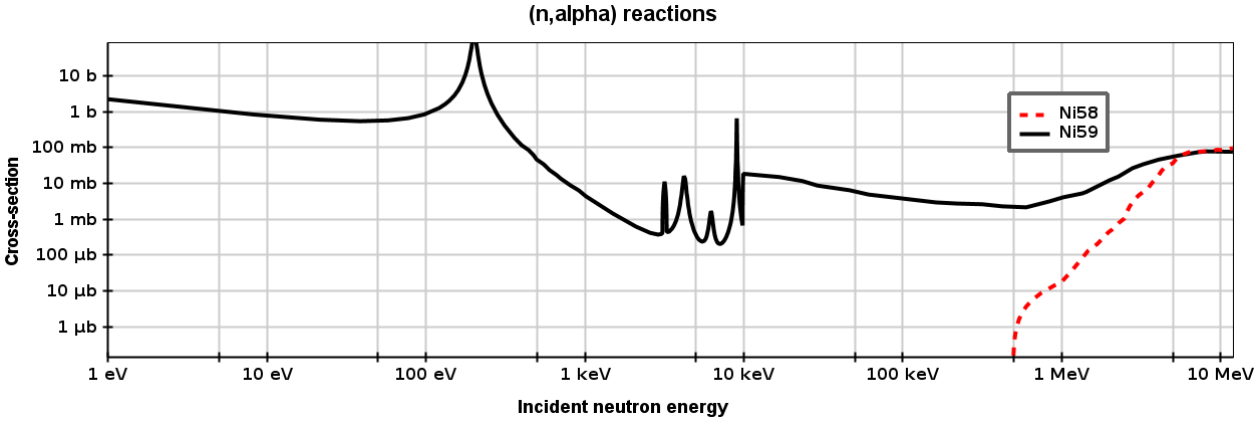

Figure 1.21: (n, α) *reaction cross-section for* ^{58}Ni *and* ^{59}Ni *(JEFF-3.1).*

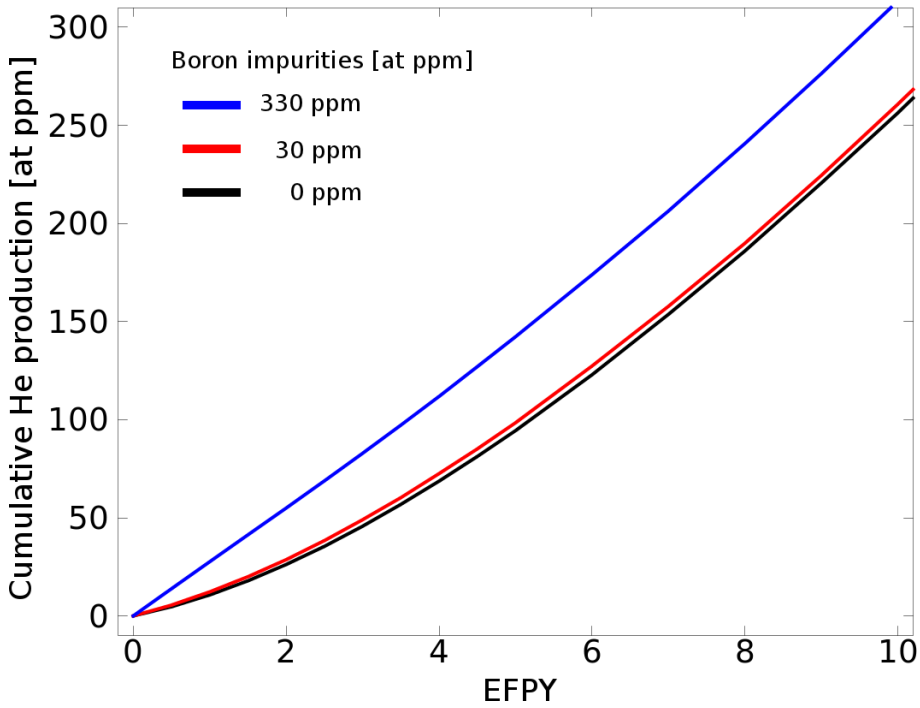

Figure 1.22: *Cumulative helium production in the primary salt container material at core mid-line.*

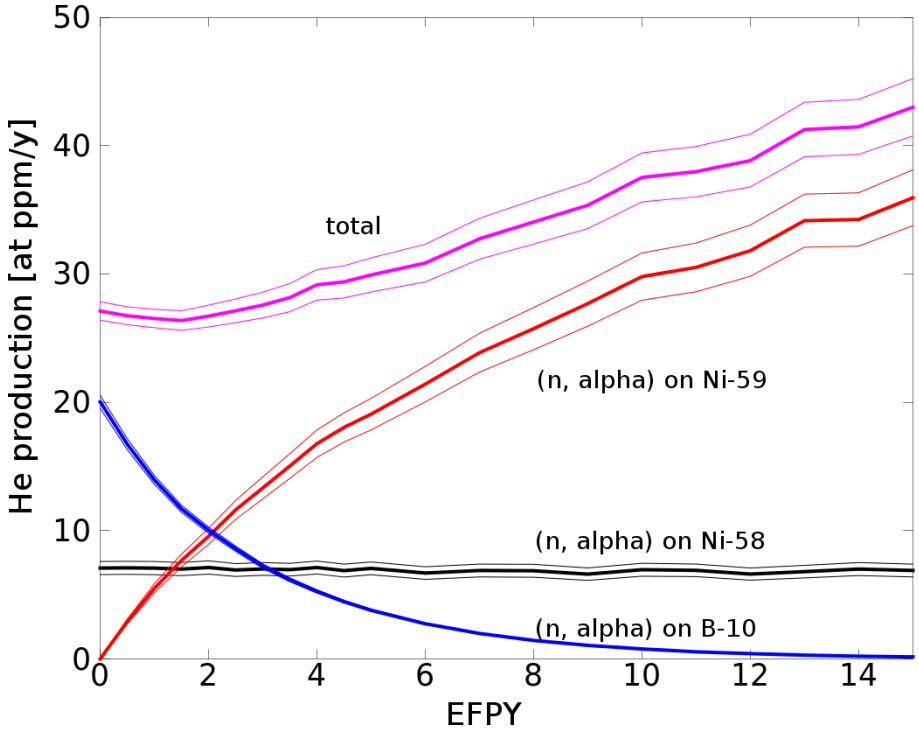

Figure 1.23: *Helium production rate in the primary salt container material at core mid-line.*

Helium bubbles formation at grain boundary is responsible of embrittlement of Ni-based alloys, which acts in combination with other radiation-induced phenomena. In general, the prediction of the mechanical properties worsening for a given set of alloy parameters (i.e. composition, irradiation temperature and neutron spectrum) is difficult and experimental tests are required (Angeliu *et al.*, 2007). The largest acceptable limit of cumulative helium production in the MSFR alloy has not been determined. A tentative value of 100 ppm has been proposed in previous works available in literature (Delpech *et al.*, 2009a; Merle-Lucotte *et al.*, 2009).

Here, results achieved by means of isotopic evolution simulations adopting the SERPENT-2 code are presented, both for the primary salt container and the axial reflectors. Figure 1.22 shows the cumulative helium production in the primary salt container, averaged in the whole nominal thickness (2 cm), at core mid-line. The different lines are relative to simulations with different content of boron impurities. The blue line represents a simulation with a boron impurity content of 330 at. ppm. In the case of the primary salt container, the limit of 100 at. ppm of helium in the alloy is reached in about 3 years. Even in the simulations with low or zero content of boron impurities (red and black lines), very high cumulative helium production is reached quickly. Figure 1.23 shows the contribution of the three phenomena to the helium production rate. The contribution of (n, α) reactions on boron is dominant in the first months, then rapidly decreases as the ^{10}B is consumed. On the other hand, the contribution of (n, α) reactions on ^{59}Ni grows as ^{59}Ni is progressively produced from ^{58}Ni, and it becomes dominant after few years. Hence, neglecting the contribution of ^{59}Ni, as sometimes assumed in fast reactors calculations and in works related to MSFR (e.g., Delpech *et al.*, 2009a; Merle-Lucotte *et al.*, 2009), may lead to sizeable underestimation of helium production.

Table 1.6: *Cumulative helium production [at. ppm] in the axial reflector for increasing distance from the core reference line (see Figure 1.1).*

Time [years]	Distance from the core reference line [cm]					
	0-2	2-4	4-8	8-16	16-32	32-64
2	16.6	9.74	5.12	1.49	0.16	-
5	57.6	34.6	18.5	5.52	0.63	0.02
10	151	91.5	51.1	15.8	1.89	0.06
20	400	241	138	45.3	5.92	0.19
50	1441	886	519	178	27.2	1.01

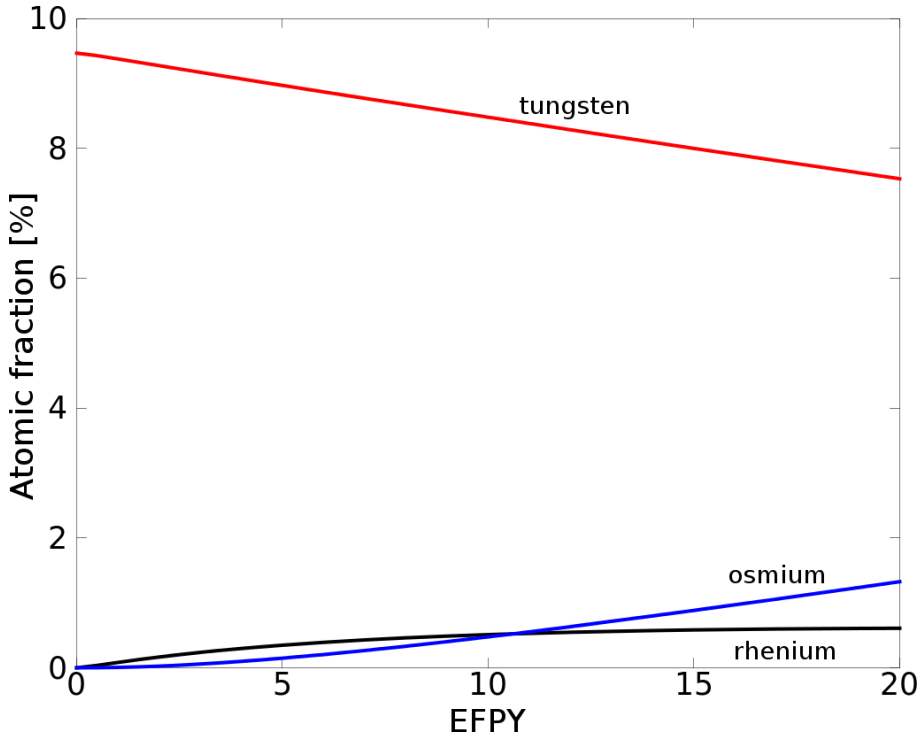

Figure 1.24: *Atomic fraction of tungsten, rhenium and osmium in the primary salt container material, as funcion of the time.*

Simulations have been performed also for the axial reflectors. Table 1.6 shows the average cumulative production of helium for different distances from the core. As expected, the helium production is progressively lower far from the core. Nonetheless, the necessity of replacement of the first 15 to 20 cm of the reflector during the reactor operation, pointed out in previous works (Merle-Lucotte *et al.*, 2009), is confirmed.

Figure 1.24 shows the atomic fraction of tungsten, rhenium and osmium in the primary salt container material near core mid-plane. Tungsten isotopes present relatively high neutron capture cross-sections and are progressively transmuted in rhenium and, successively, in osmium. The depletion in tungsten content might lead to a worsening of the nickel-based alloy mechanical performance. Table 1.7 shows the average tungsten depletion in at. % in the axial reflector at different coordinates. No clear indication exists on the maximum allowable tungsten transmutation limit. 1 at. % limit is suggested by Merle-Lucotte *et al.* (2009). According to the simulations performed, the limit is reached during the life of the reactor (∼60 years) both in the primary salt container and in the

Table 1.7: *Tungsten depletion [at. %] in the axial reflector for increasing distance from the core reference line (see Figure 1.1).*

Time [years]	Distance from the core reference line [cm]					
	0-2	2-4	4-8	8-16	16-32	32-64
2	0.14	0.12	0.08	0.04	0.01	-
5	0.37	0.30	0.21	0.10	0.03	0.01
10	0.74	0.59	0.42	0.20	0.07	0.01
20	1.43	1.14	0.81	0.39	0.13	0.02
50	3.37	2.72	1.92	0.93	0.31	0.06

inner layers of the reflector.

The above analyses highlight that the irradiation-induced damage of structural components is a critical issue of the MSFR technology.

1.6 Concluding remarks

In this Chapter, the extension of the SERPENT-2 Monte Carlo code has been presented and adopted to investigate the isotopic evolution of the MSFR core materials. The extended version allows to fully take into account the presence of on-line reprocessing in fuel depletion calculations. It has been assessed against the ERANOS-based EQL3D procedure. The presented extension is featured by a reactivity control algorithm, able to keep the effective multiplication factor of the system close to one during the fuel evolution. This capability is adopted to calculate the yearly production of ^{233}U for selected scenarios. Simulations of the TRU-started option, with nominal reprocessing rates and the adoption of the JEFF-3.1 evaluated nuclear data library, show a production of ^{233}U up to 200 kg/year in the first 10 years, with a first doubling time of about 25 years. In the ^{233}U-started scenario, the first doubling time is approximately 40 years. The produced uranium reveals to be of a good isotopic quality, especially the one extracted from the blanket salt, with a ^{232}U content similar to that found in other thorium based fuel cycles.

Thanks to a specific iterative equilibrium search algorithm, the extension has been applied to study the steady-state composition and behaviour of the reactor, as function of the fuel reprocessing rates. The MSFR confirms to be a very flexible reactor, with a high conversion ratio at nominal fission product removal rate (about 1.1 at 40 liters per day) and the possibility to decrease the reprocessing rate as low as few liters per day, while keeping iso-breeder conditions. The study of the concentration of trivalent elements at equilibrium suggests a similar lower limit (few liters reprocessed per day) to avoid precipitation problems.

An investigation on parameters relevant for reprocessing operations of the fuel has been presented. Results show that the handling of salt extracted from the core can be problematic due to decay heat and emission of neutrons and high energy gammas. The specific decay heat of the fuel shows a marked dependency on the content of insoluble fission products and is lowered by a fast extraction rate (e.g., with gas bubbling). In the time scales relevant to on-line reprocessing (i.e., few days to few weeks or months), the contribution of FPs on the emission of high energy photons dominates that of actinides and their daughter isotopes. The contribution of ^{208}Tl (from the ^{232}U decay chain) to the gamma emissions above 1 MeV becomes dominant only after few years of cooling time.

The long term radiotoxicity generation has been calculated for the equilibrium state at nominal conditions. The assumption of 0.1% losses for all the actinides has been made, leading to a radiotoxicity below the reference level after the decay of most of the fission products ($\sim$300 years). However, a better assessment would require a precise knowledge of the actual reprocessing losses for each element (not yet available). In particular, the extraction of uranium from the salt is often considered as a first reprocessing step, that would reduce uranium losses compared to other actinides.

Helium production and tungsten depletion in nickel-based alloys have been previously identified in the literature as possible phenomena limiting the life of structural materials surrounding the core. In this Chapter, the contribution of the three main (n, α) reactions responsible of helium production has been investigated. The contribution of ^{59}Ni, not present in the natural isotopic composition of nickel and sometimes neglected in previous works, becomes dominant after few years. The evaluation of helium production and tungsten depletion in both the primary salt container and the axial reflectors confirms that irradiation induced damage of structural components is a relevant issue for the deployment of the MSFR technology. In particular, the accurate estimation of an acceptable limit for the cumulative helium production and further investigation about the mechanisms leading to helium embrittlement need to be addressed.

A sensitivity analysis on the cross-sections data libraries adopted has been performed to assess the impact of nuclear data uncertainty on the results. The comparison between results obtained with JEFF-3.1 and ENDF/B-VII shows noticeable differences in the predicted performance of the system (i.e., conversion ratio, doubling time and yearly production of ^{233}U). The main reason of this discrepancy appears to be the uncertainty on the ^{233}U capture cross-section. This leads to a difference up to a factor two in the fission-to-capture ratio between the two libraries, at energies typical of the MSFR spectrum.

A more accurate uncertainty analysis is required for this system, to improve the reliability of the breeding performance and reactor kinetic parameters estimations. In this direction, a research activity is presently ongoing towards the implementation of sensitivity capabilities in SERPENT (see Section A.3 in the Appendix).

More in general, accurate measurements of the ^{233}U capture cross-section in the 1 to 100 keV energy range should be carried out, especially, considering the growing interest of the scientific community on these systems in recent times.

Nomenclature

Latin symbols

$b_{j \to i}$	branching ration from nuclide j to nuclide i
c_i	atomic fraction of the isotope i in the feed vector
$FY_{k \to l}$	fission yield for the production of the fission product l from a fission of the heavy metal k
k_{eff}	effective multiplication factor
$k_{eff,tgt}$	target effective multiplication factor for the reactivity control algorithm
k_{inf}	infinite multiplication factor
N_i	atomic density of the generic isotope i [cm^{-3}]
r	radial coordinate [m]
r_{abs}	absorption rate [s^{-1}]
r_{capt}	capture rate [s^{-1}]
z	axial coordinate [m]

Greek symbols

ε	user-defined tolerance for the reactivity control algorithm
λ_i	decay constant of the generic nuclide i
$\lambda_{l,repro}$	effective removal constant for the reprocessing of the fission product l
ρ	reactivity
$\sigma_{j \to i}$	one-group transmutation cross-section from nuclide j to nuclide i
$\sigma_{k,f}$	one-group fission cross-section of the heavy metal nuclide k
ϕ	neutron flux [cm^{-2} s^{-1}]

Acronyms

ARR	Advanced Recycling Reactor
CR	Conversion Ratio
CRAM	Chebyshev Rational Approximation Method
EFPY	Effective Full Power Years
EVOL	Evaluation and Viability of Liquid Fuel Fast Reactor Systems
FP	Fission Product
HM	Heavy Metal
LWR	Light-Water Reactor
MSFR	Molten Salt Fast Reactor
MSR	Molten Salt Reactor
pcm	per cent mille
ppm	parts per million
PSI	Paul Scherrer Institut
RHS	Right-Hand Side
TRU	Transuranium isotopes

CHAPTER 2

Multiphysics modelling

In this Chapter, the development of a multiphysics model adopting the open-source C++ library OpenFOAM for the transient analysis of non-moderated Molten Salt Reactors is discussed. The model features the adoption of an implicit Runge-Kutta scheme and the coupling among neutron diffusion, Reynolds-Averaged Navier-Stokes equations for mass and momentum conservation, and energy and delayed neutron precursor balance equations, to accurately catch thermal feedbacks on neutronics. The development of the OpenFOAM solver, which started in the last months of 2011, follows previous works carried out at Politecnico di Milano on multiphysics modelling of MSRs, mainly based on the commercial software Comsol. The adoption of the OpenFOAM libraries allowed more flexibility in the choices of the coupling strategies and the time-integration schemes, which required most of the development efforts. The solver is designed to perform fast-running simulations of the full-core three-dimensional Molten Salt Fast Reactor geometry. It is thought to be useful in the onging phase of design optimization of fuel loop components within the EVOL Project. As example of the capability of the model, an unprotected MSFR single pump failure accidental scenario is simulated and discussed in this Chapter.

In the frame of a collaboration with INOPRO (Villard-de-Lans, France), the solver has been further developed and several analyses of the optimized 3D MSFR geometry have been performed. One of this transient simulations is presented in this Chapter as example of the capabilities of the model.

The main results presented here have been submitted for publication in: Manuele Aufiero, Antonio Cammi, Olivier Geoffroy, Mario Losa, Lelio Luzzi, Marco E. Ricotti, Hervé Rouch, "Development of an OpenFOAM model for the Molten Salt Fast Reactor transient analysis.", submitted to Chemical Engineering Science. The methods implemented have been presented at the 7^{th} OpenFOAM workshop in Darmstadt, Germany[1].

More recently, in the frame of a collaboration with the Paul Scherrer Institut (Switzerland), the extension of this multiphysics coupling approach to Discrete Ordinates and Monte Carlo neutron transport has been investigated. A description of these research activities can be found in the Appendix (Section A.4).

[1] see presentation at: **http://www.openfoamworkshop.org/2012/downloads/Workshop-Documents/Presentations-Talks/AufieroManuele/final_ManueleAufieroSlidesOFW7.pdf**

2.1 Introduction

TRADITIONALLY, nuclear reactor analysis is performed by coupling neutron kinetics and thermal-hydraulic codes (Avramova and Ivanov, 1997). These coupled codes techniques are often based on the "operator-splitting" approach, in which the time-dependent solution is reached using the output from one code (e.g., the neutron kinetics code) as input to another code (e.g., the thermal-hydraulic code) at each time step. Often, the nonlinearities due to the coupling are not resolved in the time step, possibly reducing the overall accuracy (Ragusa and Mahadevan, 2009; Mahadevan *et al.*, 2012).

In MSRs, the presence of a strong coupling between the different phenomena calls for the adoption of suitable modelling approaches, while performing reactor analysis. In the reference (Cammi *et al.*, 2011a), a detailed description and comparison of recent works related to MSR multiphysics modelling can be found. More recently, at Politecnico di Milano, a coupled model for the Molten Salt Fast Reactor (MSFR) has been developed adopting the mutiphysics code COMSOL. The COMSOL model has been compared to an in-house code developed at Delft University of Technology, showing a good agreement for several transient case studies (Fiorina *et al.*, 2014).

Both models (COMSOL and TUDelft) rely on multi-group diffusion for the neutronics and involve a simplified, two-dimensional (2D) axial-symmetric representation of the MSFR. This approximation is considered to be appropriate for the purpose of preliminary transient analyses. Nonetheless, there are several situations in which a full-core three-dimensional (3D) representation of the primary circuit is desirable. Namely, asymmetric transients (e.g., single pump failure) can not be properly simulated with 2D simulations. Moreover, recent studies performed by INOPRO in the framework of the EVOL Project (Deliverable EVOL D2.2, 2013) highlighted the fact that in some of the expected operating conditions of the MSFR, the 2D axial-symmetric approximation of the turbulent flow might lead to a prediction of the flow structures with significant differences with respect to results obtained from accurate 3D simulations of the reactor core. These differences in the turbulent viscosity and velocity fields have major impact on the fuel temperature distribution in the core, which is a key parameter for the reactor analysis in both nominal and accidental conditions.

In this Chapter, the development and assessment of a multiphysics model dedicated to the transient analysis of the Molten Salt Fast Reactor is discussed. More in general, the proposed tool is aimed at studying the dynamic behaviour of non-moderated MSRs. Its distinguishing feature, with respect to previous works available in literature (e.g., see Fiorina *et al.*, 2014), is the capability to deal with full-core 3D analysis, while allowing an accurate description of the in-core turbulent fuel flow and limiting the demand for computational resources. For this purpose, a specific modelling approach has been developed, adopting the multiphysics toolkit OpenFOAM (Weller *et al.*, 1998). The work is focused on the implementation of accurate and consistent time-integration and coupling techniques, and the adoption of strategies for the reduction of computational requirements. The main purpose of the proposed model is to serve as fast-running computational tool in the phase of design optimization of fuel loop components. More in general, the present tool is of valuable help to investigate the peculiarities of the reactor physics of circulating-fuel systems, especially in presence of strong thermal feedbacks on neutronics. Detailed safety analysis is not dealt with in the present Chapter and would require

layout specifications of the core and fuel circuit components, which are not available in the present phase of the EVOL Project.

In order to reduce the computational requirements, the one-speed neutron diffusion approximation has been preferred along with the adoption of suitable albedo boundary conditions, which limit the computational domain to the fuel circuit only. In Chapter 3, where a more detailed neutronic analysis is required, the OpenFOAM model is extended to a multi-group approach. In Appendix, the extension of this work to neutron transport is investigated as well (Section A.4).

The suitability of neutronic approximations has been verified through a comparison of the shape of the scalar flux between the OpenFOAM model and Monte Carlo simulations, whereas the time-dependent response of the model to a super-prompt-critical reactivity insertion has been compared to results from the aforementioned COMSOL and TUDelft models.

The Chapter is organized as follows. In Section 2.2, the adopted methodology is discussed. In Section 2.3, the assessment of the developed model against other tools is presented, along with results from a pump failure simulation. A few concluding remarks are drawn in Section 2.4. The main equations implemented in the multiphysics model are summarized at the end of the Chapter.

A brief description of the Molten Salt Fast Reactor (MSFR) was given in the Introduction of the thesis and details about the MSFR concept can be found in the references (Merle-Lucotte *et al.*, 2009, 2011; Brovchenko *et al.*, 2012). In the following, the geometry adopted in the simulations of this Chapter is briefly discussed.

The preliminary choice of a square-cylindrical shape for the MSFR comes primarily from the neutron economy point of view (Merle-Lucotte *et al.*, 2009, 2011). In nominal flow-rate conditions, large recirculation vortices appear near the core wall when this shape is considered, which might lead to excessive structural material temperatures. For this reason, a core shape optimization process is ongoing within the EVOL Project (Rouch, 2013; Rouch *et al.*, 2014), aimed at the elimination of high-temperature zones. This issue and the strong influence of the CFD modelling on the prediction of the MSFR behaviour (Losa, 2013) calls for the adoption of realistic three-dimensional geometries, while performing multiphysics transient or steady-state reactor analysis. In this work, the "toroidal-shaped" geometry proposed by INOPRO in the EVOL Project has been adopted (Deliverable EVOL D2.2, 2013; Rouch, 2013; Rouch *et al.*, 2014). In Figure 2.1, a spatial finite-volume mesh adopted for the modelling of one quarter of the MSFR is shown. The "toroidal" reshaping of the radial fuel salt container to avoid recirculation is clearly visible, along with four external loops.

2.2 Modelling approach

In this Section, the methodologies adopted in the development of the proposed model are described and discussed.

2.2.1 Fluid-dynamics and heat transfer modelling

The model of the fluid flow (molten salt mixture) is based on the Reynolds-Averaged Navier-Stokes (RANS) equations for mass and momentum conservations. In the present work, the standard and the *realizable* k-epsilon turbulence models for incompressible

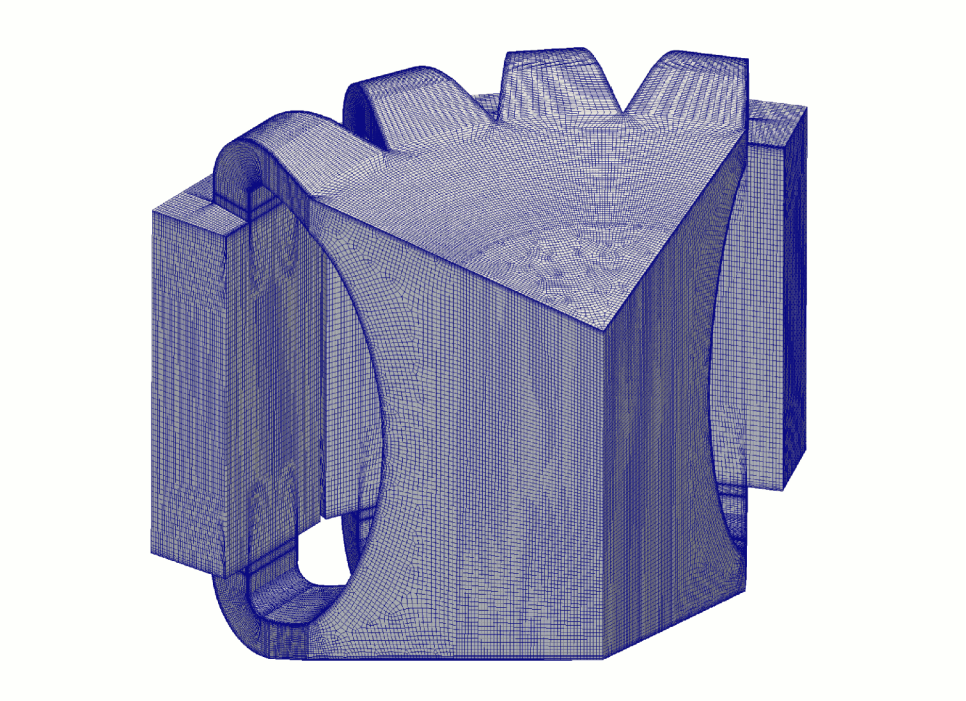

Figure 2.1: *Spatial mesh adopted for the modelling of the MSFR fuel circuit.*

Table 2.1: *Fuel salt thermophysical properties adopted in the present work (Deliverable EVOL D2.2, 2013).*

Density	4125 $kg \cdot m^{-3}$
Kinematic viscosity	$2.46 \cdot 10^{-6}$ $m^2 s^{-1}$
Thermal Conductivity	1.01 $W \cdot m^{-1} K^{-1}$
Coefficient of thermal expansion	$2.14 \cdot 10^{-4}$ K^{-1}

flows have been adopted, along with the standard wall function treatment. The buoyancy effects have been taken into account through the Boussinesq approximation.

The classical energy balance equation is solved for the calculation of the in-core temperature distribution. Turbulent heat diffusivity is considered and modelled from the turbulent viscosity, adopting an effective uniform value of the turbulent Prandtl number equal to 0.85 in the whole domain. The thermophysical properties of the molten salt mixture are considered constant and are relative to a fluid temperature of 700 °C. The main thermophysical quantities adopted are summarized in Table 2.1.

In order to reduce the computational efforts, the heat transfer in structural materials and in the blanket has been neglected, thus, thermal insulation has been applied to the boundaries of the fuel circuit.

At present, the design specifications of the MSFR fuel circuit components (e.g., primary pumps and heat exchangers) are not fully defined. Within the EVOL Project there is an ongoing research activity aimed at the definition of the most suitable options. In order to allow for the simulation of a wide range of accidental scenarios, a simplified description of the pumps and the heat exchangers has been introduced in the multiphysics model. The pumps have been simulated through a momentum source in the 16 out-of-core circuits. In order to accurately take into account possible blockage of one or more pumps,

Table 2.2: *Main specifications of the corrugated plate-type heat exchanger adopted in the present work.*

Arrangement	countercurrent flow
Plate thickness	2 mm
Channel width (fuel salt)	3 mm
Channel height	50 cm
Corrugation pattern angle	30°C

the momentum sources have a dependency on the flow rate in each branch. In case of pump blockage, this acts as additional head loss in the circuit. Lacking any detailed information about the pump characteristic, it as been assumed that the pressure loss due to a broken pump is proportional to the power of 2 of the flow rate and reaches a value of 1.5 bar at nominal flow rate. This approach, although very simplified, allows to captures the main dynamics of the system in case of malfunctioning of the fuel circuit components. Moreover, it is consistent with previous works (Fiorina *et al.*, 2014) and therefore allows for accurate comparisons with other models.

Due to the limited operating pressure of both the fuel circuit and the intermediate salt circuit, plate-type heat exchangers (HEX) are envisaged as possible option due to their compactness and simplicity. Following this option, the heat exchanger specifications (e.g., plate thickness, channel dimensions, etc.) have been preliminary optimized by INOPRO within the EVOL Project, and are reported in Table 2.2. The optimization process has followed the criteria of a compromise aimed at the minimization of both the primary salt volume in the exchanger and the head losses. It resulted in a total fuel salt volume in the 16 heat exchangers of 6.8 m^3. Similarly to what has been performed for the pumps, the HEX modelling has been introduced as 16 distributed sources of momentum and heat sinks. The pressure losses in the heat exchangers have been estimated for several flow rates through suitable correlations, also accounting for the changes in the flow regime. In a similar way, the heat exchange coefficient has been calculated for different operating conditions of both the fuel and the intermediate circuit. For the sake of simplicity, the dependency of the head losses and the heat exchange on the flow conditions has been introduced in the multiphysics model as a polynomial interpolation of the calculated points, between 5% and 100% of the nominal flow. In Figure 2.2, the calculated curves for the head losses and the heat exchange coefficient are depicted.

2.2.2 Neutronics modelling

The one-speed neutron diffusion approximation (Duderstadt and Hamilton, 1976) is adopted for the modelling of the reactor neutronics. In order to further reduce the computational burden of the simulations, the albedo boundary conditions have been adopted both in the upper and lower limit of the core (axial reflectors) and in the radial wall (blanket salt). In this way, the solution of the neutron diffusion equation is limited to the fuel salt circuit, thus reducing the computational requirement of the calculations. The group constants adopted in the model have been calculated by means of the Monte Carlo code SERPENT (SERPENT, 2011), adopting the JEFF-3.1 evaluated nuclear data library (Koning *et al.*, 2006) and the fuel composition relative to the ^{233}U-started MSFR option (see Chapter 1). In order to take into account the thermal feedback on neutronics, a dependency of the cross sections on the fuel temperature and density has been introduced in the model. In particular, the Doppler effect is described through a logaritmic dependence of the

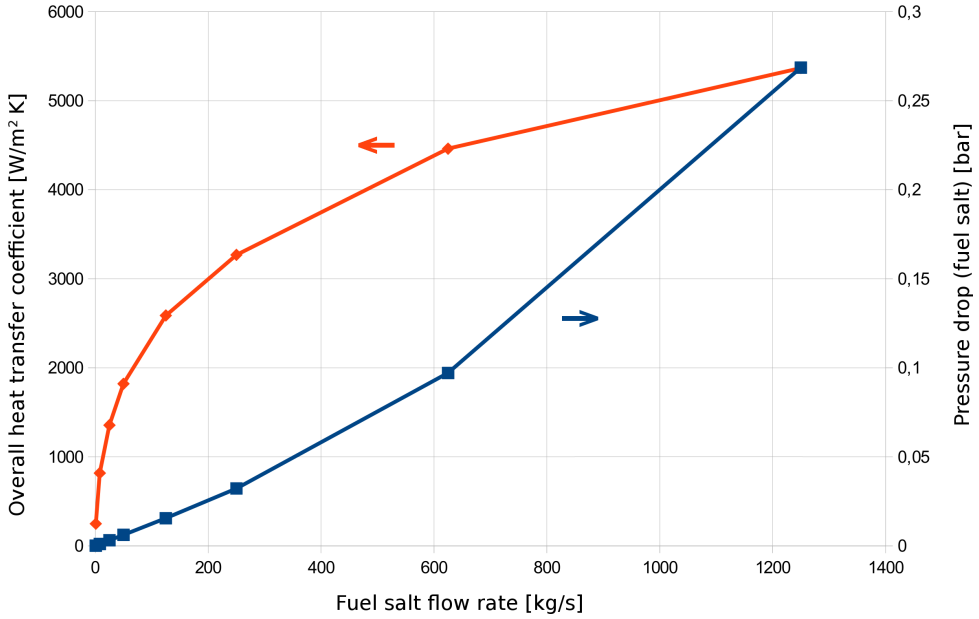

Figure 2.2: *Head loss and heat exchange coefficient in the heat exchanger as function of the primary salt flow rate (intermediate salt at nominal flow rate).*

fuel capture and fission cross sections, which has been calculated interpolating several Monte Carlo runs at different fuel temperatures. As mentioned in Section 2.2.1, the fluid flow in the fuel circuit is described adopting the incompressible Navier-Stokes equations. Nonetheless, in order to fully capture the effect of fuel thermal expansion on neutronics, a temperature-dependent effective fuel density is considered when solving the neutron diffusion equation. In particular, a linear dependency on the salt density has been introduced for the the cross sections and the diffusion coefficient.

This simple and computationally lightweight neutronics model showed able to accurately describe the space and time dependence of the neutron fluxes in the MSFR. In Figure 2.3, the neutron flux is shown as function of the axial and radial coordinates, as predicted by the OpenFOAM model and by the Monte Carlo code SERPENT. Note that the SERPENT estimates extend also in the blanket salt and in the axial reflectors, whereas the OpenFOAM calculations are limited to the fuel salt in the core. The two curves are in a good agreement (with maximum relative errors in the order of few percent) and the small discrepancies can be considered acceptable for the purpose of the present work.

The drift of delayed neutron precursors plays an important role in reactor dynamics of molten salt reactors. In the present model, the balance equations for eight groups of precursors are adopted. The decay constants of the delayed neutron precursors are taken from the JEFF-3.1 library (Koning *et al.*, 2006). Due to the adoption of the one-group approximation, the effective (adjoint weighted) delayed neutron fractions ($\beta_{eff,i}$) were considered, instead of the physical delayed neutron fractions ($\beta_{0,i}$). This allowed to take into account the different effectiveness of delayed and prompt neutrons, due to emission spectra, under the assumption that energy and spatial effects can be separated. This simplifying approximation has proved to be accurate in the case of the MSFR, and is further discussed in Chapter 3. The $\beta_{eff,i}$ values have been calculated by means of SERPENT and are shown in Table 2.3, along with the respective decay constants (λ_i)

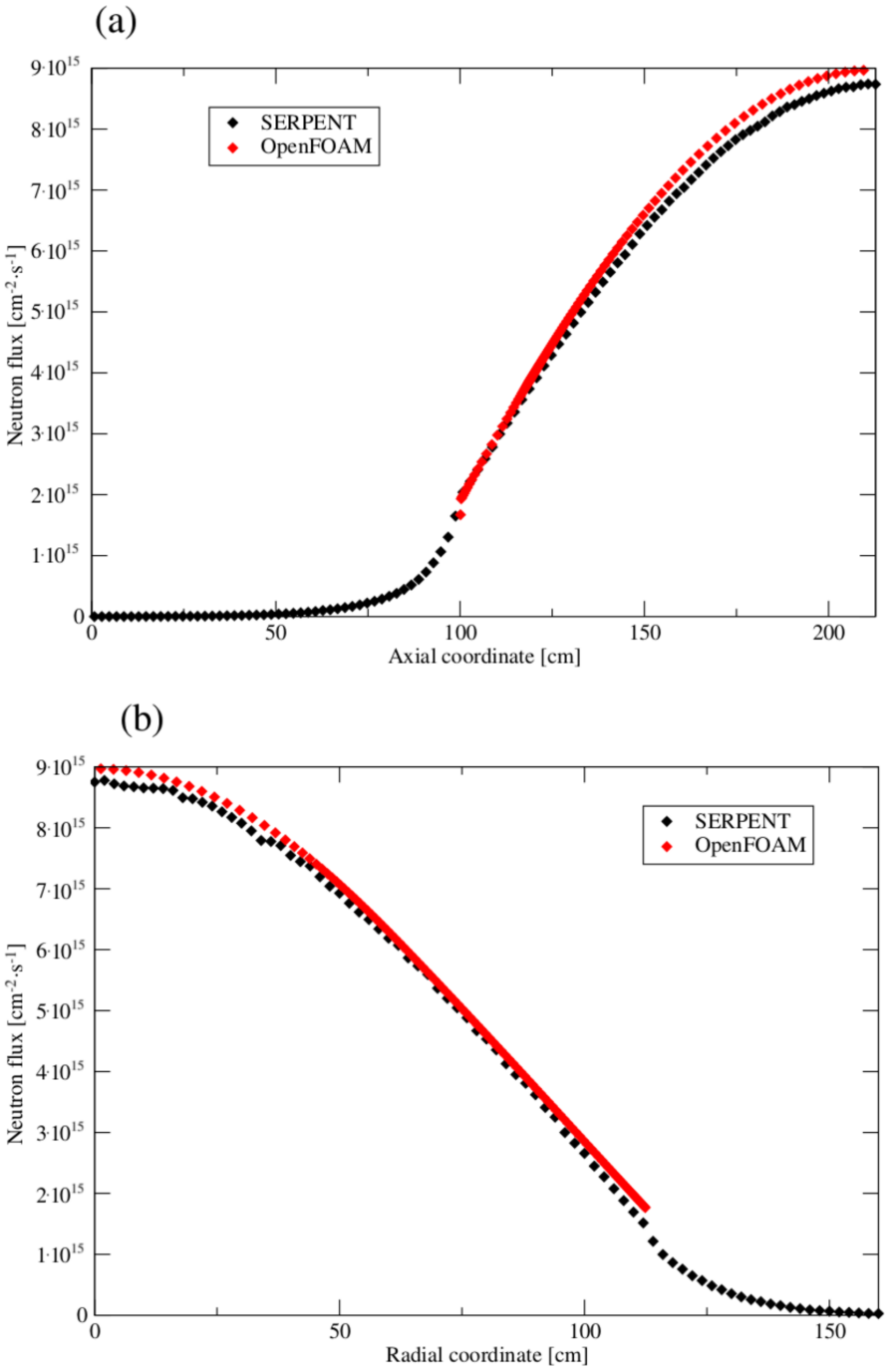

Figure 2.3: *Neutron flux as function of the axial (a) and radial (b) coordinates, as predicted by the OpenFOAM model and by the Monte Carlo code SERPENT.*

Table 2.3: *Effective delayed neutron fractions and decay constants.*

Group	$\beta_{eff,i}$ [pcm]	λ_i [s^{-1}]
1	21.8	$1.25 \cdot 10^{-2}$
2	47.6	$2.83 \cdot 10^{-2}$
3	39.3	$4.25 \cdot 10^{-2}$
4	63.5	$1.33 \cdot 10^{-1}$
5	103.5	$2.92 \cdot 10^{-1}$
6	18.1	$6.66 \cdot 10^{-1}$
7	22.8	1.63
8	5.2	3.55

adopted in the present work.

Also, the modelling of the decay heat is introduced by means of the superposition of three exponentially decaying terms. These therms are obtained by a curve fitting on the output of a SERPENT burn-up simulations, also allowing for on-line fuel reprocessing and bubbling extraction of gaseous fission products, adopting the extended code version presented in Chapter 1. In Figure 2.4, the decay heat curve for the ^{233}U-started MSFR after long operation at nominal power is shown for the first five minutes. The decay heat is expressed as fraction of the nominal power. The black dots represent SERPENT results. The red line represents the exponential interpolation adopted for the simulations presented in this Chapter. The blue dots show the modulus of the relative interpolation error. The choice of three terms represents a compromise between the accuracy in the description of the decay heat curve and computational requirements. This approximation can be judged appropriate for transient simulations that are limited to a time scale of several minutes. Both decay heat and delayed neutron precursors are transported by the fluid flow. In Chapter 3, it will be pointed out that the turbulent diffusion of delayed neutron precursors might have a non-negligible effect on the effective delayed neutron fraction and thus on reactor kinetics. For this reason, in addition to the convective term, turbulent diffusion is also considered for these quantities, adopting a turbulent Schmidt number of 0.85.

2.2.3 Time integration scheme and multiphysics coupling technique

In general, the coupled neutronics/thermal-hydraulics problem involves the solution of particularly stiff equations and is featured by the presence of fast time scale modes, hence the choice of an implicit time integration scheme appears mandatory. This is particularly true in the case of the Molten Salt Fast Reactor, in which the average prompt neutron lifetime is in the order of 1 μs. Moreover, the possibility of adopting accurate higher order integration techniques might be useful in many relevant situations. For these reasons, the adoption of implicit Runge–Kutta methods has been preferred in this work. In particular, a 6 stages, 4^{th} order explicit, singly diagonally implicit Runge-Kutta (ESDIRK) scheme from Kennedy and Carpenter (2003) was adopted. This scheme also features an embedded 3^{rd} order error estimator, which might be used for evaluating the time integration accuracy, in view of adaptive time-stepping. In Table 2.4, the Butcher table of the adopted scheme is reported.

The conventional operator-splitting technique adopted in reactor analysis involves the sequential solution of the different physics, once per time step. While this technique might offer several practical advantages, it is "nonlinearly inconsistent" in the coupling (Ragusa

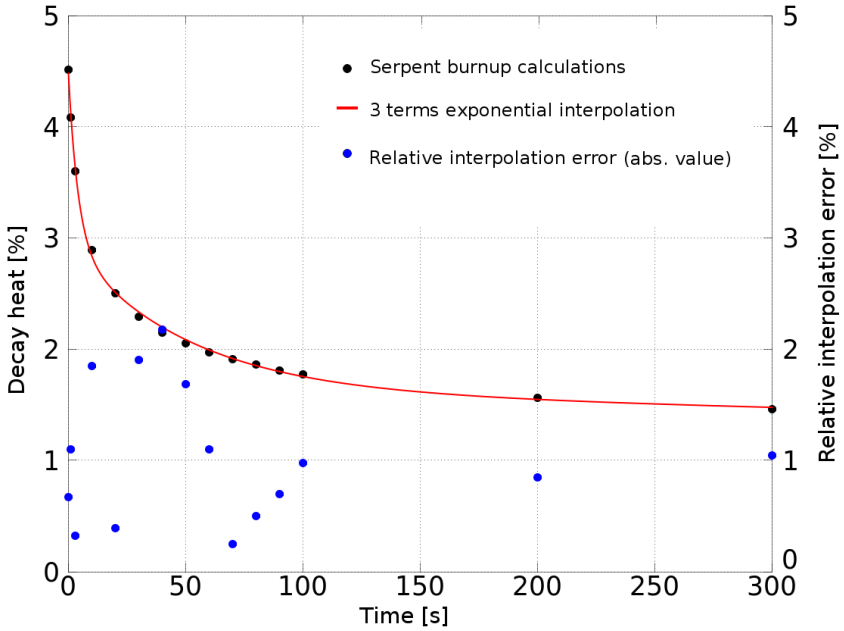

Figure 2.4: *Decay heat as function of time. ^{233}U-started MSFR after long operation. SERPENT burn-up calculations and 3 terms exponential interpolation.*

Table 2.4: *Butcher table of the adopted explicit, singly diagonally implicit Runge-Kutta integrator Kennedy and Carpenter (2003), with embedded error estimator.*

c_i	a_{ij}					
0	0					
$\frac{1}{2}$	$\frac{1}{4}$	$\frac{1}{4}$				
$\frac{83}{250}$	$\frac{8611}{62500}$	$\frac{-1743}{31250}$	$\frac{1}{4}$			
$\frac{31}{50}$	$\frac{5012029}{34652500}$	$\frac{-654441}{2922500}$	$\frac{174375}{388108}$	$\frac{1}{4}$		
$\frac{17}{20}$	$\frac{15267082809}{155376265600}$	$\frac{-71443401}{120774400}$	$\frac{730878875}{902184768}$	$\frac{2285395}{8070912}$	$\frac{1}{4}$	
1	$\frac{82889}{524892}$	0	$\frac{15625}{83664}$	$\frac{69875}{102672}$	$\frac{-2260}{8211}$	$\frac{1}{4}$
b_i	$\frac{82889}{524892}$	0	$\frac{15625}{83664}$	$\frac{69875}{102672}$	$\frac{-2260}{8211}$	$\frac{1}{4}$
b_i^*	$\frac{4586570599}{29645900160}$	0	$\frac{178811875}{945068544}$	$\frac{814220225}{1159782912}$	$\frac{-3700637}{11593932}$	$\frac{61727}{225920}$

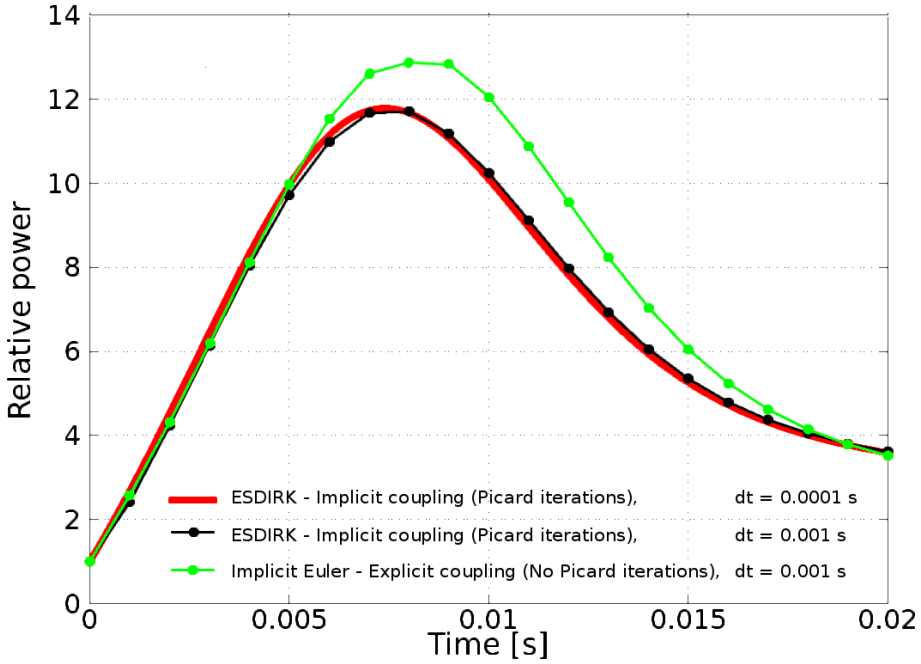

Figure 2.5: *150 pcm reactivity insertion. Comparison between implicit and explicit coupling strategies.*

and Mahadevan, 2009) and might lead to inaccurate results in case of strong feedback between the physics, as in the case of the present work.

Among the various techniques available to fully solve the non-linearities due to the coupling of the different phenomena, the adoption of Picard iterations has been preferred for the simplicity of implementation and verification. At each implicit stage of the ESDIRK scheme, all the equations are iteratively solved and the coupling terms are updated at each sweep, until the residuals of any physics drop below a user-defined tolerance. After the solution of the last stage, both a 3^{rd} order and 4^{th} order estimates of the solution for all the variables are available, whose comparison might be adopted as error estimate. While this method might be outperformed by more efficient techniques, it offers the possibility to adopt optimized linear solvers for each physics and allows for a simpler verification of both the single-physics and the whole code implementation. This was considered of primary importance, also because of the little availability of both well assessed multiphysics solvers for MSRs and experimental data on fast system, similar to the MSFR.

In Figure 2.5, the reactor power after a reactivity insertion of 150 pcm (about one \$) from nominal, steady state conditions is shown. This transient involves a rapid power rise and a fast increase of temperature, which promptly induces negative neutronics feedbacks and reduces the power. The red line shows the results from a simulation with a constant time step of $1 \cdot 10^{-4}$ s, adopting the time integration scheme described above (reference solution). The black dots were obtained adopting the same scheme and a time step of $1 \cdot 10^{-3}$ s. It can be appreciated that both the power rise and the action of the negative reactivity feedbacks are accurately resolved. The green dots show results obtained with the operator-splitting approach, commonly adopted in nuclear reactor analysis: each physics is solved sequentially and the coupling terms are updated once per time step. Thanks to the implicit nature of the single-physics time integrators adopted, and despite the stiffness

of the neutronics, even this coupling scheme is able to accurately describe the steep power increase. Nonetheless, when the dynamics of the system becomes dominated by the couplings between the physics (temperature feedbacks), the operator-splitting approach fails to accurately describe the transient evolution.

Different strategies have been tested, in order to reduce the computation time of the coupled solver. The adoption of the classical Aitken acceleration technique gave limited improvements, with a minor reduction of the total number of Picard iterations required to reach tolerances of practical interest for the purpose of the present analyses. On the other hand, the adoption of an accurate guess for the initial value of the unknown variables significantly improved the performance of the solver. In particular, the explicit Runge-Kutta scheme (ERK) associated to the adopted ESDIRK (Kennedy and Carpenter, 2003) has been employed at each implicit stage to estimate a first guess for the iterations sweep. This provided an efficient way to make use of the available information from the previous stages, with a minimal computational cost.

The 3D modelling of the fluid flow in the MSFR proved to require fine spatial meshes in order to correctly catch the reactor behaviour (few millions of cells for the full-core model). In this conditions, the solution for the variables related to the fluid flow (e.g., velocity, pressure, turbulent kinetic energy, etc.) requires a large amount of computational time. Considering also that in some of the transients of interest the time steps might be initially limited to few tens of μs, fully embedding the RANS equations in the integration scheme described above was considered too computationally expensive. For this reason, the solution for the fluid flow inside the reactor core has been obtained adopting the transient SIMPLE algorithm (Versteeg, 1995), once per time step. The convective terms for the energy and precursors balance equations are kept constant during the time step. Several considerations were made in favour to the adoption of this simplification. In particular, it should be taken into account that in the fast transient, in which the coupling between the physics needs to be more accurately resolved (i.e., reactivity insertions close to or above prompt-criticality), the reactor response is dominated by the evolution of neutron fluxes, fuel temperature and delayed neutron precursors concentration. As a clarifying example, in the 200 pcm reactivity insertion presented as test case in Section 3.3, the reactor power reaches 150 times the nominal value, and is then reduced by a factor of ten by the strong reactivity feedbacks in about 0.01 s. In this time period, the fluid flow structures barely changed.

The general structure of the adopted coupling scheme is sketched in Figure 2.6.

2.2.4 Initial steady-state conditions and parallel computing

In order to find the nominal steady-state conditions, the coupled neutronic-thermal hydraulic eigenvalue problem is solved iteratively adopting the standard power iteration method. In this way, it is possible to find the effective multiplication factor (k_{eff}) that brings the system to criticality by taking into account the spatial dependence in the core of both the fuel temperature field and delayed neutron source distribution.

OpenFOAM offers the embedded capability to run applications in parallel thanks to the domain decomposition method. Figure 2.7 shows an example of computational domain splitting: the fuel circuit is subdivided in different zones, and each one is assigned to a different processor core. The decomposition is performed automatically in pre-processing, trying to minimize communication and imbalance between processors. In this way, the

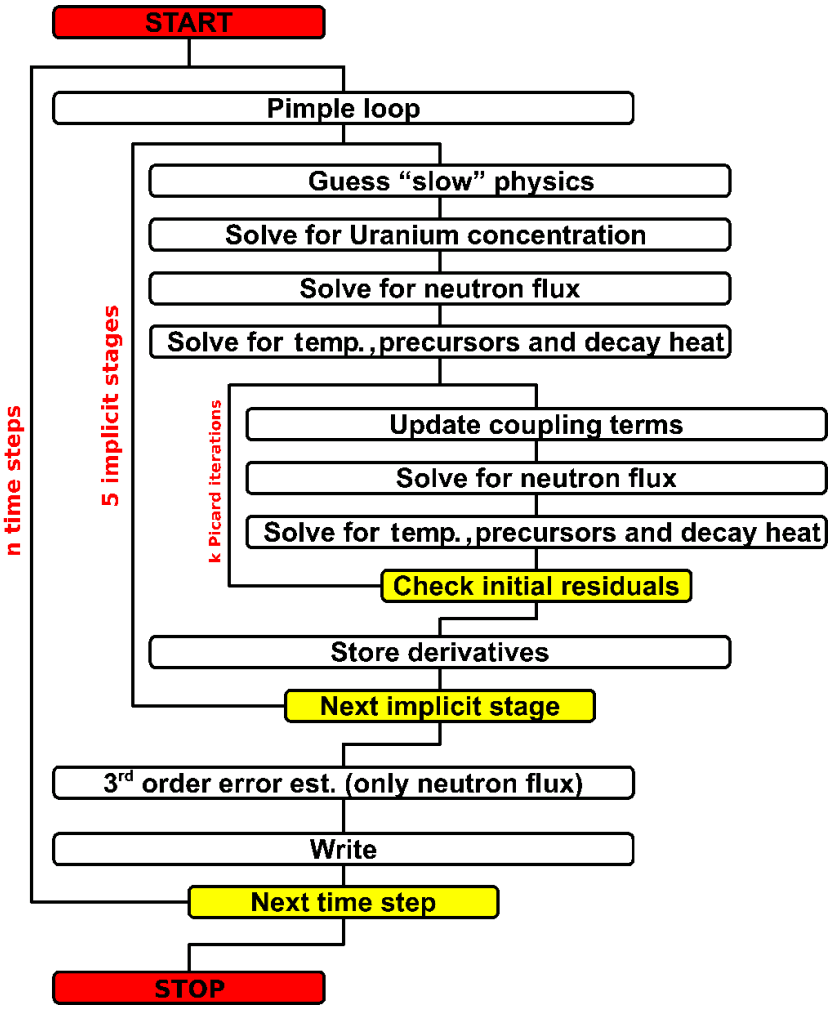

Figure 2.6: *Coupling and time integration scheme.*

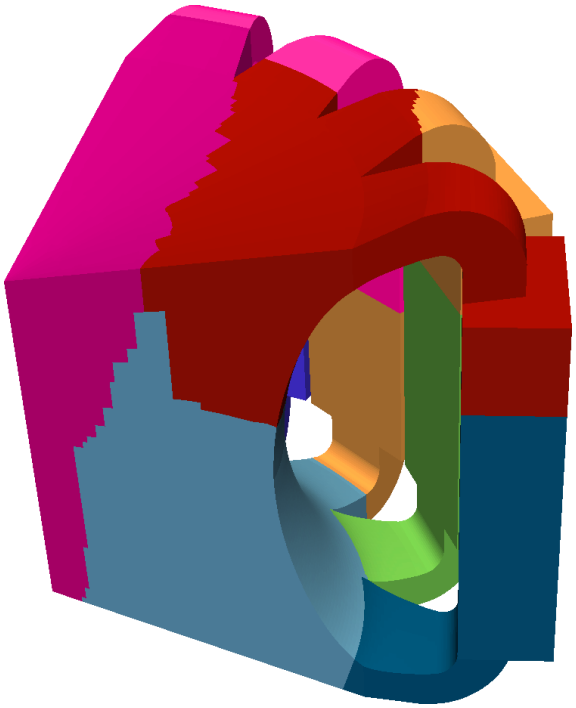

Figure 2.7: *Example of decomposed domain for parallel computing. Each zone is assigned to a different processor core.*

multiphysics solver can efficiently run in parallel. Although a systematic scalability study has not been preformed yet, the solver showed a good behaviour in all the parallel run tests.

In Section 2.3.1, results from a super prompt-critical reactivity insertion transient are shown. The 10 seconds simulation refers to a simple 2D geometry, with about $2 \cdot 10^5$ cells. In order to give an idea of the typical running time for simple case studies, the simulation was run on a machine with an Intel®Xeon™ E5440 CPU with 8 cores and a clock speed of 2.83 GHz and was completed in approximately 1 hour. For the sake of comparison, the COMSOL model with a similar number of degrees of freedom took approximately 22 hours to run the transient on the same machine[2].

2.3 Numerical results

2.3.1 Assessment against COMSOL and TUDelft models

The capability of the developed model has been assessed through a comparison with other multiphysics tools. Because no results are available in the open literature, which refer to 3D full-core simulations of non-moderated MSR on realistic geometries, the comparison has been carried out on a simplified case.

In Figure 2.8, the nominal in-core temperature distribution, as predicted by OpenFOAM (right), is compared to results from COMSOL (left) and TUDelft (center) models

[2]The COMSOL model features a different time integration technique (third order backward differentiation formula), a different error estimation method and a different spatial discretization (finite element methods). For this reason, the computational performance of the two tools can be only roughly compared. The main limiting task for the COMSOL model has been found to be the solution of the turbulent flow (k-epsilon).

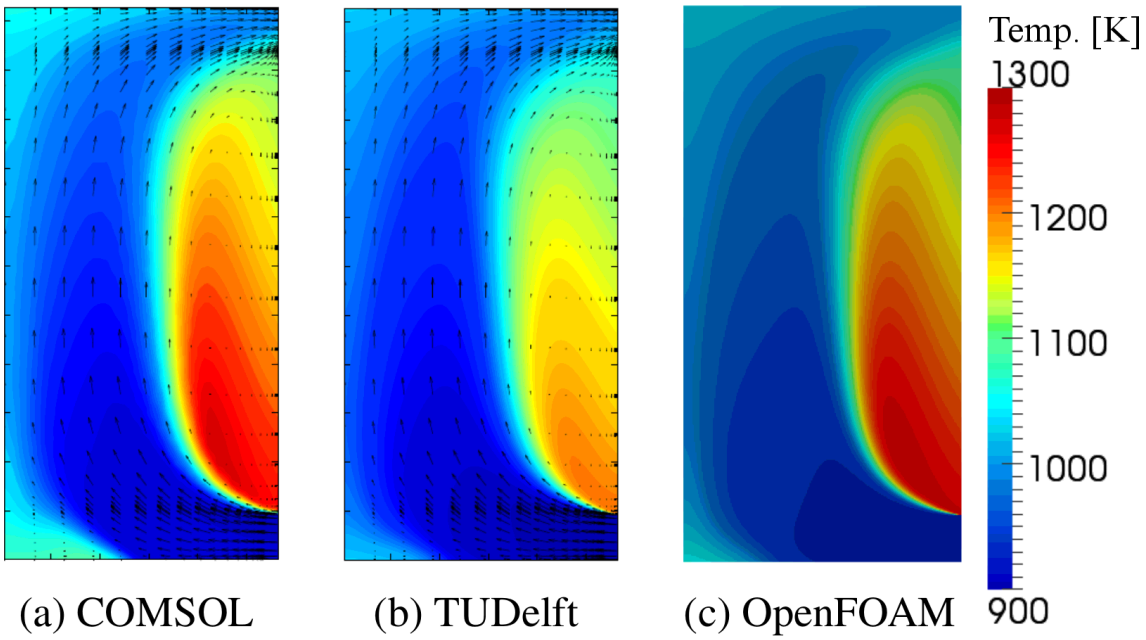

Figure 2.8: *Fuel temperature field at nominal conditions. Comparison between OpenFOAM, COMSOL and TUDelft model. Simplified 2D, axial-symmetric MSFR test case.*

(Fiorina *et al.*, 2014). The simulations refer to the simplified 2D, axial-symmetric MSFR geometry presented in Chapter 1, and the k-epsilon turbulence model has been adopted in the three different tools. A good agreement on the temperature field prediction can be appreciated, especially with the COMSOL results.

In Figure 2.9, the evolution of the total reactor power after the step-wise reactivity insertion of 200 pcm is shown. A step-wise reactivity insertion is a particularly demanding transient analysis from a numerical point of view, thus representing a good test for the models. Moreover, the insertion of 200 pcm leads to a super-prompt-critical condition, which involves a relevant power excursion and a considerable release of energy in a limited time interval.

In Figure 2.10, the average core temperature for the analysed test case is shown, as predicted by the three codes. The prompt power rise triggered by the reactivity insertion leads to a rapid temperature increase. The consequent negative reactivity insertion due to Doppler and density feedbacks quickly reduces and stabilizes the power.

A good agreement between the three solutions can be appreciated in both power and average temperature predictions. In particular, the evolution of power for the OpenFOAM and COMSOL models agrees very well even in the prompt rise, whereas the TUDelft model predicts a slightly higher power excursion. This difference is in accordance with the lower effective delayed neutron fraction value obtained with this model, as discussed in Fiorina *et al.* (2014).

2.3.2 Unprotected single pump failure

Differently from previously published works (e.g., Fiorina *et al.*, 2014), the present tool is able to deal with full core 3D MSFR geometries and can be useful to analyse asymmetric transient in which axial-symmetric simulations are not suitable. As an example of the

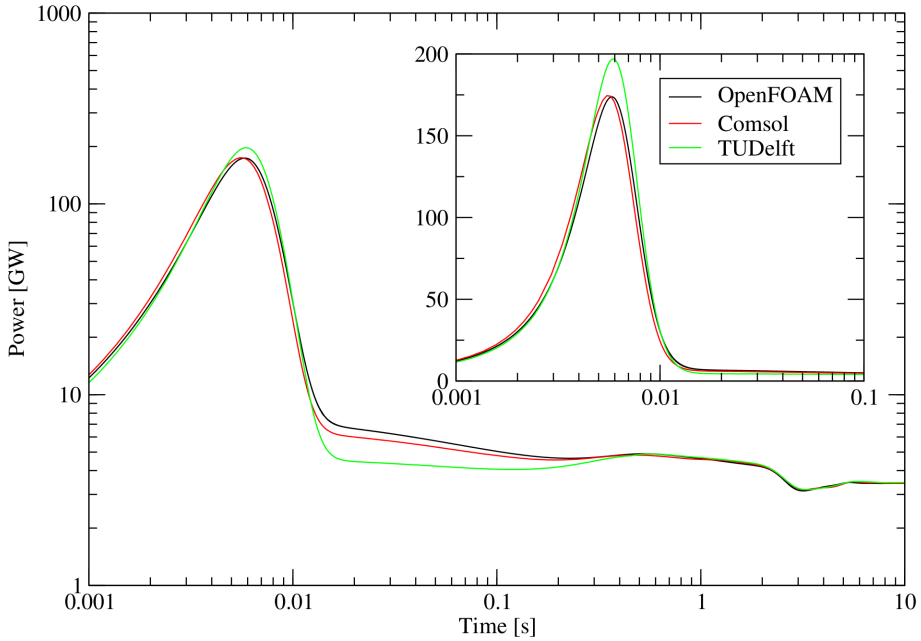

Figure 2.9: *Power excursion after step-wise insertion of 200 pcm of reactivity. Comparison between OpenFOAM, COMSOL and TUDelft model. Simplified 2D, axial-symmetric MSFR test case.*

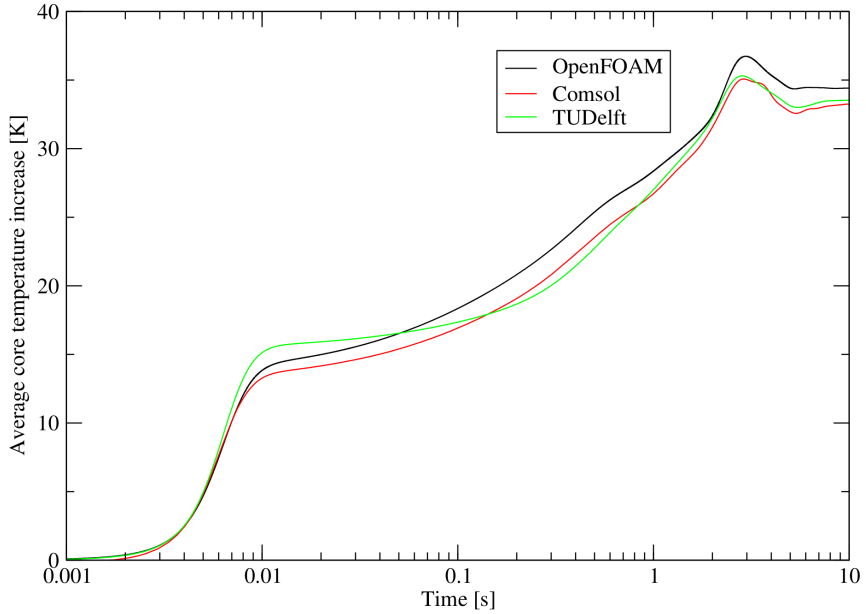

Figure 2.10: *Average core temperature after step-wise insertion of 200 pcm of reactivity. Comparison between OpenFOAM, COMSOL and TUDelft model. Simplified 2D, axial-symmetric MSFR test case.*

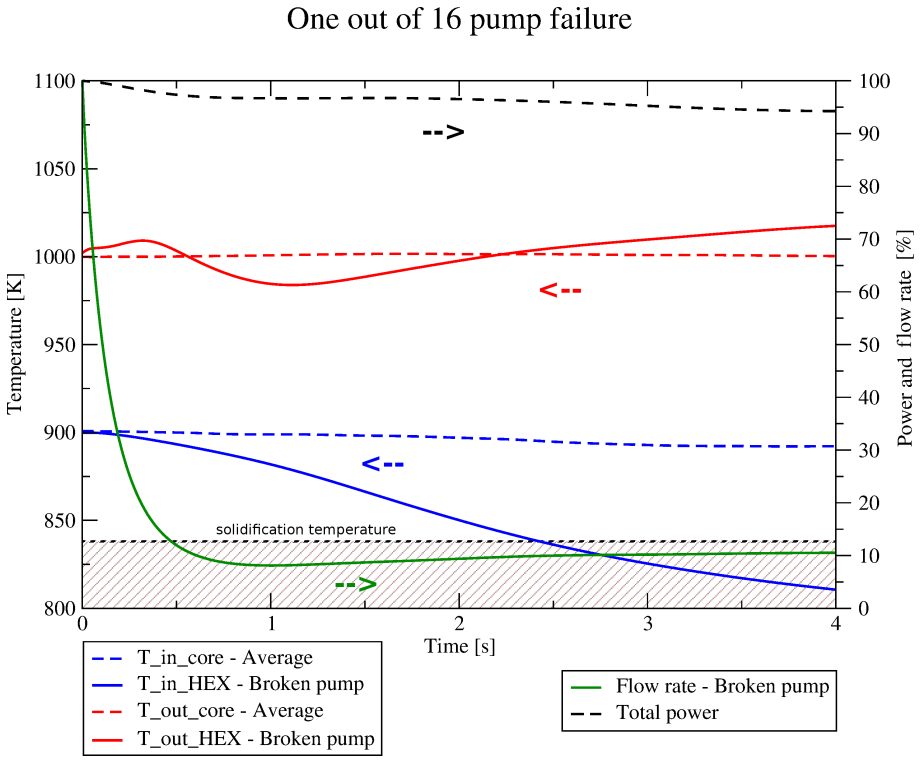

Figure 2.11: *Single pump failure unprotected scenario. Temperatures, flow rate and power. Solid lines refer to values relative to the broken pump loop. Dashed lines refer to reactor average values.*

capability of the model, a single pump failure accident is presented.

In the simulated accidental scenario, one of the 16 MSFR primary pumps undergoes a sudden bearing failure, which leads to its immediate blockage. Dealing with an unprotected scenario, no actions is taken in order to mitigate the consequences of the pump failure. In particular, the flow rate and temperature of the intermediate salt in the heat exchanger of the broken branch are kept at nominal conditions.

In Figure 2.11, the evolution of relevant quantities in the analysed accidental scenario is shown. The green line shows the flow rate in the broken branch. After bearing failure, the head losses of the blocked pump and the heat exchanger lead to a rapid decrease of the flow rate. Buoyancy effects, along with hydrodynamic effects due to neighbouring branches, provide enough thrust to keep about 10% of the nominal flow in the broken pump. The total reactor power (black line) and the average core inlet and outlet temperatures (dashed blue and red lines) are slightly affected by the single pump failure. The MSFR operating conditions deviate little from nominal ones. Nonetheless, a potential unsafe behaviour can be appreciated analysing the temperatures relative to the broken branch. In particular, solid red and blue lines show the inlet and outlet temperature of the heat exchanger located above the blocked pump, respectively. Due to mixing effects in the reactor core, the HEX inlet temperature remains close to the nominal value. On the other hand, due to the reduced flow rate in the broken branch and the nominal operation of the intermediate circuit, the temperature of the salt quickly reduces at the heat exchanger exit. If no action is taken promptly, in a few seconds the HEX outlet temperature goes below the salt solidification temperature.

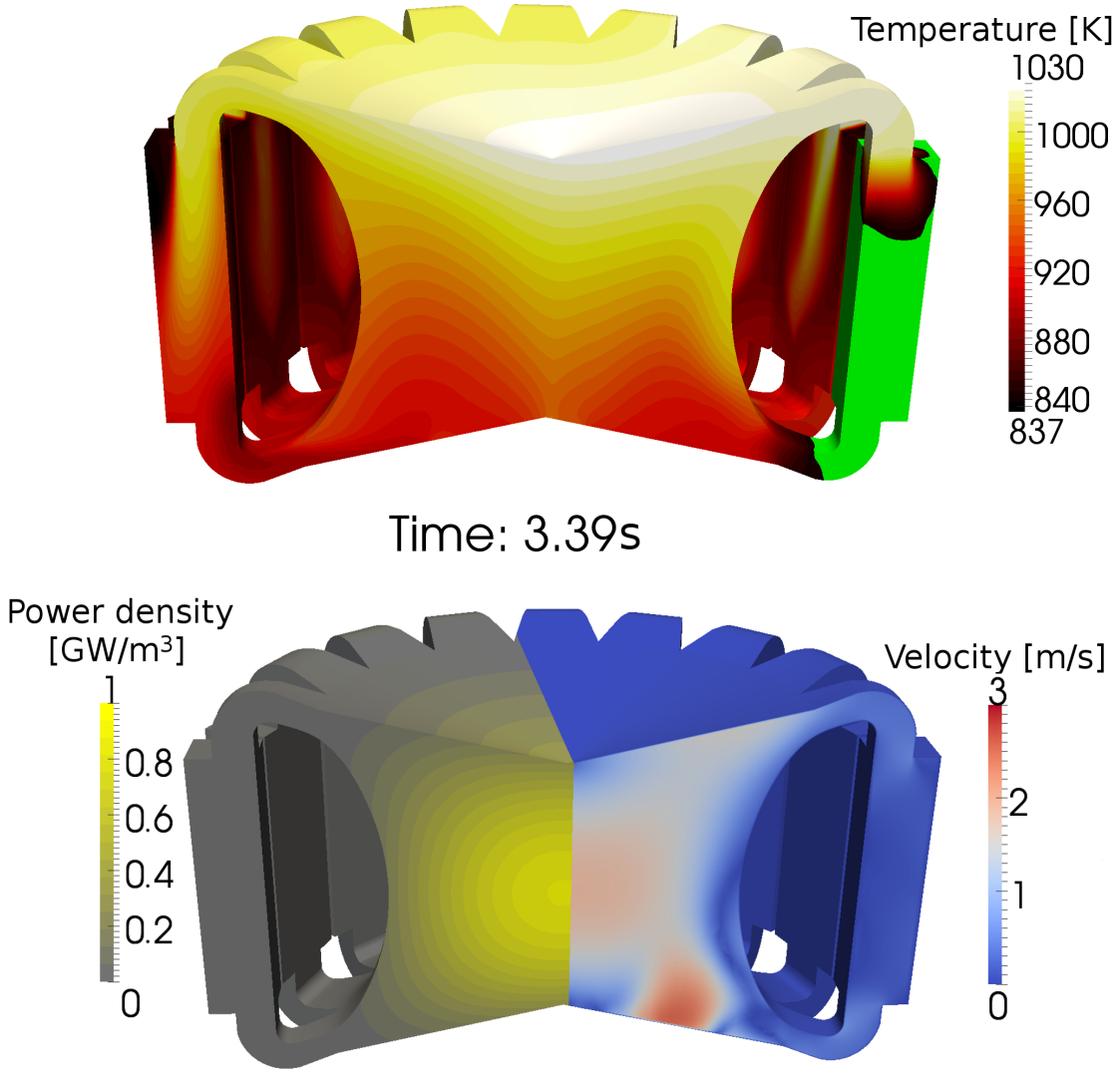

Figure 2.12: *Temperature (top), velocity and power density (bottom) fields in the MSFR after the single pump failure accident.*

Figure 2.12 shows the temperature (top), velocity and power density (bottom) fields in the MSFR about 3.4 seconds after the single pump failure accident. Temperature below melting point ($\sim$837 K) are highlighted in green. It can be appreciated that in a few seconds, most of the volume of the heat exchanger reaches almost stagnation conditions and solidification temperature. Despite the simplification adopted in the HEX modelling and the inability of the present tool to model salt phase change, the emerging of possible unsafe conditions as a consequence of a single pump failure is evident. Several mitigating features can be implemented in the MSFR design, in order to limit or avoid solidification in different accidental scenarios. A few promising solution in this direction have been preliminarily studied and presented in the framework of the EVOL Project (e.g., Geoffroy and Aufiero, 2013). Among these, the increase of the nominal intermediate salt temperature or the addition of HEX by-pass area seems feasible.

2.4 Concluding remarks

In the analysis of the Molten Salt Fast Reactor behaviour, the presence of a strong coupling between neutronics and thermal-hydraulics and fast time scales calls for the adoption of coupling techniques which are more suitable than the common operator-splitting approach. Recent works also highlighted the significant impact of CFD modelling on the MSFR analysis and the need to adopt accurate turbulence models and realistic three-dimensional geometries.

In this Chapter, the development of a multiphysics solver adopting the finite-volume open-source C++ library OpenFOAM is discussed. The work has been focused on the implementation of an accurate time-integration scheme and the adoption of suitable strategies and simplifications to enable a fast-running simulation of accidental transient on detailed full-core 3D geometries.

The neutronics capability of the multiphysics model has been assessed against Monte Carlo simulations, showing an adequate accuracy of the spatial neutron flux for the purpose of the analysis of accidental scenarios.

A super-prompt-critical reactivity insertion has been simulated with the proposed solver on a simplified geometry, for which results were already available in the literature, showing a good agreement with multiphysics models previously developed at Politecnico di Milano and Delft University of Technology.

An unprotected single pump failure accidental scenario has been simulated. Although the general reactor behaviour (total power and average temperatures) deviates only slightly from the nominal operating conditions, the results of the simulation show that unsafe situations might emerge as consequence of the possible salt freezing in the broken circuit. This transient has been discussed as example of the capability of the model, while detailed MSFR safety analysis is not the scope of this Chapter and would require layout specifications of the core and fuel circuit components (e.g., pumps), which are currently not available within the EVOL Project.

In this view, the present multiphysics full-core modelling tool, which is able to describe the transient flow field and neutronics behaviour of the MSFR, might be of relevant interest in the phase of reactor design optimization.

In addition to computationally lightweight and versatile solvers, aimed at the simulation of transient incidental scenarios, more accurate models are envisaged to provide

reference solutions. In this direction, research activities are ongoing among several institutions to develop multiphysics tools relying on more accurate neutron transport modelling. Possible extensions of the present work to deterministic (Discrete Ordinates) and Monte Carlo approaches are presented in the Appendix of the thesis (Section A.4).

Main equations of the multiphysics model

In the following, a brief summary of the main equations that are discretized and solved in the OpenFOAM multiphysics model is given.
The neutronics model of the MSFR involves the solution of the one-group neutron diffusion:

$$\frac{1}{v}\frac{\partial \phi}{\partial t} = \nabla \cdot D\nabla\phi - \Sigma_a\phi + (1-\beta_{tot})\,\nu\Sigma_f\phi + \sum_{i=1}^{8}\lambda_i c_i \tag{2.1}$$

where ϕ is the neutron flux, β_{tot} is the total delayed neutron fraction, v is the average neutron velocity, D is the diffusion coefficient, and Σ_a and $\nu\Sigma_f$ are the absorption and the neutron production cross-sections, respectively. c_i is the delayed neutron precursor concentration of the i^{th} group, and λ_i and β_i are the relative decay constant and delayed neutron fraction. The dependencies of the cross-sections on the fuel temperature T and density ρ have been introduced as follows:

$$\Sigma(T,\rho) = \left(\frac{\rho}{\rho_0}\right)\left[\Sigma_0 + \alpha_\Sigma\, log\left(\frac{T}{T_0}\right)\right] \tag{2.2}$$

$$D(T,\rho) = \left(\frac{\rho_0}{\rho}\right)\left[D_0 + \alpha_D\, log\left(\frac{T}{T_0}\right)\right] \tag{2.3}$$

where T_0 is the fuel reference temperature and ρ_0 is the fuel density at the reference temperature. In order to limit the computational domain to the fuel circuit only, albedo boundary conditions have been adopted both in the upper and lower limit of the core:

$$\mathbf{n}\cdot(D\nabla\phi)_b = -\gamma\phi_b \tag{2.4}$$

All the group constants and their temperature dependencies (α_D and α_Σ), as well as the albedo coefficients (γ), have been calculated by means of SERPENT. Delayed neutrons have been considered through the precursor balance equations for the 8 delayed neutron groups of the JEFF-3.1 library (Koning *et al.*, 2006):

$$\frac{\partial c_i}{\partial t} = -\nabla(\mathbf{u}c_i) + \nabla\cdot\frac{\nu_T}{Sc_T}\nabla c_i - \lambda_i c_i + \beta_i\cdot\nu\Sigma_f\phi \tag{2.5}$$

In a similar way, the balance equations for the decay heat precursors have been introduced in the model:

$$\frac{\partial d_i}{\partial t} = -\nabla(\mathbf{u}d_i) + \\ +\nabla\cdot\frac{\nu_T}{Sc_T}\nabla d_i - \lambda_{heat,i}\cdot d_i + \beta_{heat,i}E_f\Sigma_f\phi \tag{2.6}$$

In Eqs. (2.5) and (2.6), d_i, $\lambda_{heat,i}$ and $\beta_{heat,i}$ are the concentration, decay constant and fraction of the i^{th} decay heat precursor. E_f represents the average energy released per fission, and $\mathbf{u}$ is the fuel salt velocity. Sc_T is the turbulent Schmidt number, which has been assumed equal to 0.85 in the simulations shown in this Chapter. In Chapter 3, a sensitivity analysis to this parameter is presented.

The temperature field in the MSFR fuel circuit has been solved introducing the energy balance equation as follows:

$$\frac{\partial T}{\partial t} = -\nabla(\mathbf{u}T) + \nabla\cdot\frac{(K_{salt}+K_T)}{\rho C_p}\nabla T + \\ +(1-\beta_{heat,tot})\frac{E_f}{\rho C_p}\Sigma_f\phi + \sum_{i=1}^{3}\frac{\lambda_{heat,i}}{\rho C_p}d_i \tag{2.7}$$

The terms K_{salt} and K_T refer to the laminar and turbulent salt thermal conductivity, respectively. The latter, is calculated with a constant and uniform turbulent Prandtl number equal to 0.85. ρ and C_p are the fluid density and specific heat, respectively.

Homogeneous Neumann boundary conditions have been adopted at the walls of the fuel circuit for temperature and concentration of delayed neutrons and decay heat precursors.

The model of the fluid flow is based on the incompressible form of the Reynolds-Averaged Navier-Stokes (RANS) equations. The proposed tool fully benefits from the availability of pre-implemented turbulence models and wall functions in OpenFOAM. In particular, the comparisons shown in Section 2.3.1 have been obtained adopting the standard k-epsilon model, which is also available in COMSOL and TUDelft simulation tools, whereas the other results of the present work have been achieved by means of the *realizable* k-epsilon model, which is thought to be more accurate for the MSFR flow conditions, according to the analysis performed at INOPRO.

CHAPTER 3

Effective delayed neutron fraction

This Chapter deals with the calculation of the effective delayed neutron fraction (β_{eff}) in circulating-fuel nuclear reactors. Three different approaches have been implemented and compared. The first approach involves the extension of the Monte Carlo code SERPENT-2 to allow for delayed neutron precursors drift, according to the fuel velocity field. The second approach consists in the extension of the OpenFOAM solver presented in Chapter 2 to solve the forward and adjoint eigenvalue multi-group diffusion problems. Finally, an analytical formula for the circulating-to-static β_{eff} correction factor has been derived, under simple hypotheses, and explicitly takes into account the spatial dependence of the neutron importance.

Adjoint-weighting is achieved in SERPENT-2 via the adoption of the Iterated Fission Probability (IFP) technique. A brief description of the IFP methodology and implementation in the code is given in the Appendix (Section A.2). The OpenFOAM solver makes use of the *"Block-coupled"* libraries developed by Ivor Clifford, and available in the extended version of the library, which greatly simplified the coding efforts.

The main results presented in this Chapter have been published in: Manuele Aufiero et al., "Calculating the Effective Delayed Neutron Fraction in the Molten Salt Fast Reactor: Analytical, Deterministic and Monte Carlo Approaches.", Annals of Nuclear Energy, 65 (2014) 78-90.

3.1 Introduction

THE effective delayed neutron fraction (β_{eff}) is an important reactor kinetics parameter. The contribution of delayed neutrons is of primary importance for the safe control of any nuclear reactor. β_{eff} is often adopted as unit of experimental reactivity (*dollar*) (Bell and Glasstone, 1979). Many efforts have been devoted to the measurement (e.g., Sakurai *et al.*, 1999; Rudstam *et al.*, 2002) and calculation (e.g., Meulekamp and van der Marck, 2006; Carta *et al.*, 2011) of physical and effective delayed neutron fractions. The traditional definition of β_{eff} involves the calculation of both the forward and adjoint solution of the neutron transport equations, which makes its accurate calculation by means of continuous energy Monte Carlo codes a hard task, even for static-fuel reactors (Nagaya *et al.*, 2010). In circulating-fuel systems, the motion of

delayed neutron precursors complicates the calculation of the effective delayed neutron fraction. In molten salt reactors, the adoption of the Thorium cycle (with ^{233}U as fissile) or the envisaged incineration of Minor Actinides (Merle-Lucotte *et al.*, 2011), and the fuel motion itself, may lead to β_{eff} values much lower than those typical of Light Water Reactors (LWR). Moreover, loss of flow accidental scenarios in fluid-fuel systems involve the introduction of positive reactivity due to delayed neutron source term redistribution (Guerrieri *et al.*, 2013). The quantification of the introduced reactivity requires to take into account the difference in delayed neutron effectiveness between static and circulating conditions (Dulla, 2005). For these reasons, accurate and reliable β_{eff} calculations for molten salt reactors are desirable.

In circulating-fuel reactors, the effective delayed neutron fraction (β_{eff}) differs from the physical delayed neutron fraction (β_0) for two distinct reasons. The first reason (common to solid-fuelled reactors) is that the emission spectrum of delayed neutrons is softer than that of prompt neutrons: on average, the former are emitted with a lower energy. This may imply a difference in the importance of delayed and prompt neutrons. The second reason is that delayed neutron precursors are transported by the fluid flow in the fuel circuit and might decay in position of low importance and even out of the core. Spatial effects due to fuel motion are more relevant and always reduce the values of β_{eff}. Energy effects are, in general, of lesser relevance and might reduce or increase the effective delayed neutron fraction, according to the neutronic characteristics of the core.

One-dimensional approaches have often been adopted to correct the effective delayed neutron fraction calculation in order to take into account the fuel motion. One of the most common employed method consists in the correction of static-fuel β_{eff} calculations (obtained by means of commonly available Monte Carlo or deterministic codes, and allowing for energy effects) by means of the fraction of precursors decaying inside the reactor core and not in the out-of-core part of the loop (Lecarpentier, 2001; Cammi *et al.*, 2011b; Guerrieri *et al.*, 2013). This fraction is calculated under the hypothesis that the production of precursors has a flat or sinusoidal dependence on the axial coordinate in the core. This approach neglects the effects on β_{eff} due to the inhomogeneous spatial importance of neutrons inside the core. More precisely, this method considers the delayed neutrons produced within the core to have a relative effectiveness of one, regardless of their position, while those produced outside the core have zero importance. On average, precursors are created in a position with a higher spatial neutron importance with respect to the place where they will decay. For this reason, this approach may lead to a significant overestimation of the effective delayed neutron fraction in circulating conditions. In Section 3.2.1, a new analytical formula for the β_{eff} correction factor is derived, which takes into account the in-core spatial importance effect. Moreover, the proposed approach allows for radial redistribution of the delayed neutron precursors that re-enter in the core.

A more accurate approach involves the adoption of deterministic neutronic calculations to solve the adjoint and forward neutron transport problem. Then, the effective (i.e., adjoint weighted) delayed neutron fraction is calculated. For example, Mattioda *et al.* (2000) adopted the multi-group neutron diffusion approximation along with precursors drift in one-dimensional geometry. Kópházi *et al.* (2009) proposed a model for the analysis of moderated MSRs based on neutron diffusion and precursor convection and applied it to the MSRE (Molten Salt Reactor Experiment). In Section 3.2.2, the solution of the equations of neutron diffusion and precursor transport by means of the multi-physics

Table 3.1: *Design parameters of the simplified axial symmetric (r, z) MSFR geometry.*

Core diameter	2.25 m
Core height	2.25 m
Blanket thickness	50 cm
Boron carbide layer thickness	20 cm
Axial reflector thickness	1 m

open-source toolkit OpenFOAM (Weller *et al.*, 1998) is discussed. The proposed solver allows the solution of the forward and adjoint eigenvalue problems for arbitrary geometries based on detailed spatially-dependent velocity fields.

Monte Carlo has often been regarded as reference method for verifying the results of deterministic calculations. Commonly available Monte Carlo codes are not suitable for β_{eff} calculation in circulating-fuel systems. Kópházi *et al.* (2004) evaluated the reactivity loss due to fuel circulation in the MSRE by means of an extended version of Monte Carlo N-Particle Transport Code (MCNP). In that work, the decay position of delayed neutron precursors was recalculated under simple hypotheses, and neutrons emitted outside of the core were considered lost. More recently, Kiedrowski (2012) also considered the effect of precursors diffusion in fissile solution systems. In both works, the velocity profiles, adopted as input in the Monte Carlo simulations, were simple analytical functions of the position. In Section 3.2.3, an extension of the Monte Carlo code SERPENT-2 for β_{eff} calculation in circulating-fuel systems is presented. The extended version features a suitable algorithm for the transport of delayed neutron precursors. The algorithm is intended for an accurate and efficient tracking of the precursors, making use of more realistic velocity fields obtained from Computational Fluid Dynamics (CFD) simulations.

As in the previous Chapters, the Molten Salt Fast Reactor (MSFR) is adopted as case study for the presented methods. In Section 3.2, the three presented methods for β_{eff} calculation are discussed. In Section 3.3, the main results are reported and discussed. Finally, in Section 3.4, a few concluding remarks are drawn.

The Molten Salt Fast Reactor has been already described in the Introduction of the thesis and further details about the MSFR concept can be found in the references (Merle-Lucotte *et al.*, 2009, 2011; Brovchenko *et al.*, 2012). In this Chapter, both the simplified axial-symmetric geometry and the optimized 3D shape introduced in previous Chapters are employed. In particular, in Section 3.3, the effects of both the reactor core shape and the fluid flow path on β_{eff} are discussed. The analysis is carried out by means of a comparison between three different case studies. The first one (referred to as "k-epsilon case study" in the following) concerns the reference MSFR geometry adopted for the neutronic calculation benchmark within the EVOL Project, and presented in Chapter 1. The axial-symmetric (r, z) cylindrical shape, which can be easily modelled by most of the neutron transport codes, is presented again in Figure 3.1, along with the main dimensions (Table 3.1). The fuel velocity field inside the core is solved adopting the RANS turbulence treatment for incompressible flow and the k-epsilon turbulence model. As discussed in Chapter 2, in nominal conditions, large recirculation vortex appears near the core wall which would lead to excessive structural material temperatures. For this reason, a core shape optimization process is ongoing within the EVOL Project, aimed at the elimination of high-temperature zones. A second configuration (referred to as "uniform velocity case study") is analysed in the present Chapter, as representative of optimized flow path condi-

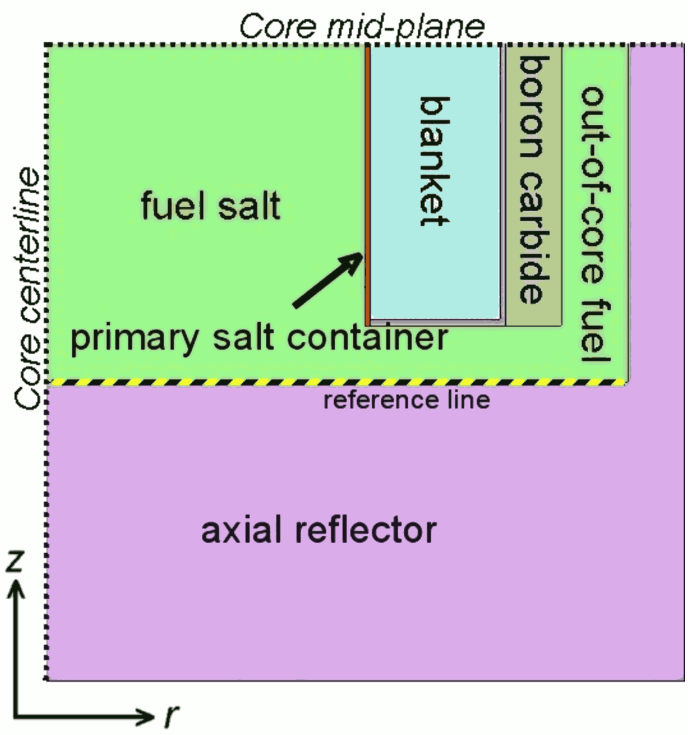

Figure 3.1: *Simplified axial symmetric (r, z) MSFR geometry.*

tions. In this case study, the simplified cylindrical geometry is adopted along with a fairly uniform fuel velocity field in the core. Finally, the optimized 3D core shape presented in Chapter 2 is considered as third case study ("optimized geometry, 3D case study").

Different fuel materials have also been considered for the calculation of the effective delayed neutron fraction in both circulating and static conditions. Thorium is adopted as fertile material in the fuel mixture. As fissile material the following options have been studied: i) ^{235}U at 20 % at. enrichment; ii) only ^{233}U; iii) a mixture of transuranic (TRU) elements from PWR spent fuel; and iv) a mixture of transuranic elements and ^{235}U at 13 % at. enrichment. Details about the iii) and iv) fuel isotopic compositions can be found in (Merle-Lucotte *et al.*, 2009, 2013).

3.2 Methods

In this Section, the three proposed approaches adopted to calculate the effective delayed neutron fraction in the MSFR are described.

3.2.1 Analytical approach

In the following, an analytical formula for the circulating-to-static correction factor of the effective delayed neutron fraction is derived. It features an explicit consideration of the in-core spatial neutron importance. This leads to significant difference with respect to non adjoint-weighted approaches (see Figure 3.5).

We can write the correction factor for the effective delayed neutron fraction as:

$$cf_{circ} \equiv \frac{\beta_{eff}^{c}}{\beta_{eff}^{s}} = \frac{\int\limits_{core} D^{c}(\mathbf{r}') \cdot I^{c}(\mathbf{r}')\, d\mathbf{V}'}{\int\limits_{core} D^{s}(\mathbf{r}') \cdot I^{s}(\mathbf{r}')\, d\mathbf{V}'} \tag{3.1}$$

where $D^{c}(\mathbf{r}')$ and $D^{s}(\mathbf{r}')$ are the probabilities to have a precursors decay in the position $\mathbf{r}'$ in circulating and static conditions, respectively, and $I(\mathbf{r}')$ is the spatial dependence of the neutron importance.

We can write $D(\mathbf{r}')$ as:

$$D(\mathbf{r}') = \int\limits_{core} K(\mathbf{r}', \mathbf{r})\, S(\mathbf{r})\, d\mathbf{V} \tag{3.2}$$

where $S(\mathbf{r})$ is the probability to have the production of a precursor in the position $\mathbf{r}$ and $K(\mathbf{r}', \mathbf{r})$ is the kernel function of the integral transform operator that allows transforming the probability density function of the precursor production into the probability density function of the precursor decay. In a simpler way, $K(\mathbf{r}', \mathbf{r})$ can be seen as the conditional probability to have the decay of a precursor in the position $\mathbf{r}'$, given that it was produced in the position $\mathbf{r}$. $K(\mathbf{r}', \mathbf{r})$ is independent from $S(\mathbf{r})$ and $I(\mathbf{r}')$ and depends only on the precursor decay constant and the fluid-fuel flow.

For the static-fuel conditions, any delayed neutron precursors will decay where it has been created:

$$K^{s}(\mathbf{r}', \mathbf{r}) = \delta(\mathbf{r}' - \mathbf{r}) \tag{3.3}$$

thus

$$D^{s}(\mathbf{r}') = S^{s}(\mathbf{r}') \tag{3.4}$$

Now, we can rewrite Equation (3.1) as:

$$cf_{circ} = \frac{\iint\limits_{core\, core} \left[K^{c}(\mathbf{r}', \mathbf{r})\, S^{c}(\mathbf{r})\, d\mathbf{V}\right] I^{c}(\mathbf{r}')\, d\mathbf{V}'}{\int\limits_{core} S^{s}(\mathbf{r}') \cdot I^{s}(\mathbf{r}')\, d\mathbf{V}'} \tag{3.5}$$

Due to the fact that delayed neutrons are very few compared to prompt neutrons, we can consider that the spatial source of precursors (that are mainly produced by prompt neutrons) is the same for static and circulating cases. We have that: $S^{c}(\mathbf{r}) \simeq S^{s}(\mathbf{r}) \simeq S(\mathbf{r})$.

Under the one-group neutron diffusion hypotheses, recalling again that delayed neutrons are few compared to prompt neutrons, we have that the spatial dependence of the neutron flux and the adjoint flux is the same: $\phi(\mathbf{r}') \simeq \phi^{*}(\mathbf{r}')$. In the case of homogeneous core composition, the source of delayed neutrons is proportional to the neutron flux and the spatial neutron importance is proportional to the adjoint flux.

Under these hypotheses, in the case of a cylindrical core, we obtain:

$$S(\mathbf{r}) \simeq I(\mathbf{r}) \simeq cos\left(\frac{\pi\, z}{H_e}\right) J_0\left(\frac{2.405\, r}{R_e}\right) \tag{3.6}$$

where H_e and R_e are the extrapolated height and radius, respectively, at which ϕ and ϕ^* go to zero. $S(\mathbf{r})$ and $I(\mathbf{r})$ are both normalized to be equal to one at core center.

Now, only the term $K^c(\mathbf{r}', \mathbf{r})$ is missing in Equation (3.5). In the following, $K^{\lambda T}(r'z' \leftarrow rz)$ is derived for the general case of precursor decay constant λ, fuel salt loop circulation period T and in-core-to-total fuel volume ratio γ. H_a and R_a are the core active height and radius, respectively. As further hypotheses, uniform (axial) velocity in the core and complete mixing in the out-of-core part of the primary loop (i.e., in the pump and the heat exchanger) have been assumed.

In order to simplify the solution, we can split the problem in two parts:

$$K^{\lambda T}(r'z' \leftarrow rz) = p_1^{\lambda T}(r'z' \leftarrow rz) + p_2^{\lambda T}(r'z' \leftarrow rz) \tag{3.7}$$

where $p_1^{\lambda T}(r'z' \leftarrow rz)$ is the conditional probability for the decay in $(r'z')$ during the first passage in the core and $p_2^{\lambda T}(r'z' \leftarrow rz)$ is the probability to have a decay during the further N passage in the core, with $N \to \infty$.

In general, for a precursor created at time $t = 0$, the probability to have a decay between t_1 and $t_1 + \varepsilon$ is: $p = \int_{t_1}^{t_1+\varepsilon} \lambda e^{-\lambda t}\, dt$ for $t_1 \geq 0$ and $p = 0$ for $t_1 < 0$. Similarly, the probability density function for a precursor created in z to have a decay, during the first loop, in z' is:

$$p(z' \leftarrow z) = \int_{T\gamma\frac{z'-z}{H_a}}^{T\gamma\left(\frac{z'-z}{H_a}+\frac{dz'}{H_a}\right)} \lambda e^{-\lambda t}\, dt \tag{3.8}$$

for $z' \geq z$ and $p = 0$ for $z' < z$. Thus, due to the zero radial velocity in the core, we have:

$$\begin{aligned} p_1^{\lambda T}(r'z' \leftarrow rz) &= \frac{1}{2\pi r}\delta(r'-r)dr' \cdot \int_{T\gamma\frac{z'-z}{H_a}}^{T\gamma\left(\frac{z'-z}{H_a}+\frac{dz'}{H_a}\right)} \lambda e^{-\lambda t}\, dt = \\ &= \frac{1}{2\pi r}\delta(r'-r)dr' \cdot e^{-\lambda T\gamma\frac{z'-z}{H_a}}\left(1 - e^{-\lambda T\gamma\frac{dz'}{H_a}}\right) \end{aligned} \tag{3.9}$$

It can be shown that the limit of $p_1^{\lambda T}$ for $\lambda T \to +\infty$ is:

$$\lim_{\lambda T \to +\infty} p_1^{\lambda T}(r'z' \leftarrow rz) = \frac{1}{2\pi r}\delta(r'-r)dr' \cdot \delta(z'-z)dz' \tag{3.10}$$

Then, as expected, for very low fuel velocity the decay will occur near the precursor production position. The limit for very fast fuel velocity ($\lambda T \to 0^+$) is:

$$\lim_{\lambda T \to 0^+} p_1^{\lambda T}(r'z' \leftarrow rz) = 0 \tag{3.11}$$

It means that the probability to have a decay during the first passage in the core tends to zero as fuel velocity increases.

For finite value of λT, we can proceed to first order Taylor series expansion around $dz' = 0$:

$$p_1^{\lambda T}(r'z' \leftarrow rz) = \frac{1}{2\pi r}\delta(r'-r)dr' \cdot e^{-\lambda T\gamma\frac{z'-z}{H_a}} \cdot \lambda T\gamma\frac{dz'}{H_a} \tag{3.12}$$

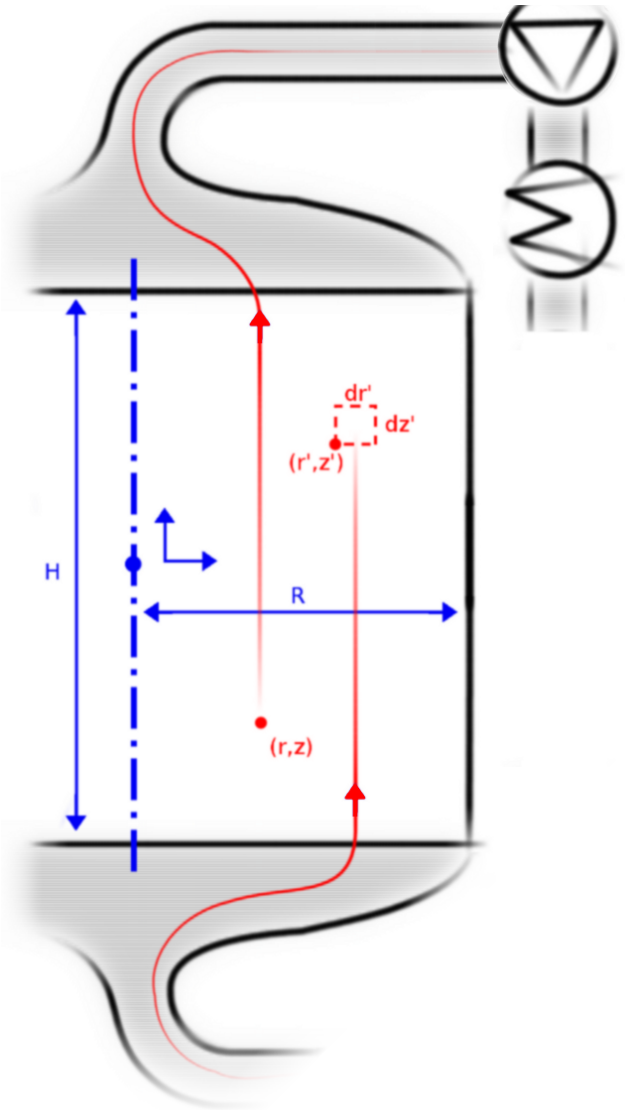

Figure 3.2: *Schematic representation of the reactor model adopted in the derivation of the analytical approach.*

After the first loop, if the precursor has not yet undergone the decay, it might emit the neutron in the out-of-core part of the fuel loop or come back in the core at $z' = -\frac{H_a}{2}$ in any radial position (see Figure 3.2). If the precursor is still "alive" after the second passage in the core, it might decay outside or come back again at $z' = -\frac{H_a}{2}$, and so on:

$$p_2^{\lambda T}(r'z' \leftarrow rz) = \frac{2\pi r' dr'}{\pi R_a^2} \cdot \left[\int_{T\gamma\frac{z'-z}{H_a}+T}^{T\gamma\left(\frac{z'-z}{H_a}+\frac{dz'}{H_a}\right)+T} \lambda e^{-\lambda t}\, dt + \right.$$
$$\left. + \int_{T\gamma\frac{z'-z}{H_a}+2T}^{T\gamma(...)+2T} \lambda e^{-\lambda t}\, dt \; + \int_{T\gamma\frac{z'-z}{H_a}+3T}^{T\gamma(...)+3T} \lambda e^{-\lambda t}\, dt \; + \; ... \right] \quad (3.13)$$

$p_2^{\lambda T}(r'z' \leftarrow rz)$ can be rewritten as:

$$p_2^{\lambda T}(r'z' \leftarrow rz) = \frac{2\pi r' dr'}{\pi R_a^2} \cdot \left(\sum_{N=1}^{\infty} e^{-N\lambda T} \right) e^{-\lambda T \gamma \frac{z'-z}{H_a}} \left(1 - e^{-\lambda T \gamma \frac{dz'}{H_a}} \right) \quad (3.14)$$

The limit for very low fuel velocity ($\lambda T \to +\infty$) is:

$$\lim_{\lambda T \to +\infty} p_2^{\lambda T}(r'z' \leftarrow rz) = 0 \quad (3.15)$$

As λT tends to $+\infty$, the probability to have a decay during a passage in the core different from the first one tends to zero.

The sum $\sum_{N=1}^{\infty} e^{-N\lambda T}$ converges to $\frac{1}{e^{\lambda T}-1}$ and we obtain:

$$p_2^{\lambda T}(r'z' \leftarrow rz) = \frac{2\pi r' dr'}{\pi R_a^2} \cdot \frac{1}{e^{\lambda T}-1} \cdot e^{-\lambda T \gamma \frac{z'-z}{H_a}} \left(1 - e^{-\lambda T \gamma \frac{dz'}{H_a}} \right) \quad (3.16)$$

The limit of $p_2^{\lambda T}$ for $\lambda T \to 0^+$ is:

$$\lim_{\lambda T \to 0^+} p_2^{\lambda T}(r'z' \leftarrow rz) = \gamma \cdot \frac{2\pi r' dr'}{\pi R_a^2} \cdot \frac{dz'}{H_a} \quad (3.17)$$

For very fast fuel velocity, the probability to have a precursor decay in a certain position becomes uniform in the core and all the dependencies on the production position are lost. As expected, as λT tends to 0^+, the integral probability to have a decay inside the core tends to the in-core-to-total volume ratio γ.

After first order expansion of $p_2^{\lambda T}$ around $dz' = 0$, we can finally write the general expression for $K^{\lambda T}$:

$$K^{\lambda T}(r'z' \leftarrow rz) = p_1^{\lambda T}(r'z' \leftarrow rz) + p_2^{\lambda T}(r'z' \leftarrow rz) =$$
$$= e^{-\lambda T \gamma \frac{z'-z}{H_a}} \cdot \lambda T \gamma \frac{dz'}{H_a} \left[H(z'-z) \cdot \frac{1}{2\pi r} \delta(r'-r) dr' + \frac{1}{e^{\lambda T}-1} \cdot \frac{2\pi r' dr'}{\pi R_a^2} \right] \quad (3.18)$$

where $H(z'-z)$ is the heavyside step function defined as $\int_{-\infty}^{z'} \delta(s-z)\, ds$ and is zero for $(z' < z)$ and one for $(z' > z)$.

Now, all the terms of Equation (3.5) are known and the correction factor can thus be calculated for any λT. An *Octave/Matlab* script employed for numerical integration of Equation (3.5) is reported at the end of the Chapter. The values of the parameters for the MSFR are: H_a =2.24 m, R_a =1.12 m, H_e =2.6 m, R_e =1.3 m, $\gamma = 0.5$.

3.2.2 Deterministic approach

The second approach presented in this Chapter involves the solution of the forward and adjoint multi-group diffusion eigenvalue problems, along with precursor transport using CFD techniques. In this context, the fluid velocity field enters as an external operator in the system of equations (Mattioda *et al.*, 2000; Lapenta *et al.*, 2001) for the convective transport of the delayed neutron precursors. Commonly available neutronics codes (used for solid-fuelled systems) are unable to model this convective transport and are therefore not suitable. For this reason, the OpenFOAM solver presented in Chapter 2 is extended to solve the equations related to multi-group neutron diffusion and neutron precursor transport. The coupled solution of the multi-group neutron diffusion equation within this framework is based on the work of Clifford and Jasak (2009). The fluid flow inside the reactor core has been obtained adopting the SIMPLE algorithm for incompressible flows along with RANS turbulence treatment. In particular, the standard k-epsilon turbulence model available in OpenFOAM has been adopted. For the simulations presented in this Chapter, the spatially-dependent fluid velocity field is considered to be a fixed input to the neutronics calculation. Calculations refer to "zero-power" conditions and temperature feedbacks to both the fluid flow and the neutronics have been neglected. In the following, the equations implemented in the developed solver are reported.

$$\nabla \cdot D_g \nabla \phi_g - \Sigma_{a,g}\phi_g - \sum_{g' \neq g} \Sigma_{s,gg'}\phi_g + \sum_{g' \neq g} \Sigma_{s,g'g}\phi_{g'} + \\ + (1-\beta_0)\,\chi_{p,g} \sum_{g'=1}^{6} \frac{1}{k_{eff}} \left(\nu\Sigma_f\right)_{g'} \phi_{g'} + \sum_{i=1}^{8} \chi_{d,g}\lambda_i c_i = 0 \quad (3.19)$$

$$-\nabla\left(\mathbf{u}c_i\right) + \nabla \cdot \frac{\nu_T}{Sc_T}\nabla c_i - \lambda_i c_i + \beta_{0,i} \sum_{g=1}^{6} \frac{1}{k_{eff}} \left(\nu\Sigma_f\right)_g \phi_g = 0 \quad (3.20)$$

Equations (3.19) and (3.20) are related to the forward eigenvalue problem. Here, the delayed neutron source ($\sum_{i=1}^{8} \chi_{d,g}\lambda_i c_i$) is explicitly written as function of the precursors concentration (c_i) and decay constants (λ_i), which is not usually the case in solid fuel eigenvalue problems, where the delayed neutron source term can be eliminated in the neutron balance. In fact, the eigenvalue solution is independent of the decay constants of the delayed neutron precursors only in static-fuel cases. The first two terms of the delayed neutron precursor balance equations (Equation 3.20) represent the convection and diffusion of fission products responsible for neutron emissions. $\mathbf{u}$ is the fuel velocity field and ν_T is the turbulent viscosity. These fields are calculated in OpenFOAM, before starting the power iteration solution of the eigenvalue problem. The turbulent Schmidt number (Sc_T) is defined as the ratio of the turbulent momentum diffusivity (eddy viscosity) ν_T

and the turbulent mass diffusivity D_T:

$$Sc_T = \frac{\nu_T}{D_T} \tag{3.21}$$

Sc_T can be seen as the equivalent of the turbulent Prandtl number (Pr_T) for mass transport and is commonly adopted in CFD calculations to model the species diffusion (Tominaga and Stathopoulos, 2007). Due to the unavailability of accurate studies on turbulent mass transport in the MSFR carrier salt and operating conditions, a tentative value of 1 has been adopted for Sc_T. A sensitivity analysis to the value of Sc_T for one case study is presented in Section 3.3.

The laminar diffusion coefficients of the different chemical species constituting delayed neutron precursors have not been measured for the MSFR carrier salt. In general, diffusion coefficients in molten fluorides at operating temperature typical of nominal reactor conditions are very low (Salanne *et al.*, 2009; Rollet *et al.*, 2010) compared to turbulent diffusivity. For this reason, the laminar diffusion of the precursors has been neglected in the present work. Moreover, some of the delayed neutron precursors are constituted by metallic species that are not soluble in the molten fluoride matrix. These precursors may leave the fuel circuit due to extraction by gas bubbling or deposition in cold metallic surfaces in the out-of-core part of the loop. According to previous studies (Doligez, 2010), the extraction will affect at most about 1% of the precursors before delayed neutron emission, in the nominal MSFR conditions.

Hereafter, the equations related to the adjoint eigenvalue problem are presented:

$$\nabla \cdot D_g \nabla \phi_g^* - \Sigma_{a,g}\phi_g^* + \sum_{g' \neq g} \Sigma_{s,gg'}\phi_g^* - \sum_{g' \neq g} \Sigma_{s,g'g}\phi_{g'}^* + \\ + (1-\beta_0)\frac{1}{k_{eff}}\left(\nu\Sigma_f\right)_g \cdot \sum_{g'=1}^{6} \chi_{p,g'}\phi_{g'}^* + \frac{1}{k_{eff}}\left(\nu\Sigma_f\right)_g \cdot \sum_{i=1}^{8} \beta_{0,i} c_i^* = 0 \tag{3.22}$$

$$-\nabla\left(\textbf{-u}c_i^*\right) + \nabla \cdot \frac{\nu_T}{Sc_T}\nabla c_i^* - \lambda_i c_i^* + \lambda_i \sum_{g=1}^{6} \chi_{d,g}\phi_g^* = 0 \tag{3.23}$$

c_i^* (Eqs. (3.22) and (3.23)) is not present in classical solid fuel adjoint problem. It represents the importance of a precursor injected in a certain position (i.e., it is the average importance of the delayed neutrons emitted).

In the present work, the six energy-groups structure employed in previous works (Fiorina *et al.*, 2013b) has been adopted and it is reported in Table 3.2. The JEFF-3.1 evaluated nuclear data library (Koning *et al.*, 2006) has been adopted for the delayed neutron group decay constants and fractions. This library adopts eight groups of precursors, with the same time constants for any fissioning isotope. In Table 3.3, the decay constants of the different groups are reported along with the physical fractions ($\beta_{0,i}/\beta_{0,tot}$) for some fissile isotopes. The value of the cross sections, diffusion coefficients and neutron emission spectra have been calculated by means of the SERPENT Monte Carlo code (SERPENT, 2011), adopting the same library.

Neumann conditions are applied to the forward and adjoint precursor equations at the boundaries of the fuel salt domain. The albedo boundary condition has been applied to

Table 3.2: *6 energy-groups structure adopted in the deterministic approach.*

Energy-group #	1	2	3	4	5	6
Upper energy boundary [MeV]	$7.485 \cdot 10^{-4}$	$5.531 \cdot 10^{-3}$	$2.479 \cdot 10^{-2}$	$4.979 \cdot 10^{-1}$	2.231	20

Table 3.3: *Decay constants of delayed neutron precursors. Physical delayed neutron fractions of some isotopes are also reported, for incident neutron energy of 1 eV. JEFF-3.1 nuclear data library.*

Group #	1	2	3	4	5	6	7	8
Decay constant [s^{-1}]	$1.25 \cdot 10^{-2}$	$2.83 \cdot 10^{-2}$	$4.25 \cdot 10^{-2}$	$1.33 \cdot 10^{-1}$	$2.92 \cdot 10^{-1}$	$6.66 \cdot 10^{-1}$	1.63	3.55
	Effective physical fractions [%] ($\beta_{0,i}/\beta_{0,tot}$)							
U-235	3.4	15.0	9.9	20.0	31.2	9.3	8.8	2.4
U-233	8.0	15.7	13.4	20.9	30.8	3.7	6.2	1.3
Pu-239	2.9	22.5	9.5	14.9	35.1	3.7	9.7	1.7

the neutron diffusion equations (3.19) and (3.22), with the albedo coefficients calculated from SERPENT results.

The bi-conjugate gradient solution algorithm with ILU preconditioning has been used for all equations. A traditional power iteration has been employed for the steady-state nonlinear eigenvalue solution for both the forward and adjoint cases. Here, the fission rate and delayed neutron precursor concentrations from the previous iteration are supplied as source terms for the solution of the multi-group neutron diffusion equation.

Once the forward and adjoint problems have been solved, the effective delayed neutron fractions can be calculated as follows (Mattioda *et al.*, 2000):

$$\beta_{eff,i} = \frac{\int \sum_{g=1}^{6} \phi_g^* \chi_{d,g} \lambda_i c_i}{\int \sum_{g=1}^{6} \phi_g^* \chi_{d,g} \sum_{k=1}^{8} \lambda_k c_k + \int \sum_{g=1}^{6} \phi_g^* \chi_{p,g} \sum_{g'=1}^{6} \phi_{g'} \left(\nu \Sigma_f\right)_{g'}} \tag{3.24}$$

In Figure 3.3, the velocity field and stream lines of the three different cases are presented. On the top left, the axial-symmetric solution of the velocity field obtained with k-epsilon turbulence model is shown for the nominal flow rate conditions in the axial-symmetric MSFR geometry. On the top right, the case study with uniform in-core velocity is shown as representative of conditions of optimized fluid flow path. On the bottom, results obtained in the full-core optimized geometry with the k-epsilon turbulence model are shown. The effects of recirculation vortex and core geometry are discussed in Section 3.3.

3.2.3 Monte Carlo approach

The third approach presented is based on the continuous energy Monte Carlo method. The Monte Carlo code SERPENT-2 has been extended, in order to take into account the presence of a circulating fuel. In common Monte Carlo criticality source simulations, when the emission of a delayed neutron is sampled, this affects only the energy of the new particle, which is sampled according to the emission spectrum of the particular delayed neutron group. In the extended version, the initial position of the new history is corrected according to the fuel velocity field and the delayed neutron emission time, which is sampled according to the group decay constant.

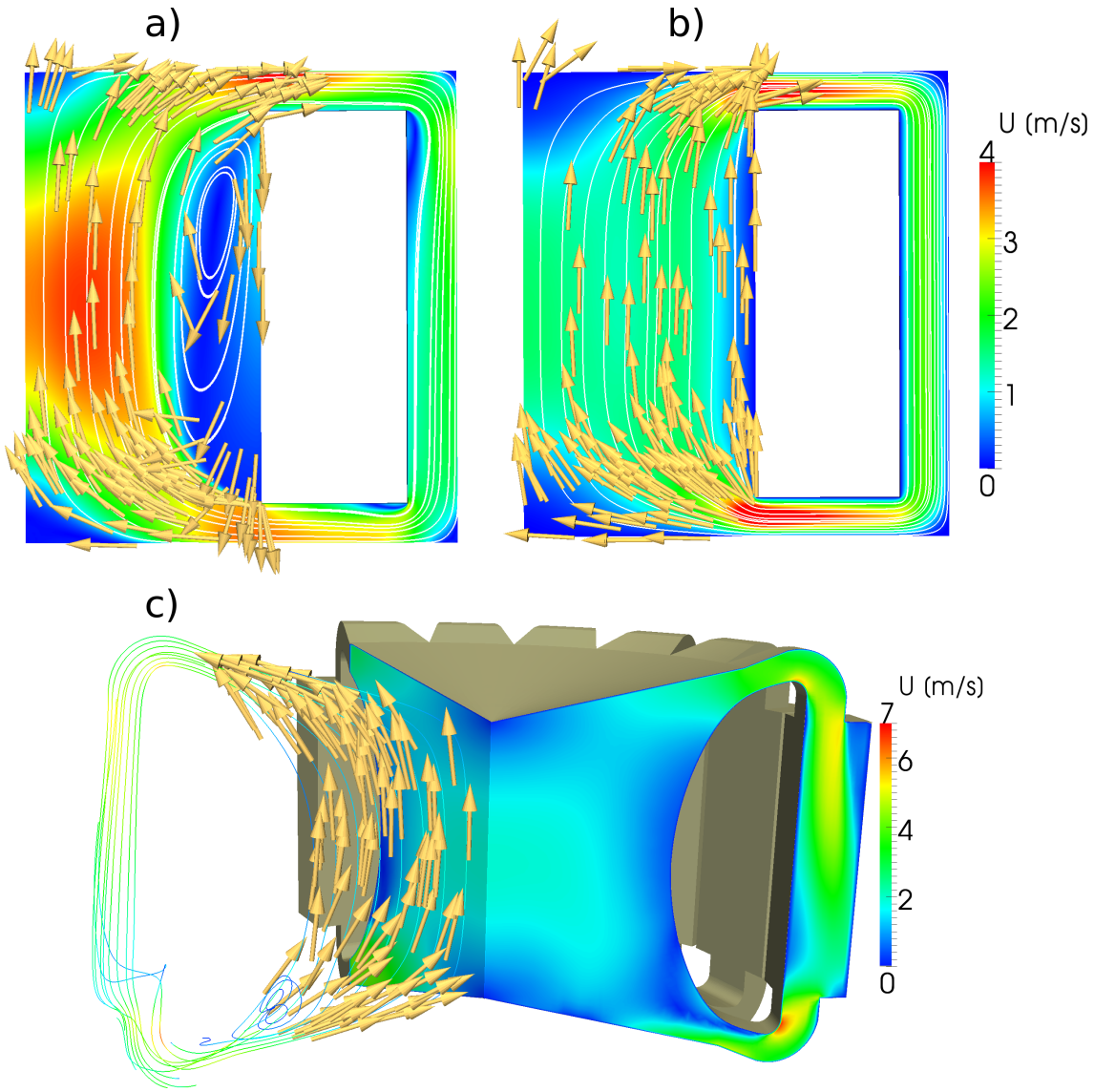

Figure 3.3: *Stream lines and velocity fields of the 3 analysed cases: a) k-epsilon case study b) uniform velocity case study c) optimized geometry, 3D case study.*

As tracking algorithm, a fifth-order Runge-Kutta explicit integrator with embedded fourth-order error estimation is adopted (Dormand and Prince, 1980). The velocity fields employed have been calculated by means of OpenFOAM, adopting the k-epsilon turbulence model, and mapped to an axial-symmetric cartesian mesh. In Table 3.4, the coefficients of the Dormand-Prince algorithm are reported. The adoption of an error estimation technique allows a continuous correction of the tracking time-step, according to the adopted mesh and the input velocity field. In principle, an *a priori* choice of the time-step is a difficult task. Independent of the particular integration algorithm adopted, if too long time-steps are employed, tracking errors might lead to inaccurate results due to a wrong spatial distribution of the delayed neutron source. On the other hand, the adoption of too short time-steps might lead to an unacceptable increase of the computational time. Nonetheless, the choice of the tolerance adopted for error check and adaptive time-stepping, is still a delicate task.

In the following, the algorithm adopted in SERPENT-2 for the transport of delayed neutron precursors is reported:

When the emission of a delayed neutron is sampled:

(1) Sample the delayed neutron group according
to the physical delayed neutron fractions $\beta_{0,i}$

(2) Sample the neutron emission time EM_{time}
according to the decay constant λ_i

(3) Start the precursors tracking loop
$TRK_{time} = 0$
$\Delta t = \Delta t_{zero}$ (initial guess)

(4) while $(TRK_{time} < EM_{time})$

(5) for all the **k** stages of the Dormand-Prince algorithm

(6) Calculate $\mathbf{u}_k^x$, $\mathbf{u}_k^y$, $\mathbf{u}_k^z$ from the Cartesian mesh

(7) Calculate the new precursor position
at the end of the time-step Δt

(8) Calculate the tracking error estimation ERR

(9) if $(ERR < \varepsilon_{min})$
where ε_{min} is a user defined tolerance

(10) Increase the time-step Δt

(11) if $(ERR > \varepsilon_{max})$
where ε_{max} is a user defined tolerance

(12) Reduce the time-step Δt

(13) $TRK_{time} = TRK_{time} + \Delta t$

(14) Sample the new neutron energy
according to the delayed neutron group

Start the new neutron history

Unfortunately, the availability of the correct energy and spatial distribution of the delayed neutrons is not enough to guarantee an accurate estimation of the delayed neutron fraction. As already mentioned, β_{eff} is an adjoint-weighted quantity and can not be es-

Table 3.4: *Butcher table of the adopted explicit Runge-Kutta integrator (Dormand and Prince, 1980), with embedded error estimator.*

c_i	a_{ij}						
0							
1/5	1/5						
3/10	3/40	9/40					
4/5	44/45	-56/15	32/9				
8/9	19372/6561	-25360/2187	64448/6561	-212/729			
1	9017/3168	-355/33	46732/5247	49/176	-5103/18656		
1	35/384	0	500/1113	125/192	-2187/6784	11/84	
b_i	35/384	0	500/1113	125/192	-2187/6784	11/84	0
b_i^*	5179/57600	0	7571/16695	393/640	-92097/339200	187/2100	1/40

timated by means of a simple criticality source simulation. A detailed review of the different techniques for effective delayed neutron fraction calculation in Monte Carlo can be found in the references (e.g., Meulekamp and van der Marck, 2006; Nagaya *et al.*, 2010). In the following, two of the most commonly adopted methods and their applicability are briefly discussed.

Often, β_{eff} is estimated through the "prompt" method. This method involves two separated Monte Carlo simulations, with and without the production of delayed neutrons. The effective delayed neutron fraction is then approximated as:

$$\beta_{eff} \simeq 1 - \frac{k_p}{k_{eff}} \tag{3.25}$$

where k_{eff} is the effective multiplication factor of the reference case and k_p is the effective multiplication factor of the simulation without delayed neutrons.

This method can be easily adopted without any modification of the available Monte Carlo codes but requires a relatively high amount of computational resources. Due to the fact that the effective delayed neutron fraction is obtained by comparison of two separate runs, to have a relative statistical error on β_{eff} in the order of 1%, k_{eff} estimations with an accuracy of few pcm are required. Moreover, if the effective contributions of the different delayed neutron groups need to be investigated, the "prompt" method looses any applicability due to the presence of $\beta_{eff,i}$ fractions as low as few pcm, whose contributions would be highly covered by uncertainty in k_{eff} and k_p estimations.

Other approaches, which employ a single simulation and involve the approximation of the adjoint weighting function, have been developed. The Meulekamp and van der Marck (2006) method approximates the neutron importance to the probability of producing a fission (next fission probability). It captures very well the difference in importance between prompt and delayed neutrons due to energy spectra but is not suitable when relevant spatial effects are present (Nagaya *et al.*, 2010) and gives wrong results in circulating-fuel conditions.

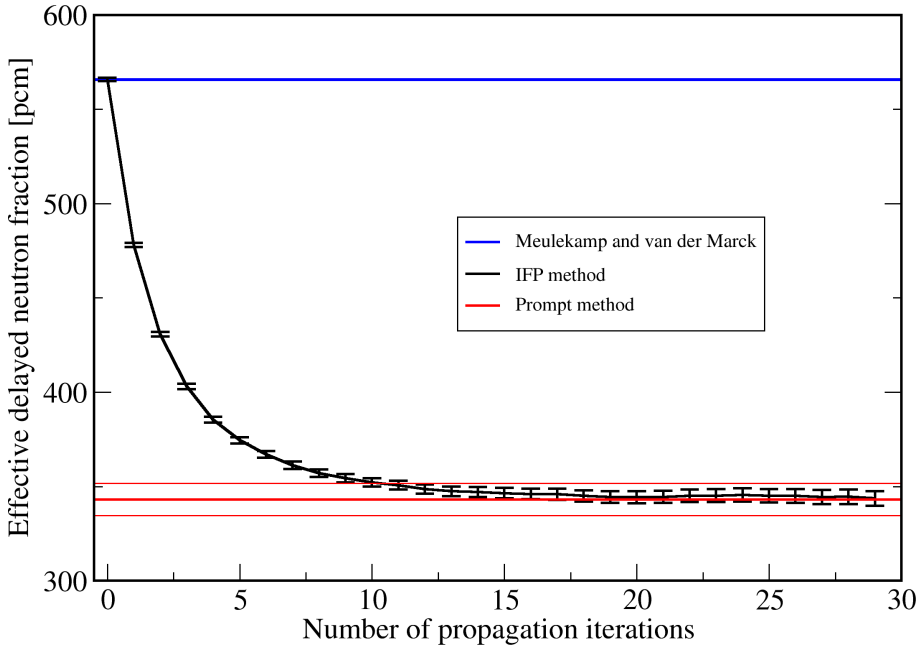

Figure 3.4: *Comparison between IFP, "prompt" and Meulekamp methods (U235-started, k-epsilon case study; nominal flow rate).*

For this reason, the Iterated Fission Probability (IFP) method (Nauchi and Kameyama, 2010; Kiedrowski *et al.*, 2011) has been implemented in SERPENT-2. This method allows to calculate directly adjoint-weighted quantities. In Figure 3.4, the comparison between the different β_{eff} estimations is shown. Results are relative to the MSFR nominal conditions (k-epsilon case study). The IFP method converges to the "prompt" method in about 20 latent generations. The Meulekamp and van der Marck (2006) method fails to give a good approximation of β_{eff}. A brief discussion of the IFP method implementation in SERPENT-2 can be found in Section **??** of the Appendix.

In order to better compare the analytical results with Monte Carlo simulations in the limit of infinite fuel velocity ($\lambda T \rightarrow 0$), a further modification of the code has been implemented. As already discussed, in case of infinite fuel velocity, any precursors that is produced has a uniform decay probability in the whole fuel loop. In this case, the starting positions of the delayed neutrons are uniformly sampled in the entire reactor geometry. If the sampled point is in the fuel circuit, the position is accepted and the new neutron history is started. If the sampled point falls in a different material (e.g., reflector, neutron shield, etc.), the position is rejected and new random coordinates are extracted.

The MSFR features the presence of radial blankets constituted by a mixture of Thorium-fluoride and Lithium-fluoride. Recent studies highlighted the necessity to actively remove the energy released in the blanket material by flowing the fluid in an external circuit. At present, no detailed studies are available on this subject. However, only few fissions occur in the blanket and few delayed neutrons are produced there. Moreover, these neutrons feature a very low importance because are likely to undergo radiative capture in the fertile material. For these reasons, precursor motion is neglected in the blanket material, and any delayed neutron produced there is emitted in the position of the originating fission event.

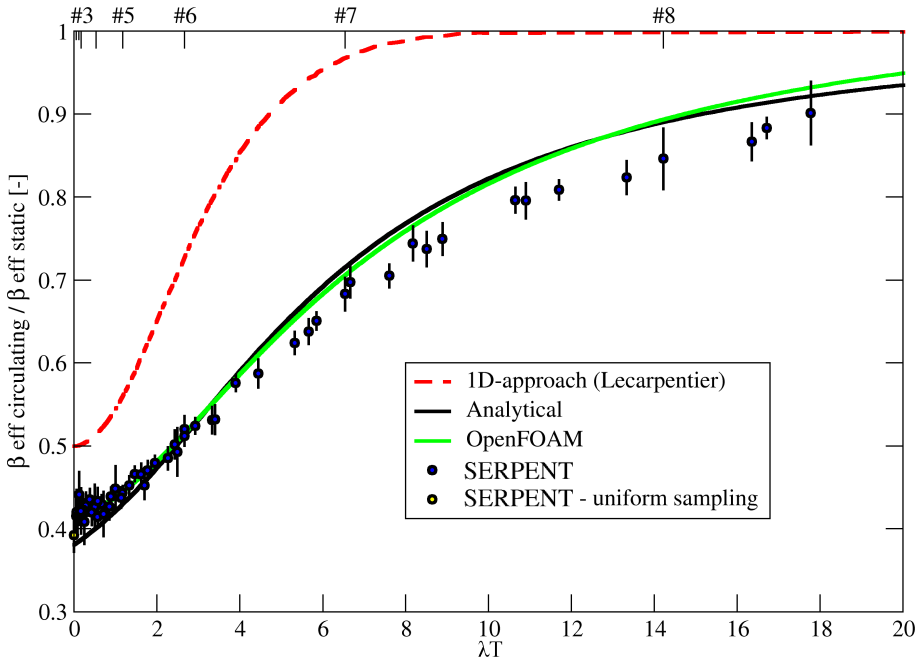

Figure 3.5: *Correction factor: comparison between analytical approach, SERPENT and OpenFOAM (uniform velocity case study).*

3.3 Numerical results

In this Section, the presented approaches are adopted to calculate the effective delayed neutron fraction in the Molten Salt Fast Reactor.

In Figure 3.5, the correction factor calculated by means of the three proposed approaches is presented, as function of the dimensionless parameter λT (see Section 3.2.1). Results are relative to the uniform velocity case study (see Figure 3.3). Results show good agreement over a wide range of λT values. It is clear that, in this case, even a simple analytical approach is able to accurately estimate the effective delayed neutron fraction, provided that a correct spatial adjoint-weighting function is adopted. For comparison, results from one of the commonly adopted 1-D approach (non adjoint-weighted) are presented[1](Lecarpentier, 2001). This and other similar methods overestimate the correction factor over the whole range of λT values, with relative errors up to 20$\sim$30%. For small values of λT, precursors are tracked for several loops over the fuel circuit in the Monte Carlo approach. In this case, tracking errors accumulate and a small bias in the estimation may arise. Nonetheless, the limit for $\lambda T \rightarrow 0$ can be studied with a simplified algorithm (see Section 3.2.3). The yellow dot shows the IFP estimation of the β_{eff} correction factor obtained with uniform sampling of the delayed neutron position in the fuel. In this case, the three methods are again in good agreement. In the top of the plot, the positions of delayed neutron constants of the JEFF-3.1[2]library are shown for a circulating period of 4 seconds (nominal MSFR flow rate).

In Figure 3.6, results from the k-epsilon case study with axial-symmetric geometry are presented. In this case, the analytical estimations significantly differ from those of

[1]Similar results were obtained also at Politecnico di Milano (e.g., see Guerrieri *et al.*, 2012)

[2]Please note that this library adopts 8 groups of delayed neutron precursors with fixed decay constants for all the Actinides.

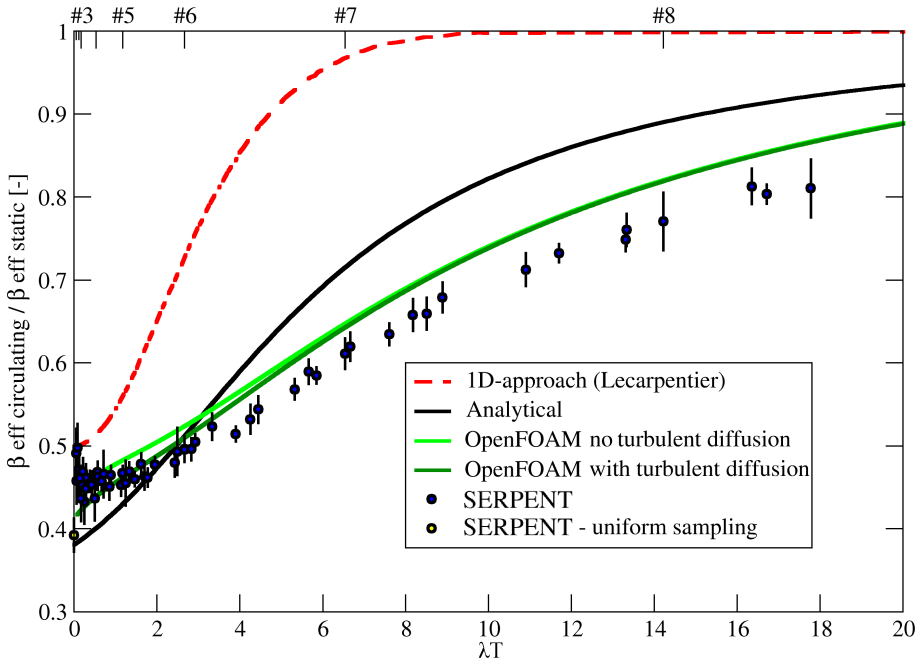

Figure 3.6: *Correction factor: comparison between analytical approach, SERPENT and OpenFOAM (k-epsilon case study).*

OpenFOAM and SERPENT. This is due to the inability of the simplified approach to capture the effects of in-core fuel recirculation (see Figure 3.3), both at high and low values of λT.

These results help in the interpretation of the effect of recirculation vortex on β_{eff}. At low λT (high recirculation velocity), the main effect is the higher in-core retention of precursors (see Figure 3.7). Precursors are "trapped" in the core and this leads to higher values of the effective delayed neutron fractions for slow-decaying groups, even if the recirculation zone presents a relatively low importance. For high values of λT, most of the precursors would decay inside the core independently of the presence of the vortex. In this case, the main effect of the vortex is the increase of the "effective" fuel velocity at core center (for a given flow rate). This leads to a faster removal of precursors from central zones of high neutron importance and the effect is a reduced $\beta_{eff,i}$ for fast-decaying groups.

In Figure 3.7, the concentration (top) and importance (bottom) of delayed neutron precursors are shown for different values of the dimensionless parameter λT. In the recirculation zone, the increase in both concentration and importance of delayed neutron precursors is evident for low values of λT.

In Figure 3.8, the effect of turbulent diffusion is analysed. The turbulent Schmidt number Sc_T is the ratio between the eddy viscosity and the eddy diffusivity and is adopted to take into account the effects of turbulent mixing (i.e., equivalent of Pr_T for mass transport). Uncertainties are present both in the evaluation of the turbulent viscosity field by means of RANS turbulence models and in the choice of an appropriate value for Sc_T. For this reason, a sensitivity to the effect of turbulent diffusion is presented for the nominal flow rate conditions. The main effect of turbulent diffusion is to reduce the retention of delayed neutron precursors in the recirculation zone. This leads to a decrease of the ef-

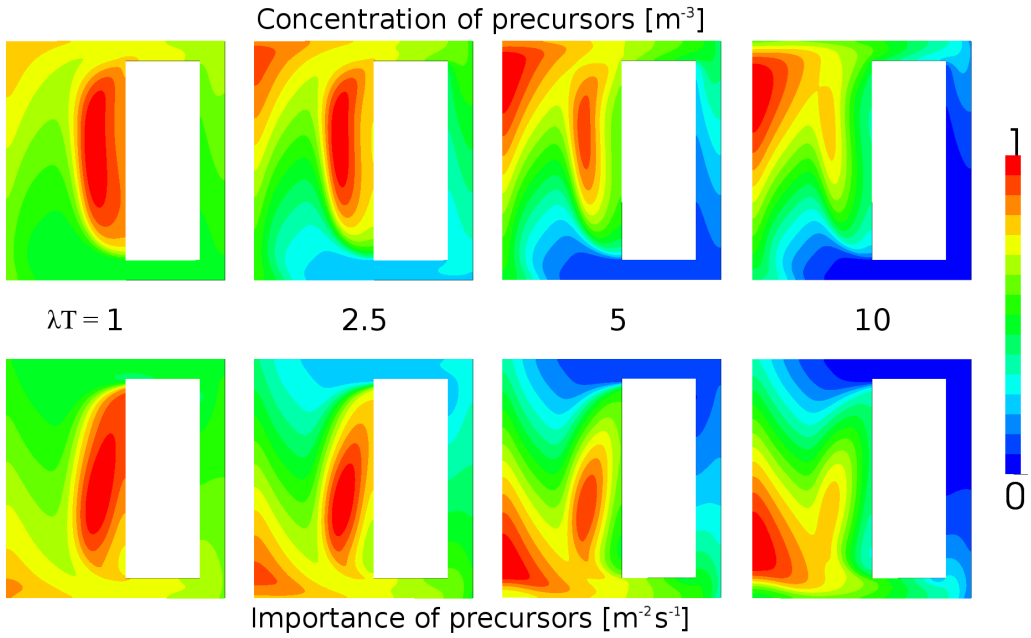

Figure 3.7: *Precursor concentration and importance for the k-epsilon case study for different values of the dimensionless parameter λT (OpenFOAM; arbitrary units).*

fective delayed neutron fraction for low Sc_T values, as delayed neutron are more likely to be emitted in the out-of-core part of the fuel loop. The effect of the turbulent diffusion term becomes very small in case of no recirculation vortex. Nonetheless, the analysed case studies highlight the important role of fluid flow modelling inside the reactor core. A proper solution of the in-core flow path (e.g., by means of CFD simulations) appears to be a first mandatory step, while calculating the effective delayed neutron fraction in circulating fuel reactors.

The adoption of the dimensionless parameter λT allows a better comprehension of the phenomena governing the reduction of the effective delayed neutron fraction and ensures a more accurate comparison between different approaches. Nonetheless, while studying the reactor behaviour, the expression of β_{eff} as function of the fuel flow rate might lead to more useful results. These data can be used to estimate the reactivity insertion/extraction as consequence of operational or accidental change in the behaviour of fuel pumps.

In Figure 3.9, the effective delayed neutron fraction is plotted against the flow rate and circulation time. Around nominal flow rate conditions (about 4 seconds of recirculation time), the reactivity loss due to fuel circulation is close to saturation and only little reactivity is inserted/removed by small variation of the flow rate. At higher recirculation time, little modifications in the operating conditions cause high reactivity insertion/removal. OpenFOAM results show a good agreement with Monte Carlo estimations. SERPENT-2 calculations adopting the IFP method are always statistically compatible with the more expensive results of the "prompt" method. Starting from nominal flow rate, the failure of the pumps might lead to the slow insertion of slightly more that 350 pcm of reactivity if stagnation conditions are reached at the end of the transient. Predictions of the analytical approach can be considered a good approximation over the range between static fuel and nominal conditions, also because the errors due to fuel recirculation shown before for fast

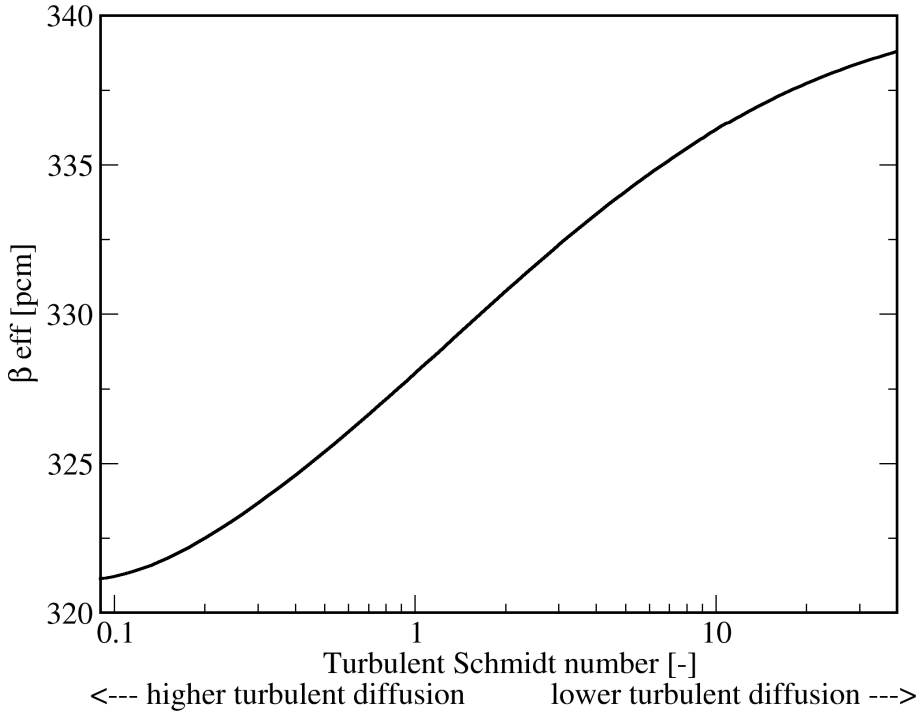

Figure 3.8: *Effective delayed neutron fraction as function of the turbulent Schmidt number Sc_T (U235-started, k-epsilon case study; nominal flow rate; OpenFOAM).*

and slow groups partially compensate each other.

The adoption of the IFP method allows a computationally "cheap" estimation of the single effective delayed neutron fractions $\beta_{eff,i}$. In Figures 3.10 and 3.11, the $\beta^c_{eff}/\beta^s_{eff}$ correction factor is shown for the different delayed neutron groups of the JEFF-3.1 library as function of the MSFR flow rate. At the top of the plots, the corresponding fuel loop circulation time (T) is shown. For better clarity, the groups are divided in "slow" and "fast". In Figure 3.10, only the interval $0 \div 10\%$ of the flow rate is shown. Slower groups reach their saturation values already at very low flow rate. At nominal conditions, the correction factor is significantly greater than 0.5 only for groups 7 and 8.

In Figure 3.12, delayed neutron fraction values are shown for different fuel compositions. The reduction in the values from β_{zero} to β^s_{eff} is due to differences in the energy spectra of prompt and delayed neutrons and is well captured by the Meulekamp and van der Marck (2006) method already available in SERPENT. In order to catch the effect of fuel motion, appropriate techniques are required (e.g., "prompt" or IFP methods). Energy effects are smaller and are dependent on the isotopic composition of the fissile material. Spatial effects are dominant and have a minor dependence on the fuel composition. In particular, $\beta^c_{i,eff}/\beta^s_{i,eff}$ correction factors calculated for the different delayed neutron groups can be considered of a certain generality, because the decay constants λ_i of the JEFF-3.1 library are not dependent on the fuel composition. Moreover, spatial and energy effects may be separated as first approximation, in the case of the MSFR.

In Figure 3.13, the spatial dependency of the delayed and prompt neutron source is shown as calculated with OpenFOAM for the 3D optimized MSFR core shape at nominal flow rate conditions. The delayed neutron source is calculated as sum over the eight delayed neutron groups. The upward shift of the fast decaying precursors is evident. The

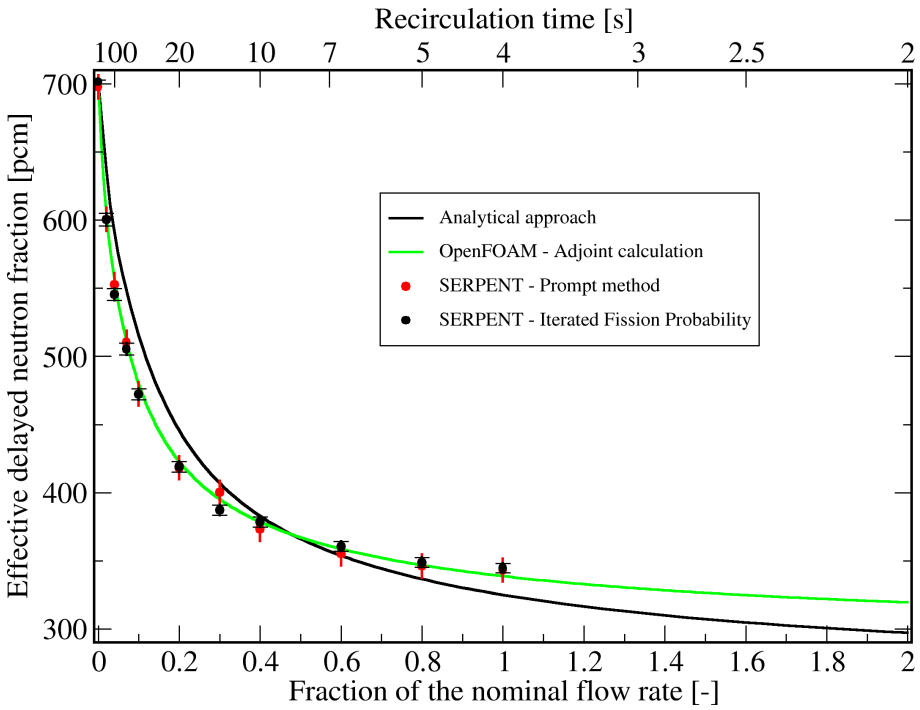

Figure 3.9: *Effective delayed neutron fraction in the MSFR as function of the flow rate: comparison between analytical approach, SERPENT and OpenFOAM (U235-started, k-epsilon case study; no turbulent diffusion).*

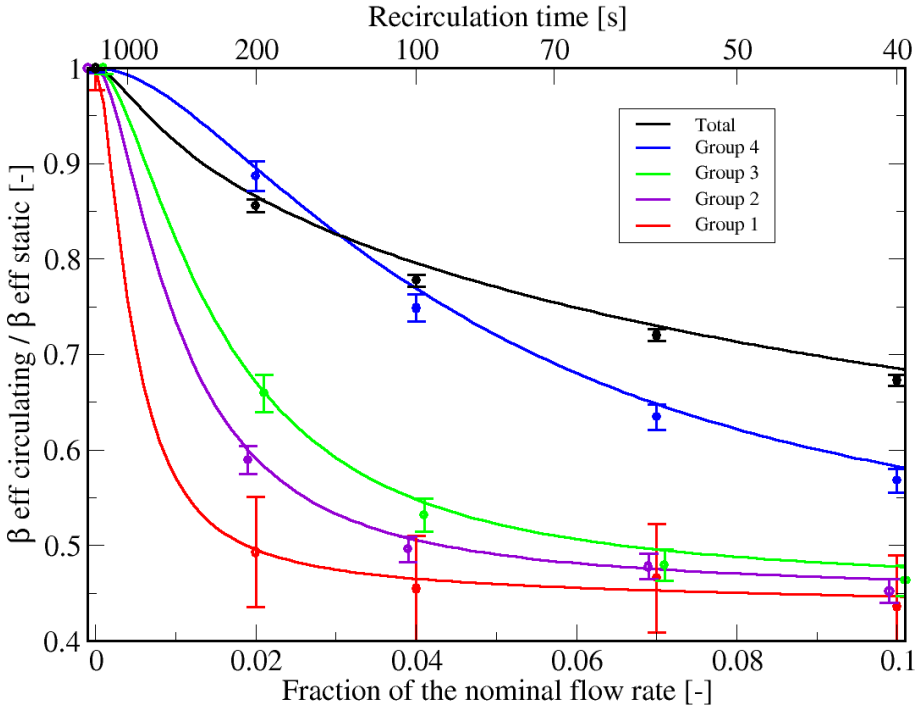

Figure 3.10: $\beta^c_{i,eff}/\beta^s_{i,eff}$ *correction factors. Solid line: OpenFOAM; dots: SERPENT (U235-started, k-epsilon case study; no turbulent diffusion).*

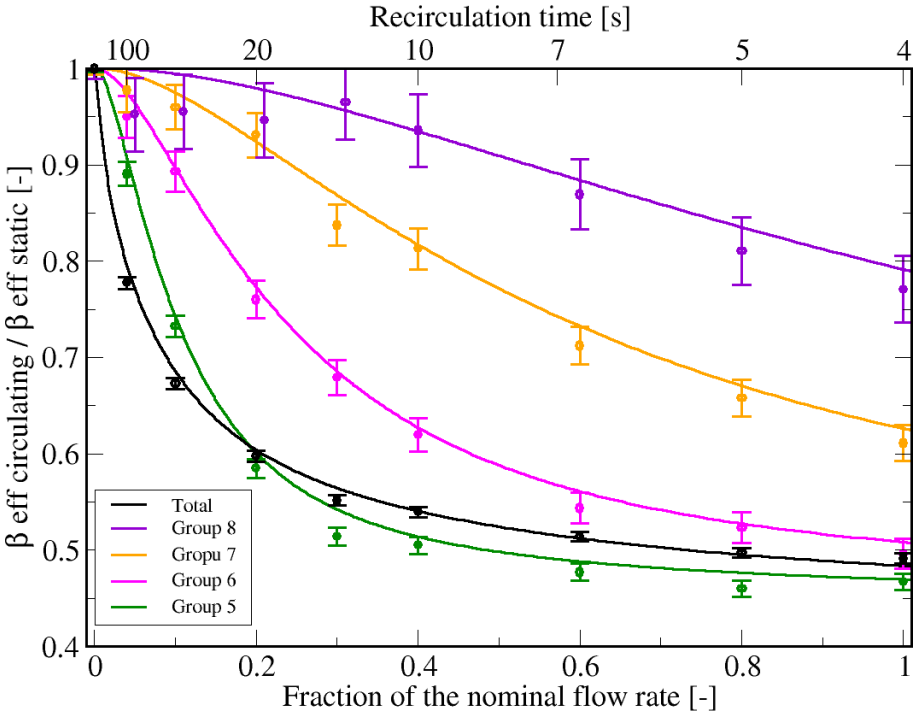

Figure 3.11: $\beta^c_{i,eff}/\beta^s_{i,eff}$ *correction factors. Solid line: OpenFOAM; dots: SERPENT (U235-started, k-epsilon case study; no turbulent diffusion).*

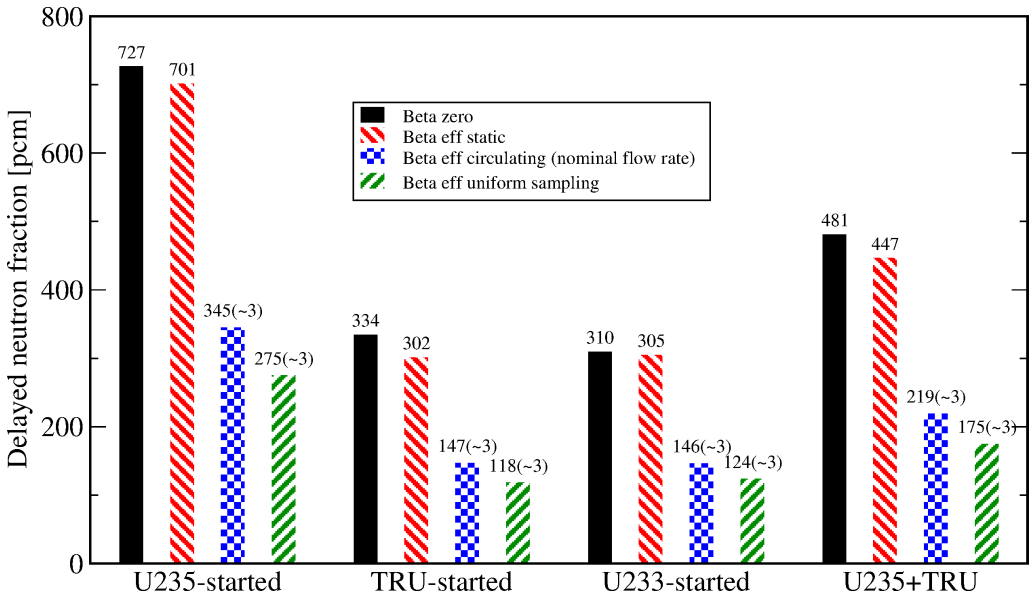

Figure 3.12: *Delayed neutron fractions in the MSFR for different fuel compositions.*

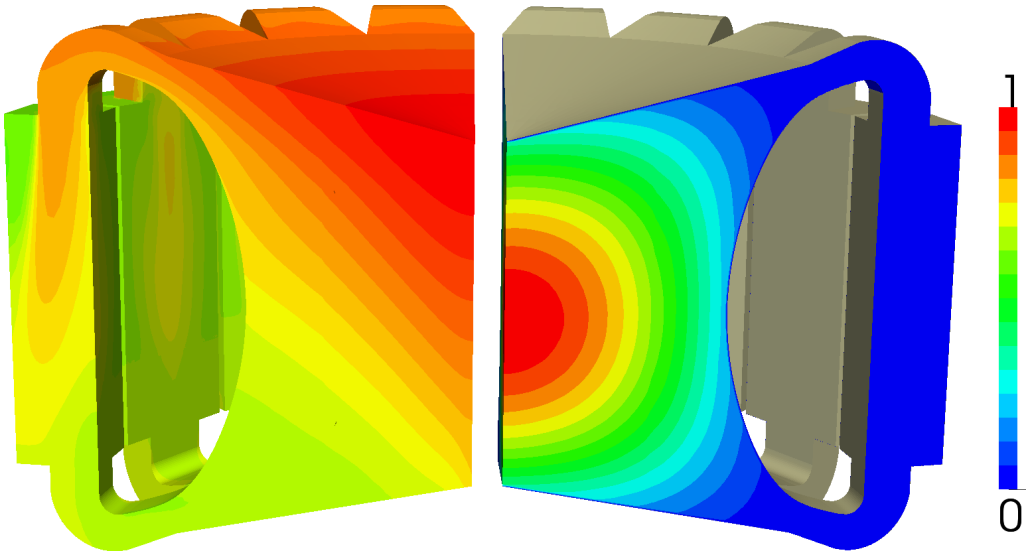

Figure 3.13: *Spatial distribution of the delayed (left) and prompt (right) neutron sources at nominal flow rate (arbitrary unit; OpenFOAM; optimized geometry, 3D case study; nominal flow rate).*

Table 3.5: *Effective delayed neutron fraction in the optimized geometry for different flow rates. Comparison between OpenFOAM and the analytical approach (U235-started, optimized geometry, 3D case study).*

Frac. of the flow rate [-]	Recirc. time [s]	OpenFOAM β_{eff} [pcm]	Analytical – $\gamma = 0.5$ β_{eff} [pcm]	rel. diff.	Analytical – $\gamma = 0.44$ β_{eff} [pcm]	rel. diff.
0.3	13.3	370.6	407.2	(+9.88%)	378.2	(+2.05%)
0.5	8	335.1	366.3	(+9.31%)	335.4	(+0.09%)
0.7	5.7	316.4	344.4	(+8.85%)	312.7	(–1.17%)
0.85	4.7	307.0	333.4	(+8.56%)	301.3	(–1.86%)
1	4	299.8	325.1	(+8.44%)	292.7	(–2.37%)
1.15	3.5	294.3	318.4	(+8.19%)	285.9	(–2.85%)
1.3	3.1	289.8	313.1	(+8.04%)	280.4	(–3.24%)
1.5	2.7	285.0	307.3	(+7.82%)	274.5	(–3.68%)

absence of in-core recirculation paths avoids precursors retention near reactor radial wall, as found in results related to the cylindrical axial-symmetric case study.

The optimized geometry and the simple cylindrical geometry have the same nominal in-core-to-total volume ratio (∼50 %). The definition of "in-core" is problematic in this kind of reactors. In the out-of-core part of the fuel circuit the neutron flux is several order of magnitude lower than the average value of the core. Nonetheless, the transition between the two zones is not sharp and defined as in solid-fuelled reactors or even graphite-moderated molten salt reactors. For simplicity, the core volume is often considered as the whole region between piping inlets and outlets, having a volume of approximately 9 m^3 for both the reference cylindrical and the optimized MSFR geometry. On the other hand, in Figure 3.13, high leakage zones near core inlets and outlets with low neutron flux can be appreciated. If we consider as "in-core" volume the region having a scalar neutron flux equal or greater than the 5% of the peak value, significant differences between the two geometries arise. The effective core volume calculated in this way results to be about 9.18 m^3 for the cylindrical axial-symmetric geometry and 7.92 m^3 for the optimized geometry, and the effective in-core-to-total volume ratio are 51% and 44%, respectively.

In Table 3.5, the results of the OpenFOAM simulations in the optimized geometry for different flow rates are presented. As discussed in Section 3.2, the analytical approach has been derived under the hypotheses of cylindrical core and uniform in-core axial velocity and does not allow for turbulent diffusion. Nonetheless, analytical results show a relative error with respect to OpenFOAM lower than 10% in the wide range from 0.3 to 1.5 of the nominal flow rate. If the effective in-core-to-total volume ratio calculated above (44%) is adopted, errors of about 3% are achieved.

3.4 Concluding remarks

The effective delayed neutron fraction is an important reactor kinetics parameter, whose calculation is particularly difficult in circulating-fuel reactors. A correct importance-weighting of the delayed neutron source has proved necessary to achieve accurate results. Approximate techniques have been often adopted in the literature, which proved inaccurate in the considered case study of the Molten Salt Fast Reactor. In this Chapter, three different approaches have been presented and adopted to study the MSFR with different geometry and flow rate conditions. The extension of the continuous energy Monte Carlo code SERPENT-2 involves the tracking of precursors according to an input velocity field. The effective delayed neutron fraction in circulating-fuel conditions is then calculated adopting the Iterated Fission Probability method. A deterministic approach is presented as well, which is based on the OpenFOAM multi-physics finite-volume tool-kit, and involves the solution of the multi-group diffusion forward and adjoint eigenvalue problems. The solver allows for the convective and turbulent diffusive terms in the delayed neutron precursors balance. An analytical formula for the circulating-to-static effective delayed neutron fraction correction factor is also presented. The formula is derived under simple hypotheses for cylindrical geometries. It takes into account the effect of the fuel motion on the effective delayed neutron fraction due to the non-uniform spatial neutron importance.

Results of the comparison show a good agreement between the Monte Carlo and the deterministic approach in the three analysed case studies. The analytical formula shows close agreement with OpenFOAM for the case study with simple geometrical and velocity field conditions. However, it offers a good approximation even in conditions far from the hypotheses under which it was derived, and gives better results than the commonly adopted analytical approaches (without importance weighting) in all the analysed cases.

The effect of in-core flow recirculation has been studied, revealing that it is responsible of a relevant increase of the effective delayed neutron fraction, due to in-core retention of slow-decaying precursors. β_{eff} revealed to be dependent on the particular geometry and flow conditions. At nominal flow rate, differences of about 10 % have been found for the analysed case studies with the same nominal in-core-to-total volume ratio of 50 %. Results highlighted the importance of a proper solution of the fluid flow inside the core for an accurate calculation of the effective delayed neutron fraction.

Nomenclature

	Latin symbols
c	Concentration of delayed neutron precursors [m^{-3}]
c^*	Importance of delayed neutron precursors [$m^{-2}s^{-1}$]
cf_{circ}	Correction factor for the effective delayed neutron fraction defined in Equation 3.1 [-]
D	Diffusion coefficient [m]
$D(\mathbf{r}')$	Space dependence of the delayed neutron precursors decay probability [-]
D_T	Turbulent mass diffusivity [m^2s^{-1}]
H_a	Active height [m]
H_e	Extrapolated height [m]
	Space dependence of the precursors importance [-]
$I(\mathbf{r}')$	Space dependence of the neutron importance [-]
$K(\mathbf{r}', \mathbf{r})$	Conditional precursor decay probability [-]
k_{eff}	Effective multiplication factor [-]
k_p	Effective multiplication factor without delayed neutrons [-]
Pr_T	Turbulent Prandtl number [-]
r	Radial coordinate [m]
R_a	Active radius [m]
R_e	Extrapolated radius [m]
$S(\mathbf{r})$	Space dependence of the precursors source [-]
Sc_T	Turbulent Schmidt number [-]
T	Fuel circulation period [s]
$\mathbf{u}$	Fuel velocity field [m s^{-1}]
z	Axial coordinate [m]
	Greek symbols
β_0	Total physical delayed neutron fraction [-]
β_{eff}	Total effective delayed neutron fraction [-]
γ	In-core-to-total fuel volume ratio [-]
λ	Decay constant of precursors [s^{-1}]
ν	Average total number of neutron emitted per fission [-]
ν_T	Eddy viscosity [m^2s^{-1}]
Σ_a	Absorption cross section [m^{-1}]
Σ_f	Fission cross section [m^{-1}]
Σ_s	Scattering cross section [m^{-1}]
ϕ	Forward neutron flux [$m^{-2}s^{-1}$]
ϕ^*	Adjoint neutron flux [$m^{-2}s^{-1}$]
χ_p	Delayed neutron yield [-]
χ_p	Prompt neutron yield [-]
	Superscripts
c	Relative to circulating-fuel conditions
s	Relative to static-fuel conditions
	Subscripts
d	Relative to delayed neutrons
g	Relative to the g^{th} neutron energy-group
i	Relative to the i^{th} delayed neutron precursor group
p	Relative to prompt neutrons

Acronyms

CFD	Computational Fluid-Dynamics
EVOL	Evolution and Viability Of Liquid fuel fast reactor systems
IFP	Iterated Fission Probability
LWR	Light Water Reactor
MCNP	Monte Carlo N-Particle transport code
MSFR	Molten Salt Fast Reactor
MSRE	Molten Salt Reactor Experiment
OpenFOAM	Open-source Field Operation And Manipulation
PWR	Pressurized Water Reactor
RANS	Reynolds-Averaged Navier–Stokes
TRU	Transuranic elements

Octave/Matlab script for the numerical computation of Equation 3.5

"circulating_beta_eff_correction_factor.m"

```
H = 2.24;                       %core height
R = 1.12;                       %core radius
He = 2.6;                       %extrapolated height
Re = 1.3;                       %extrapolated radius
gam = 0.5;                      %in-core-to-total volume ratio
ndisc = 250;                    %discretization for numerical integration

rr = 0:(R/ndisc):R;             %radial coordinate for numerical integration
zz = -(H/2):(H/ndisc):H/2;      %axial coordinate for numerical integration
zzp = -(H/2):(H/ndisc):(H/2);

%integral calculation for static-fuel case (lambdaT -> inf)
den_r = 2*pi .* rr .* (besselj(0,(rr .* 2.404825 ./ Re))).^2;
int_den_r = (R/ndisc)/2 * sum(den_r(2:length(den_r)) + den_r(1:(length(den_r)-1)));

den_z = (cos(pi .* zz ./ He)).^2;
int_den_z = (H/ndisc)/2 * sum(den_z(2:length(den_z)) + den_z(1:(length(den_z)-1)));

int_den = int_den_r * int_den_z;

%correction factor calculation for infinite_velocity case (lambdaT -> 0)
prod_r = 2*pi .* rr .* (besselj(0,(rr .* 2.404825 ./ Re)));
int_prod_r = (R/ndisc)/2 * sum(prod_r(2:length(prod_r)) + prod_r(1:(length(prod_r)-1)));

prod_z = (cos(pi .* zz ./ He));
int_prod_z = (H/ndisc)/2 * sum(prod_z(2:length(prod_z)) + prod_z(1:(length(prod_z)-1)));

int_prod = int_prod_r * int_prod_z;
int_imp = int_prod;

num_inf_vel = int_imp * int_prod * gam / (pi*R^2*H);

cf_inf_vel = num_inf_vel / int_den;

%correction factor calculation for finite values of lambaT
vector of lambdaT values
lambdaT_vec = [0.1:0.1:20];
cf_vec = zeros(size(lambdaT_vec));

%loop over lambdaT
for i=1:1:(length(lambdaT_vec))
        lambdaT = lambdaT_vec(i);

        %from second loop on: uniform radial probability (p2)
        f_p2 = (prod_z' * prod_z) .* exp(-lambdaT.*gam.*((ones(size(zz))' * zz) - (zzp' *
             ones(size(zzp))))./H);
        int_p2 = ((H/ndisc)^2)/4 * sum(sum(f_p2(1:(length(zz)-1),1:(length(zzp)-1)) +
             f_p2(2:(length(zz)),1:(length(zzp)-1)) + f_p2(1:(length(zz)-1),2:(length(zzp))) +
             f_p2(2:(length(zz)),2:(length(zzp))))) * (lambdaT*gam/(exp(lambdaT)-1)) * int_prod_r *
             int_prod_r / (pi*R^2*H);

        %first loop (if zzp >= zz): same radial coordinate (p1)
        f_p1 = (prod_z' * prod_z) .* exp(-lambdaT.*gam.*((ones(size(zzp))' * zzp) - (zz' *
             ones(size(zz))))./H) .* (triu(ones(size(f_p2)),0) + triu(ones(size(f_p2)),1))./2;
        int_p1 = ((H/ndisc)^2)/4 * sum(sum(f_p1(1:(length(zz)-1),1:(length(zzp)-1)) +
             f_p1(2:(length(zz)),1:(length(zzp)-1)) + f_p1(1:(length(zz)-1),2:(length(zzp))) +
             f_p1(2:(length(zz)),2:(length(zzp))))) * lambdaT * gam * int_den_r / H;

        %vector of circulating beta_eff correction factors
        cf_vec(i) = (int_p1 + int_p2)/int_den;
end

%add infinite velocity case
lambdaT_vec = [0 lambdaT_vec];
cf_vec = [cf_inf_vel cf_vec];

%save results
results = [lambdaT_vec' cf_vec'];
save results.dat results;

%plot circulating correction factor
plot(lambdaT_vec, cf_vec);
```

To deny a rebirth of nuclear energy is to deny human ingenuity and aspiration. This I cannot do. During my life I have witnessed extraordinary feats of human ingenuity. I believe that this struggling ingenuity will be equal to the task of creating the Second Nuclear Era. My only regret is that I shall not be here to witness its success.

Alvin Weinberg – "The First Nuclear Era"

Conclusions

MOLTEN Salt Reactors present several interesting characteristics which make them one of the most promising options for fuel cycle closure and reactor safety enhancement. The presence of a liquid fuel is one of the unique distinguishing features of these reactors, and represents one of the most challenging aspects of reactor analysis.

Throughout the thesis work, advanced modelling tools for circulating-fuel reactors have been developed and assessed. The main focus has been on efficient and consistent implementation of simulation methods, trying to avoid some of the restrictions that are sometimes present in commonly available tools.

The Monte Carlo code SERPENT-2 has been extended for the simulation of material isotopic evolution in MSRs. The extension is capable to correctly model the peculiarities of MSR fuel-cycle, namely: on-line reprocessing and reactivity control via fuel addition. Moreover, an accelerated equilibrium search algorithm has been introduced, with the purpose of minimizing the Monte Carlo transport cycles required to reach an accurate estimation of the steady-state composition. The extension proved to be computationally competitive even with traditionally fast-running codes, based on less accurate deterministic transport, and not featuring any accelerated equilibrium search technique.

A new multiphysics solver has been developed for the MSFR transient analysis, adopting the finite-volume library OpenFOAM. The solver features the adoption of efficient and consistent time integration techniques, which allow to fully catch the strong feedbacks that emerge in the coupling of the different physics. The main purpose of the model is to serve as fast-running computational tool in the ongoing phase of design optimization of core and fuel loop components of the MSFR. The solver has been assessed against previous tools, showing a good agreement and a significant reduction of the computational requirements.

A detailed investigation of the effective delayed neutron fraction in circulating-fuel reactors has been performed by means of analytical, deterministic and Monte Carlo approaches. This has been achieved via the development of new tools for the calculation of adjoint-weighted quantities, in combination with delayed neutron precursor drift. The OpenFOAM solver has been extended to solve the forward and adjoint multi-group diffu-

sion eigenvalue problems, accounting for fuel motion. Monte Carlo solutions have been also achieved via an extension of the SERPENT code, which features precursor tracking capabilities and adjoint-weighting through the Iterated Fission Probability method. An analytical formula has been derived as well. Despite the simple assumptions adopted, it is able to correctly catch the effect of inhomogeneous spatial neutron importance in the core.

The presented methods can be considered of general interest in the analysis of MSRs. Nonetheless, the development of these tools has been carried out in parallel with the analysis of the Molten Salt Fast Reactor, and focusing on its peculiarities (e.g., the fast neutron spectrum and the absence of internal core structures), especially in the multiphysics modelling approach. The new models helped in the understanding and clarification of some issues related to the MSFR system. Here below, a few results are briefly summarized, focusing on those more relevant in the framework of the EVOL Project, and those in contrast with the outcomes of recent works:

- The uncertainty in the (n,γ) cross-section of the U-233 in the energy region of interest for the MSFR is found to greatly affect the main results related to the MSFR fuel cycle. A simple comparison between JEFF-3.1 and ENDF/B-VII libraries showed that the minimum reprocessing rate required for the iso-breeding conditions, and the doubling time in nominal conditions are both affected by an uncertainty greater than 50-60%.

- Simplified analytical or one-dimensional tools, commonly adopted for transient- and control-oriented modeling, are found to overestimate the effective delayed neutron fraction in the MSFR of about 10-20% in the considered range of operating conditions.

- Large in-core recirculation zones were thought to have a detrimental effect on the β_{eff} of the MSFR. Actually, the adjoint-weighted calculations presented in this thesis show that their presence leads to a small increase of the delayed neutron fraction in nominal conditions.

- The "toroidal" MSFR optimized core shape adopted to avoid recirculation and temperature hot spots is featured by a lower β_{eff} (about 15%), with respect to the previous cylindrical geometry.

- The minimum effective reprocessing rate required to accomplish with solubility limit of the fuel salt mixture in the MSFR is found to be around 5 to 6 liters per day.

- Despite the relatively fast spectrum, the (n,α) reaction on Ni-59, produced via (n,γ) reaction on Ni-58, is found to highly contribute to the helium production in the core structural materials.

Numerous possible extensions of the present work are desirable. In the nominal MSFR conditions, a certain fraction ($\sim 1\%$) of the core volume is occupied by small gas bubbles. In these conditions, the fuel mixture is likely to present a relatively high compressibility and a very low speed of sound (compared to the pure fuel salt). In case of low-Doppler fuel compositions, a certain delay in the salt expansion feedbacks is expected to affect the reactor response to super-prompt-critical reactivity insertions. In this direction, consistent

transient analyses are desirable, at least to exclude any meaningful difference with respect to incompressible simulations.

Special accidental transients (e.g., those involving localized core voiding) are not suitable to be studied with the neutron diffusion approximation. Multiphysics models based on more accurate neutronics treatment are also desirable for the analysis and optimization of smaller and more heterogeneous reactors, envisaged as demonstrators of the MSFR technology.

As it has been pointed out, the uncertainties of the nuclear data need to be evaluated in detail. The effects of cross-sections inaccuracy should be assessed for important reactor parameters. For example, the effective delayed neutron fraction (on which Chapter 3 of this thesis is focused) is always affected by a considerable degree of uncertainty. In the case of the MSFR, the lower quality of the available delayed neutron data for ^{233}U and TRUs, adopted as fissile, should also be considered. Moreover, the uncertainties in the delayed neutron precursors decay constants is also reflected in β_{eff} due to fuel motion, while this is not the case in common solid fuel reactors. Finally, as the fuel motion itself has a large impact on β_{eff}, the uncertainty in the modelling of in-core velocity and turbulence fields should be considered as well. A consistent combined estimation of the main sources of β_{eff} uncertainty in the MSFR would be one of the most interesting step ahead in the neutronic analysis of this reactor.

To conclude, new measurements of the (n,γ) reaction on ^{233}U between 1 and 100 keV would be a nice gift for all MSR supporters.

APPENDIX $\mathcal{A}$

Appendix

An overall assessment of SERPENT results (related to the MSFR system) against other neutronics codes can be found in the Deliverable EVOL D2.2 (2013, POLIMI results). In Section A.1 of this Appendix, only a few comparisons obtained in the frame of a collaboration with LPSC/CNRS are reported. Other detailed comparisons between SERPENT and the in-house codes available at LPSC can be found in the PhD thesis of Mariya Brovchenko (2013).

Adjoint-weighted quantities can not be estimated via simple Monte Carlo criticality source simulations. Often, to overcome this problem, approximate methods have been adopted for the calculations of the effective delayed neutron fraction and generation time (e.g., see Meulekamp and van der Marck, 2006; Verboomen *et al.*, 2006). These approximations have proven to be impractical or inaccurate in several cases (Nagaya *et al.*, 2010) and are not suitable for circulating-fuel reactors. In solid-fuel reactors, the difference in importance between prompt and delayed neutrons is mainly due to the different energy spectra. In case of Molten Salt Reactors, prompt and delayed neutrons have also a strongly different spatial distribution, due to fuel motion. In Chapter 3, a Monte Carlo-based approach for the calculation of β_{eff} has been presented. This approach required the implementation of a suitable technique to achieve correct adjoint-weighting. The adopted methodology is based on the Iterated Fission Probability (IFP, Nauchi and Kameyama, 2010; Kiedrowski *et al.*, 2011) and its practical implementation in SERPENT-2 is briefly described in Section A.2.

The IFP methodology and implementation are described in details in: Leppänen, J., Aufiero, M., Fridman, E., Rachamin, R., van der Marck, S., "Calculation of effective point kinetics parameters in the Serpent 2 Monte Carlo code.", Annals of Nuclear Energy, 65 (2014) 272-279. In this paper, a wide suite of validation test cases, performed by Jaakko Leppänen, Emil Fridman and others, can be found.

As pointed out throughout the thesis, sensitivity/uncertainty analysis for the nuclear data adopted in the modelling of the MSFR is highly desirable. In this direction, in the frame of a collaboration with the Paul Scherrer Institut (PSI), the possibility to extend SERPENT for the calculation of adjoint-weighted sensitivity coefficients has been investigated. In Section A.3, preliminary results of this activity are presented. The case studies involve energy-dependent sensitivity coefficients for Jezebel (compared to ERANOS calculations from Sandro Pelloni, PSI) and a PWR pin cell (compared to Tsunami calculations from Maria Pusa (2012)).

At the end of the Appendix (Section A.4), preliminary activities concerning the extension of OpenFOAM multiphysics modelling to deterministic and Monte Carlo neutron transport are reported.

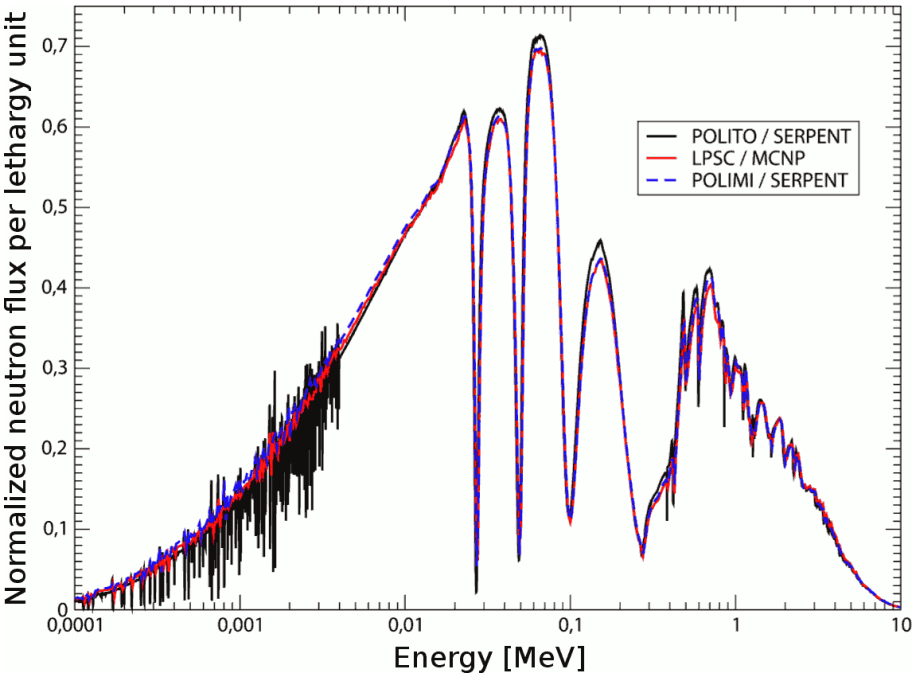

Figure A.1: *Normalized neutron flux in the MSFR. ^{233}U-started case study (from Brovchenko, 2013).*

A.1 Comparison of neutronic results within the EVOL Project

SERPENT has been assessed against neutronics codes adopted by other participants of the EVOL Project, also in the framework of the MSFR neutronic benchmark. In this Section, a few comparisons are reported. The first verifications performed in collaboration with LPSC, involved simple neutronics calculations, adopting the standard version of SERPENT. As example, in Figure A.1 the normalized neutron flux for the MSFR ^{233}U-started case study (see Chapter 1) is shown. POLIMI results appears in good agreement with calculations from Politecnico di Torino (POLITO) and Laboratoire de Physique Subatomique et de Cosmologie (LPSC/CNRS - Grenoble)[1]. In the three cases, the JEFF-3.1 library has been adopted. A second comparison is given in Figure A.2, where the main reaction rates estimates are reported for LPSC and POLIMI (^{233}U-started MSFR case study). LPSC results have been obtained adopting the Monte Carlo code MCNP. In general, in all the performed neutronic simulations, SERPENT results showed to be in agreement with MCNP results, provided that the same assumptions were adopted (e.g., nuclear data libraries, material isotopic compositions, etc.).

Further comparisons involved burn-up simulations with on-line fuel reprocessing and active reactivity control. For these calculations, the extended SERPENT version presented in Chapter 1 has been adopted. In Figure A.3, the evolution of masses for the main elements in the fuel salt is shown for the MSFR TRU-started case study. SERPENT results (POLIMI) are compared to calculations from LPSC and Kurchatov Institute (KI - Moscow). The ENDF/B-VI.8 library has been adopted. A fair agreement in the fuel isotopic evolution estimates between the three codes can be appreciated.

The decay heat curve at reactor shutdown represents a key information for safety anal-

[1]Note that POLITO results have been tallied adopting a different energy discretization.

Reaction rate R = NσΦ [mol/day]	LPSC JEFF-3.1	POLIMI SERPENT JEFF-3.1
Fission Rate ^{233}U	13.1	13.3
(n,γ) Rate ^{233}U	1.36	1.37
Fission Rate ^{232}Th	0.25	0.24
(n,γ) Rate ^{232}Th	15.9	15.8
(n,t) Rate ^{6}Li	0.157	$1.9\ 10^{-3}$
(n,γ) Rate ^{7}Li	$7.6\ 10^{-3}$	$6.85\ 10^{-3}$
(n,γ) Rate ^{19}F	0.13	0.12
(n,α) Rate ^{19}F	0.29	0.29
(n,γ) Rate TOTAL	17.3	17.29
Fission Rate TOTAL	13.3	13.55
Statistic uncertainty	< 2 %	0.1 – 5 %

Figure A.2: *Reaction rates in the MSFR. ^{233}U-started case study.*

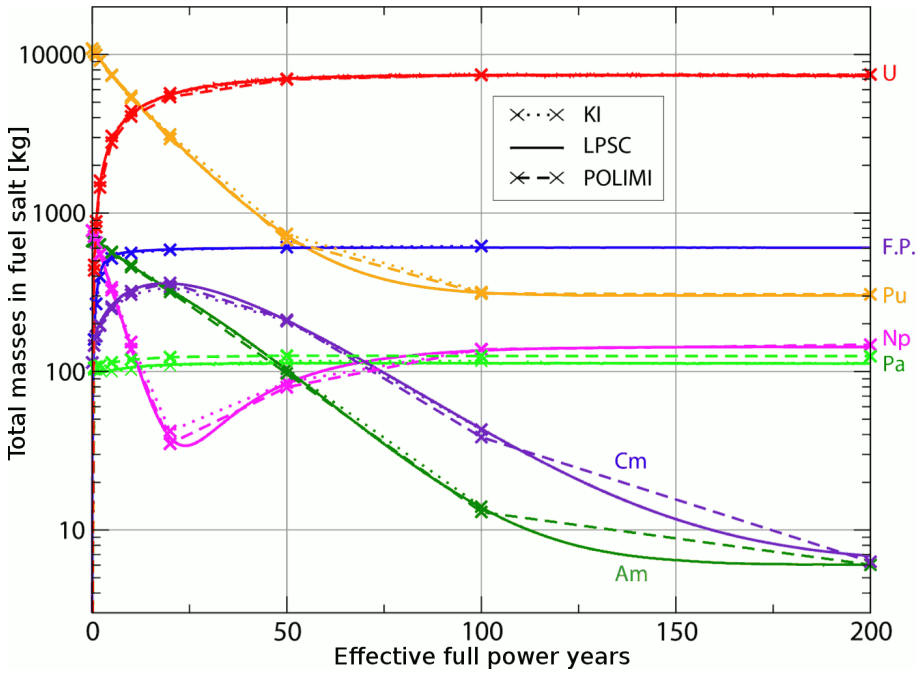

Figure A.3: *Masses evolution in the MSFR fuel salt. TRU-started case study (from Brovchenko, 2013).*

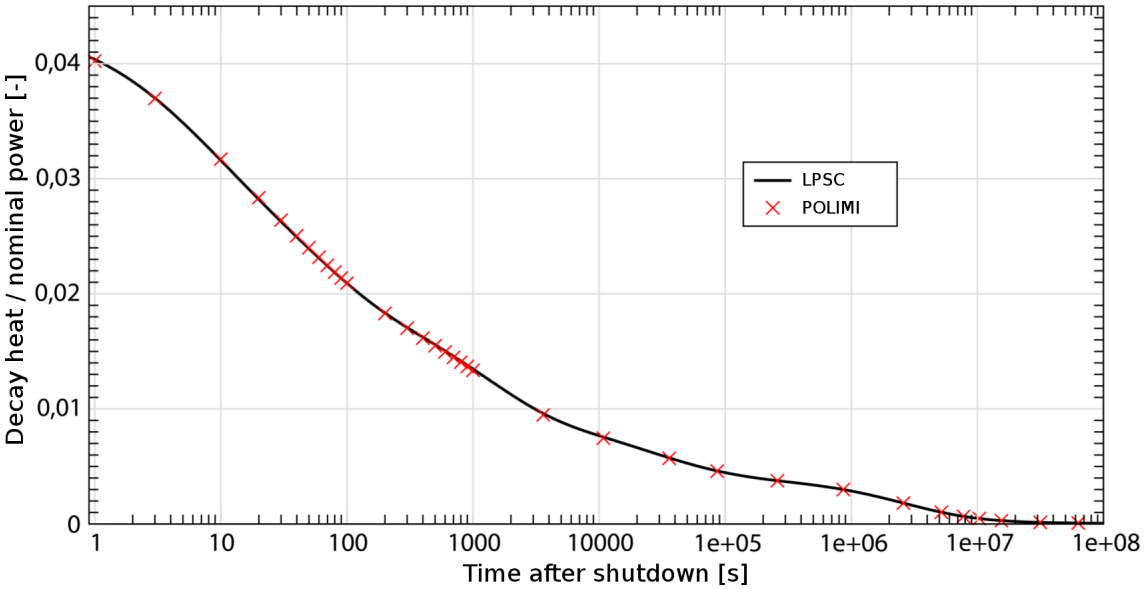

Figure A.4: *Decay heat at shutdown after long operation, normalized to the nominal reactor power (from Brovchenko, 2013).*

ysis. Many of the isotopes produced in fission reactors via nuclear reactions present very short half-life, especially among fission products. These isotopes are often neglected or treated via approximated methods in burn-up simulations. Nonetheless, they give a substantial contribution to the decay heat curve in the initial time period after shutdown. The extended SERPENT version and the in-house tools available at LPSC allow to fully consider all the isotopes available in the nuclear data libraries (a few hundreds). In this way, more reliable decay heat calculations can be performed[2]. In Figure A.4, the estimates for the decay heat after shutdown from SERPENT and the in-house REM code (LPSC) are presented. Simulations refer to the MSFR at equilibrium composition, after long operation at nominal power, adopting the JEFF-3.1 data libraries for cross-sections, fission yield data and decay data. A very good agreement between the two curves can be appreciated.

Other comparisons between SERPENT and LPSC results are reported and thoroughly discussed in the PhD thesis of Mariya Brovchenko (2013) and in the Deliverable EVOL D2.2 (2013, POLIMI results).

A.2 Adjoint-weighted kinetics parameters

The Iterated Fission Probability

Let us consider a neutron "a" that is injected in a critical zero-power core with position $\mathbf{r}$, energy E and travelling direction $\hat{\Omega}$. This neutron might induce a fission event and produce new neutrons. These new neutrons might produce other neutrons and continue the chain reaction. If the system is exactly critical, after a certain number "λ" of generations (i.e., after the convergence of the fission source to the fundamental mode), the expected value of the neutron population will attain a stable level. The value of the *asymptotic*

[2]The reliability of the decay heat calculations is always affected by the accuracy of the decay and fission yield data.

population is called *iterated fission probability*. It represents the importance of the *ancestor* neutron a and is proportional to $\psi^*(\mathbf{r}, \hat{\mathbf{\Omega}}, E)$ (Nauchi and Kameyama, 2010). We can define the set "$d_a^{(\lambda)}$" of all the neutrons which belong to the $(\alpha+\lambda)^{th}$ generation and are descendants of a single neutron ancestor "a",[3] which belongs to the α^{th} generation. The total number of neutrons members of the set $d_a^{(\lambda)}$ can be adopted as unbiased importance estimator for the ancestor a in analog Monte Carlo criticality source simulations, provided that λ is sufficiently large.

In non-analog simulations, the particle weights may be different from one and altered during tracking. This requires a correction of the IFP estimator. In the general case, the estimator of the importance of the ancestor a is:

$$I_a^{(\lambda)} = \frac{\sum\limits_{k \in d_a^{(\lambda)}} w_k}{w_a} \tag{A.1}$$

where w_a is the weight of the ancestor a and $\sum\limits_{k \in d_a^{(\lambda)}} w_k$ is the total weight of its descendants belonging to the $(\alpha+\lambda)^{th}$ generation.

Moreover, in Monte Carlo k-eigenvalue simulations, at each i generation (with $\alpha \leq i < \alpha+\lambda$), the descendant population is artificially reduced (or increased) by a factor $\frac{1}{k_{eff}^i}$, where k_{eff}^i is the multiplication factor estimated at the i^{th} generation. Thus, the importance estimator $I_a^{(\lambda)}$ should be corrected in this way:

$$I_a^{(\lambda)} = \frac{\sum\limits_{k \in d_a^{(\lambda)}} w_k}{w_a} \cdot k_{eff}^{\alpha} \cdot k_{eff}^{\alpha+1} ... k_{eff}^{\alpha+\lambda-2} \cdot k_{eff}^{\alpha+\lambda-1} = \frac{\sum\limits_{k \in d_a^{(\lambda)}} w_k}{w_a} \cdot \prod_{i=\alpha}^{\alpha+\lambda-1} k_{eff}^i \tag{A.2}$$

In the following, the implementation of the IFP scheme in SERPENT is briefly discussed. Two vectors of variables are associated to each neutron. The lifetimes and delayed neutron group index of the previous λ ancestors are stored in the two vector, respectively. At each generation, any neutron producing descendants passes to the progeny the information about itself and its last $\lambda - 1$ ancestors. In this way, any neutron has memory of scored quantities from the last λ generations, which are adopted for the estimation of Λ_{eff} and β_{eff}.

Effective generation time

The concepts of "neutron lifetime", "generation time", "reproduction time" and "removal time" are often adopted with different meanings. Here, we start from the definition of the effective generation time given by Spriggs *et al.* (1997):[4]

$$\Lambda_{\text{eff}} = \frac{{\tau_{\text{r}}}^{\dagger}}{k_{\text{eff}}} \tag{A.3}$$

[3] A detailed definition of *ancestor* or *progenitor* is given in (Kiedrowski *et al.*, 2011).

[4] Nauchi and Kameyama (2010) arrived to a conceptually similar algorithm starting from the common "deterministic" definition of effective generation time: $\Lambda_{\text{eff}} = \frac{\int \psi^{\dagger} \frac{1}{v} \psi}{\int \psi^{\dagger} \mathbf{F} \psi}$.

that estimates Λ_{eff} as the importance weighted removal lifetime divided by the multiplication factor of the system.

The IFP-based estimator of ${\tau_{\text{r}}}^{\dagger}$ at generation α is defined as:

$$\widetilde{{\tau_{\text{r}}}^{\dagger}}^{(\lambda)} = \frac{\sum\limits_{n\in\alpha} w_n \cdot l_n \cdot I_n^{(\lambda)}}{\sum\limits_{n\in\alpha} w_n \cdot I_n^{(\lambda)}} \tag{A.4}$$

Sums are performed over all the neutrons belonging to generation α. l_n is the neutron lifetime. We can substitute the importance estimator $I_n^{(\lambda)}$ with its definition given in Eq. A.2, obtaining:

$$\widetilde{{\tau_{\text{r}}}^{\dagger}}^{(\lambda)} = \frac{\sum\limits_{n\in\alpha} w_n \cdot l_n \cdot \left(\frac{\sum\limits_{k\in d_n^{(\lambda)}} w_k}{w_n} \cdot \prod\limits_{i=\alpha}^{\alpha+\lambda-1} {k_{\text{eff}}}^i \right)}{\sum\limits_{n\in\alpha} w_n \cdot \left(\frac{\sum\limits_{k\in d_n^{(\lambda)}} w_k}{w_n} \cdot \prod\limits_{i=\alpha}^{\alpha+\lambda-1} {k_{\text{eff}}}^i \right)} \tag{A.5}$$

The term $\prod\limits_{i=\alpha}^{\alpha+\lambda-1} {k_{\text{eff}}}^i$ is the same for all the neutrons belonging to the same generation and it can be taken out of the sum and simplified. Also, the weights w_n of the ancestors can be simplified in both the numerator and denominator, obtaining:

$$\widetilde{{\tau_{\text{r}}}^{\dagger}}^{(\lambda)} = \frac{\sum\limits_{n\in\alpha} l_n \cdot \left(\sum\limits_{k\in d_n^{(\lambda)}} w_k \right)}{\sum\limits_{n\in\alpha} \left(\sum\limits_{k\in d_n^{(\lambda)}} w_k \right)} \tag{A.6}$$

Considering that each neutron k living in the $(\alpha+\lambda)^{th}$ generation has one (and only one) ancestor in the $(\alpha)^{th}$ generation, further considerations can be drawn. The denominator $\sum\limits_{n\in\alpha} \left(\sum\limits_{k\in d_n^{(\lambda)}} w_k \right)$ is simply the weight of the total neutron population in the $(\alpha+\lambda)^{th}$ generation. It can be rewritten as: $\sum\limits_{k\in(\alpha+\lambda)} w_k$. Moreover, because again any neutron $k \in (\alpha+\lambda)$ is uniquely associated to one ancestor, the ancestor lifetime l_n can be written as function of the descendant neutron as $l_k^{(-\lambda)}$. $l_k^{(-\lambda)}$ should be interpreted as the lifetime of the λ^{th} ancestor of the neutron k (i.e., the ancestor who lived λ generations before). The numerator $\sum\limits_{n\in\alpha} l_n \cdot \left(\sum\limits_{k\in d_n^{(\lambda)}} w_k \right)$ can thus be rewritten as $\sum\limits_{n\in\alpha} \left(\sum\limits_{k\in d_n^{(\lambda)}} w_k \cdot l_k^{(-\lambda)} \right)$, that is equivalent to $\sum\limits_{k\in(\alpha+\lambda)} w_k \cdot l_k^{(-\lambda)}$. We can finally rewrite Eq. A.6 as:

$$\widetilde{{\tau_{\text{r}}}^{\dagger}}^{(\lambda)} = \frac{\sum\limits_{k\in(\alpha+\lambda)} w_k \cdot l_k^{(-\lambda)}}{\sum\limits_{k\in(\alpha+\lambda)} w_k} \tag{A.7}$$

It appears clear that the present estimator of the adjoint-weighted removal lifetime is the mean λ^{th} ancestor lifetime of the neutron population. In order to have unbiased results, both α and λ should be sufficiently large, to ensure the convergence of the fission source and the correct adjoint-weighting, respectively. The effective generation time can be calculated dividing the estimator of Eq. A.7 by an estimator of the effective multiplication factor. Because we are supposing that the fission source has already converged in generation α, many choices of k_{eff} estimators are possible. Among these, the simpler is the adoption of the implicit estimator of the current $(\alpha + \lambda)$ generation.

Effective delayed neutron fraction

The traditional definition of delayed neutron fraction is:

$$\beta_{\text{eff},j} = \frac{\int \psi^{\dagger}(\mathbf{r}, \mathbf{\Omega}', E')\mathbf{B}_j\, \psi(\mathbf{r}, \mathbf{\Omega}, E)}{\int \psi^{\dagger}(\mathbf{r}, \mathbf{\Omega}', E')\mathbf{F}\, \psi(\mathbf{r}, \mathbf{\Omega}, E)} \tag{A.8}$$

where $\mathbf{F}$ is the fission operator:

$$\mathbf{F}(\mathbf{r}, E, E') = \chi_t(E' \leftarrow E)\nu_t\Sigma_f(\mathbf{r}, E) \tag{A.9}$$

and $\mathbf{B}_j$ is the delayed neutron emission source operator[5]:

$$\mathbf{B}(\mathbf{r}, E, E') = \chi_{d,j}(E' \leftarrow E)\nu_{d,j}\Sigma_f(\mathbf{r}, E) \tag{A.10}$$

It can be seen as the ratio between the importance weighted rate of production of delayed neutrons of group j and the total importance weighted fission neutron production rate. Provided that the fission source is well converged at generation α, this quantity can be estimated through the ratio between the importance weighted source rate of delayed neutrons of group j and the total importance weighted fission neutron source rate:

$$\widetilde{\beta}^{(\lambda)}_{\text{eff},j} = \frac{k_{\text{eff}}\left(\sum\limits_{n\in\alpha} w_n \cdot \delta_{j,g_n} \cdot I_n^{(\lambda)}\right)}{k_{\text{eff}}\left(\sum\limits_{n\in\alpha} w_n \cdot I_n^{(\lambda)}\right)} \tag{A.11}$$

where δ_{j,g_n} is equal to one if the delayed group index of the neutron (g_n) is equal to the delayed neutron group whose effective fraction is being estimated (i.e, if $g_n = j$) and zero in the other cases. Note that prompt neutrons are assigned a delayed group index g_n equal to zero. Following a procedure similar to the one adopted for the generation time, the estimator can be simplified and rewritten as function of the descendant neutrons living in the $(\alpha + \lambda)^{th}$ generation:

$$\widetilde{\beta}^{(\lambda)}_{\text{eff},j} = \frac{\sum\limits_{k\in(\alpha+\lambda)} w_k \cdot \delta_{j,g_k^{(-\lambda)}}}{\sum\limits_{k\in(\alpha+\lambda)} w_k} \tag{A.12}$$

where $g_k^{(-\lambda)}$ is the delayed neutron index of the λ^{th} ancestor of the neutron k. The present estimator of the delayed neutron fraction $\beta_{\text{eff},j}$ can be simply interpreted as the fraction of

[5] In case of circulating fuel reactors, the delayed neutron precursor concentration needs to be explicitly considered (see Chapter 3).

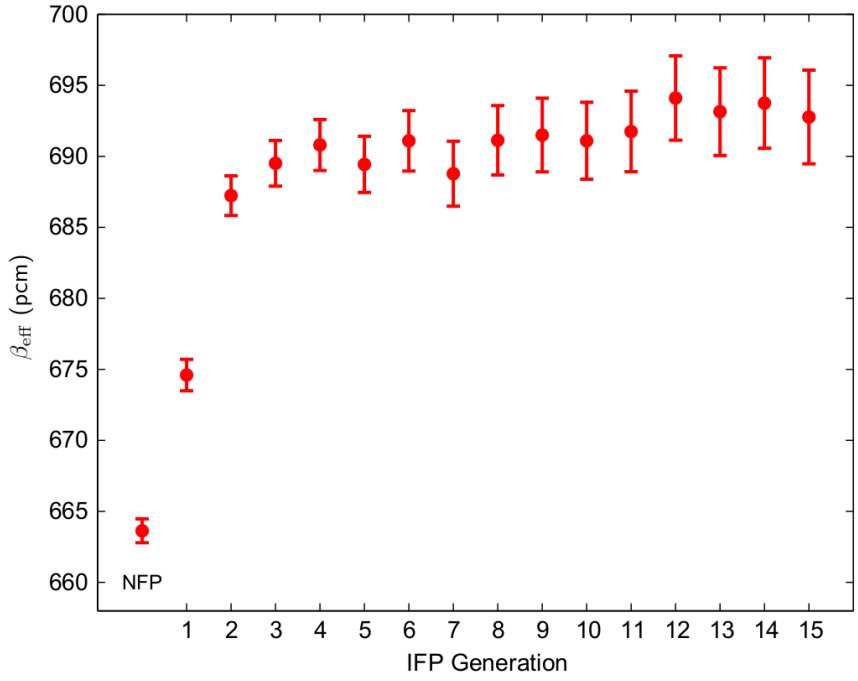

Figure A.5: β_{eff} *as function of IFP generation in the Topsy case (from Leppänen* et al.*, 2014).*

neutrons of the total population, whose λ^{th} ancestor was a delayed neutron of the group j. The estimation of the total effective delayed neutron fraction $\widetilde{\beta_{\text{eff}}}$ can be obtained in a similar way, calculating the total fraction of neutrons whose λ^{th} ancestor was a delayed neutron.

In Figure A.5, the convergence of the of the IFP β_{eff} estimation is shown for the Topsy critical assembly (highly enriched uranium sphere surrounded by a thick reflector of natural uranium, see NEA Nuclear Science Committe, 2011). In all the tested critical assemblies (see Leppänen *et al.*, 2014), the convergence is reached within 10 to 15 latent generations. In most cases, a few generations are enough to get accurate adjoint-weighting. In case of circulating fuel reactors (see Figure 3.4 in Chapter 3), much more generations might be required.

Approximated adjoint-weighting approaches based on the "next fission probability" (e.g., the method developed by Meulekamp and van der Marck (2006)) involve the estimation of the fraction of neutrons produced by delayed neutrons (i.e., whose first ancestor was a delayed neutron). In this view, the iterated fission probability approach appears clearly as a simple generalization of the next fission probability to the λ^{th} ancestor.

In Figures A.6 to A.9, a comparison between different methods for β_{eff} calculation is presented for four critical assemblies (NEA Nuclear Science Committe, 2011). Results are in pcm and have been obtained adopting the JEFF-3.1 library and 14 latent generations ($\pm 2\sigma$ error bars are also shown). The implemented iterated fission probability method is statistically in agreement with the "prompt" method (see Chapter 3). The adoption of the commonly employed Meulekamp and van der Marck (2006) method leads to errors in the β_{eff} estimates in the order of $\sim$5% in both the bare and the reflected assemblies considered.

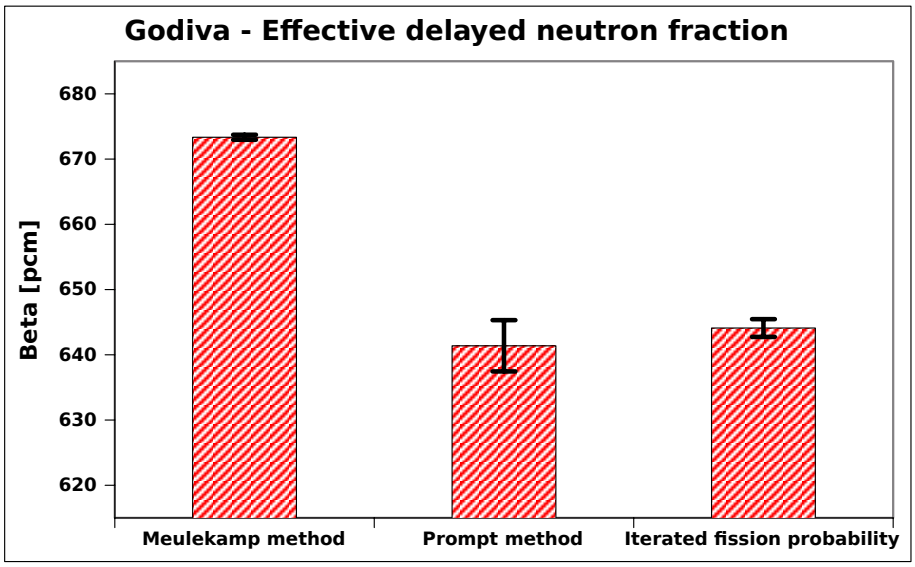

Figure A.6: *β_{eff} calculation in SERPENT-2: comparison between Meulekamp and van der Marck (2006) method, prompt method and the iterated fission probability. Godiva critical assembly (NEA Nuclear Science Committe, 2011).*

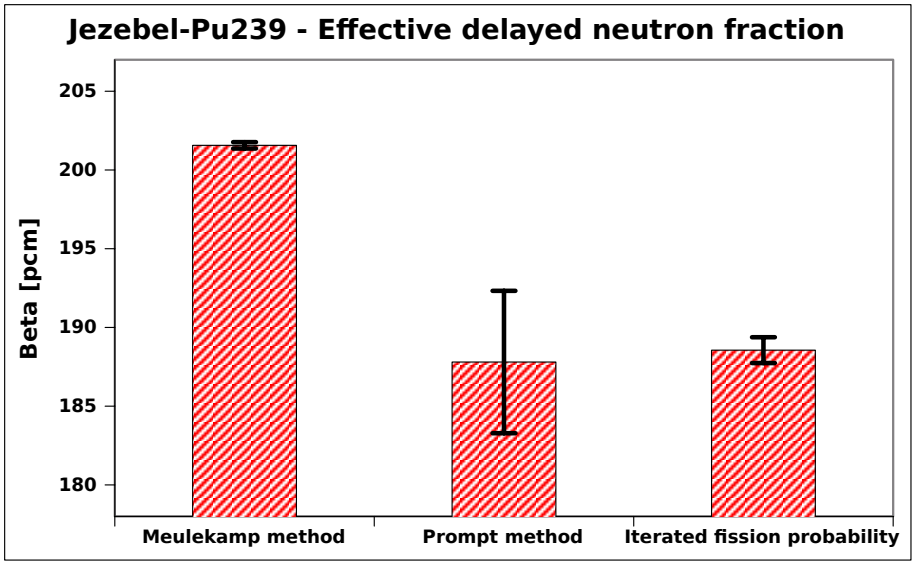

Figure A.7: *β_{eff} calculation in SERPENT-2: comparison between Meulekamp and van der Marck (2006) method, prompt method and the iterated fission probability. Jezebel (^{239}Pu) critical assembly (NEA Nuclear Science Committe, 2011).*

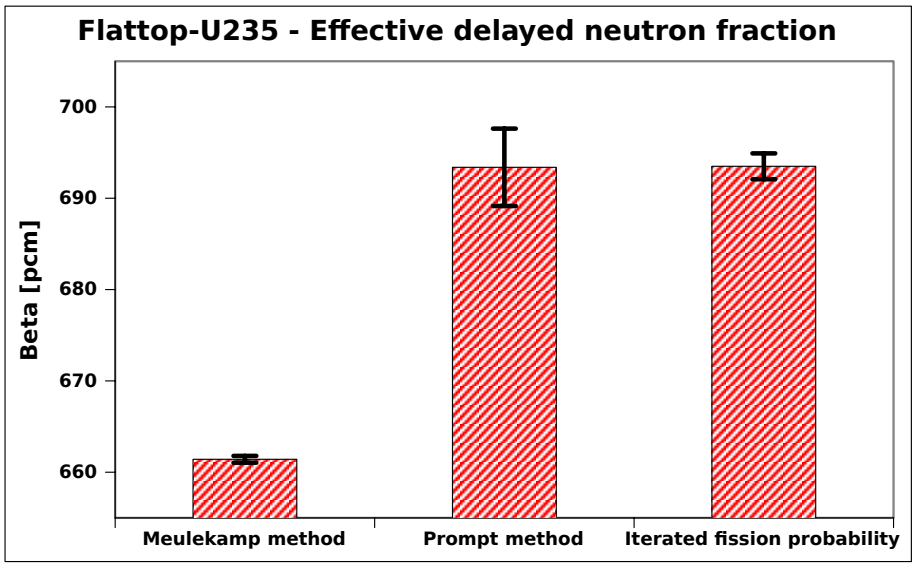

Figure A.8: *β_{eff} calculation in SERPENT-2: comparison between Meulekamp and van der Marck (2006) method, prompt method and the iterated fission probability. Flattop (^{235}U) critical assembly (NEA Nuclear Science Committe, 2011).*

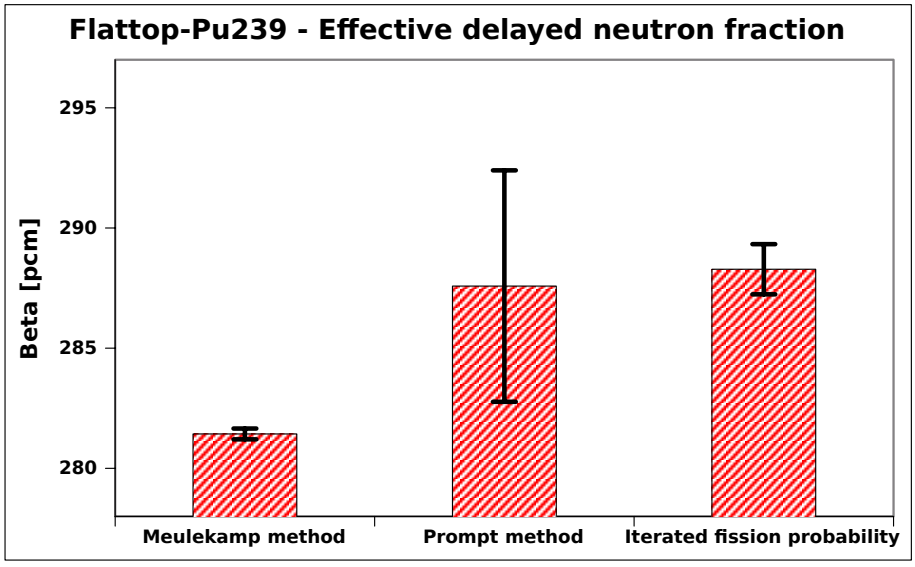

Figure A.9: *β_{eff} calculation in SERPENT-2: comparison between Meulekamp and van der Marck (2006) method, prompt method and the iterated fission probability. Flattop (^{239}Pu) critical assembly (NEA Nuclear Science Committe, 2011).*

A.3 Adjoint-weighted k_{eff} sensitivity coefficients

Adjoint-weighted sensitivity coefficients represent the first step toward the uncertainty analysis of the main reactor parameters. In this Section, the first results from the SERPENT extension for the calculation of k_{eff} sensitivity coefficients are briefly presented. The implementation represents an extension of the method presented in the previous Section.

Increasing cross-sections and rejecting collisions

In an analog particle transport simulation, after artificially increasing the cross-sections by an arbitrary factor f, fair (unbiased) game can be ensured if the sampled collisions are consistently rejected with a probability $p = \left(1 - \frac{1}{f}\right)$. Let us consider the simple case with $f = 2$ and $p = \frac{1}{2}$. In this way, on average, half of the collisions are rejected. In Figure A.10, the history of a neutron travelling in the modified framework is simply sketched. In red, the accepted and rejected collisions of the present (λ) generation are shown. In green, the history is tracked back to the "father" in the $\lambda - 1$ generation. In blue, the tracks of previous ancestors are indicated.

In the collision rejection framework described above, the effect of "small" cross-sections perturbations on the particles weight can be easily derived. In Figure A.10, the perturbed particle weight (w^*) is expressed as function of the unperturbed weight (w^0) and the perturbed cross sections. k_{eff} analog sensitivity coefficient estimators can be defined by simply accounting the number of accepted and rejected collisions. Adjoint-weighting is achieved by propagating the information over multiple generations, in a way similar to the one presented in the previous Section.

Jezebel

In Figures A.11 to A.14, the SERPENT results for the k_{eff} sensitivities of the Jezebel ^{239}Pu critical assembly (NEA Nuclear Science Committe, 2011) are compared against ERANOS results. The JEFF-3.1 nuclear data library has been adopted, along with the 175 groups Vitamin-J energy structure. Black lines represent SERPENT results (thin lines are $\pm 1\sigma$). Reference ERANOS results (red lines) were obtained by Sandro Pelloni adopting P_5 approximation of the anisotropic scattering and S_{100} one-dimensional quadrature set. In general, fair agreement can be observed in the plots. The presence of low lethargy width intervals (e.g., close to 300 keV and 2.3 MeV) results in evident "spikes" in the SERPENT results, due to low scoring efficiency.

Similar comparisons have been performed for the Flattop ^{239}Pu critical assembly (NEA Nuclear Science Committe, 2011). Satisfactory agreement was found, also in this case, for most of the reactions. Nonetheless, a very high number of latent generations turned out to be necessary to achieve full convergence of the results, in case of reactions involving strong spatial modification of the fission source.

PWR pin cell

In this Sub-Section, a PWR pin cell is considered. The case study is the TMI-1 cell (hot zero power conditions) of the UAM benchmark (Ivanov *et al.*, 2007). In Figures A.15 to A.18, SERPENT estimates are compared to Tsunami-1D results provided by Maria Pusa

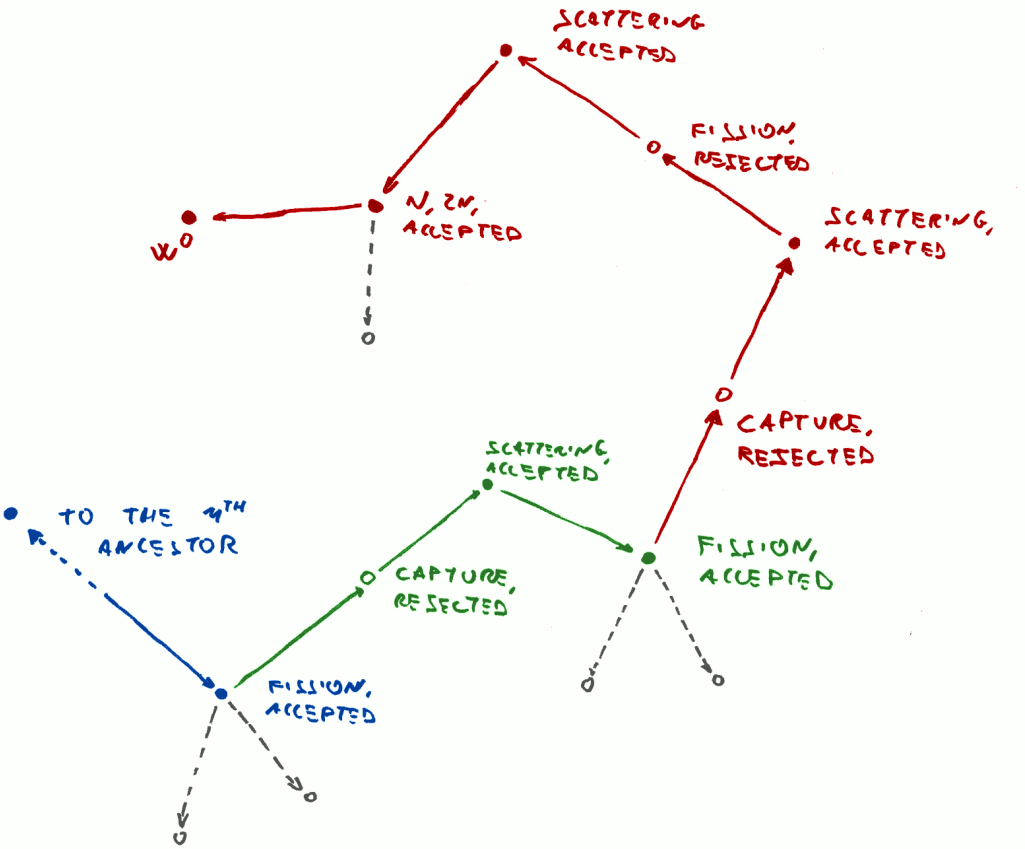

$$w^* \simeq w^0 \cdot \left(1+\frac{\partial\Sigma_{n,2n}}{\Sigma_{n,2n}}\right)\cdot\left(1+\frac{\partial\Sigma_s}{\Sigma_s}\right)\cdot\left(1-\frac{\partial\Sigma_f}{\Sigma_f}\right)\cdot\left(1+\frac{\partial\Sigma_s}{\Sigma_s}\right)\cdot\left(1-\frac{\partial\Sigma_c}{\Sigma_c}\right)\ldots$$
$$\ldots\left(1+\frac{\partial\Sigma_f}{\Sigma_f}\right)\cdot\left(1+\frac{\partial\Sigma_s}{\Sigma_s}\right)\ldots\left(1+\frac{\partial\Sigma_f}{\Sigma_f}\right)\ldots$$

Figure A.10: *Neutron weight change due to small cross-sections perturbation.*

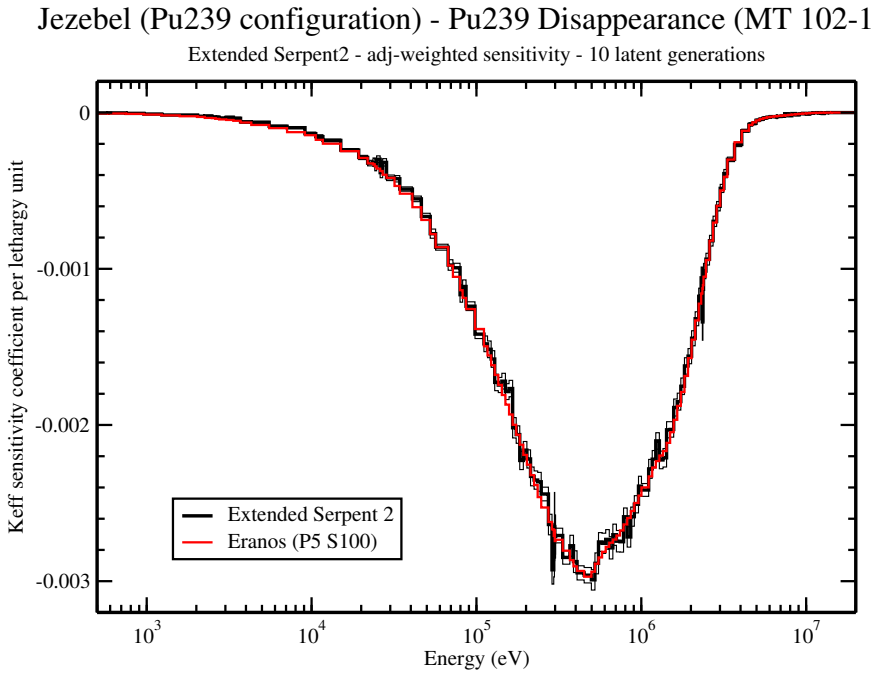

Figure A.11: *Adjoint-weighted k_{eff} sensitivity coefficients for the Jezebel critical assembly. ^{239}Pu capture cross-section.*

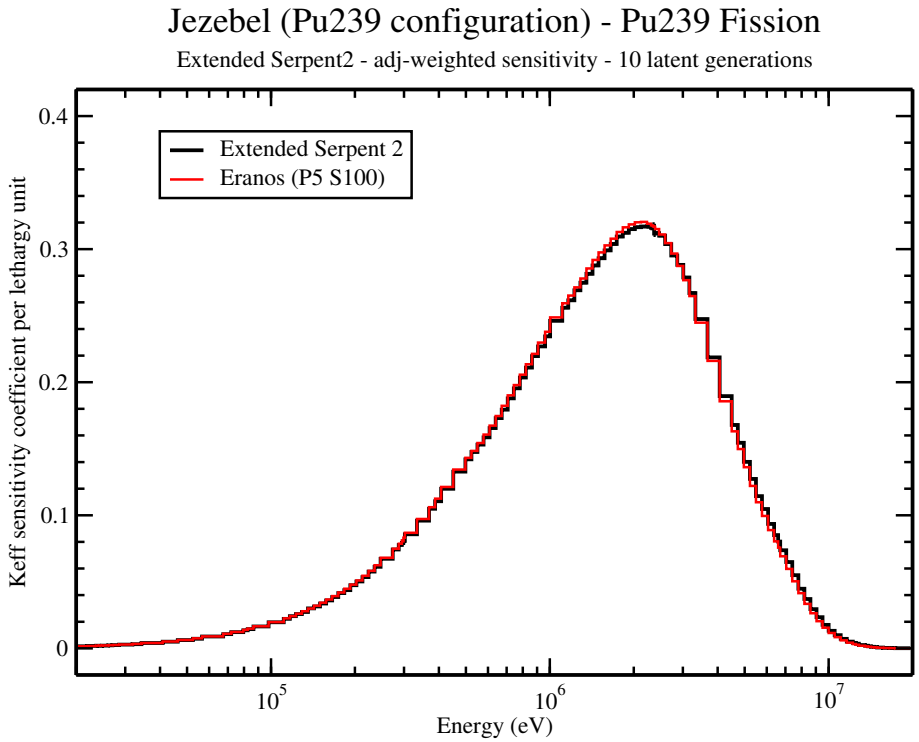

Figure A.12: *Adjoint-weighted k_{eff} sensitivity coefficients for the Jezebel critical assembly. ^{239}Pu fission cross-section.*

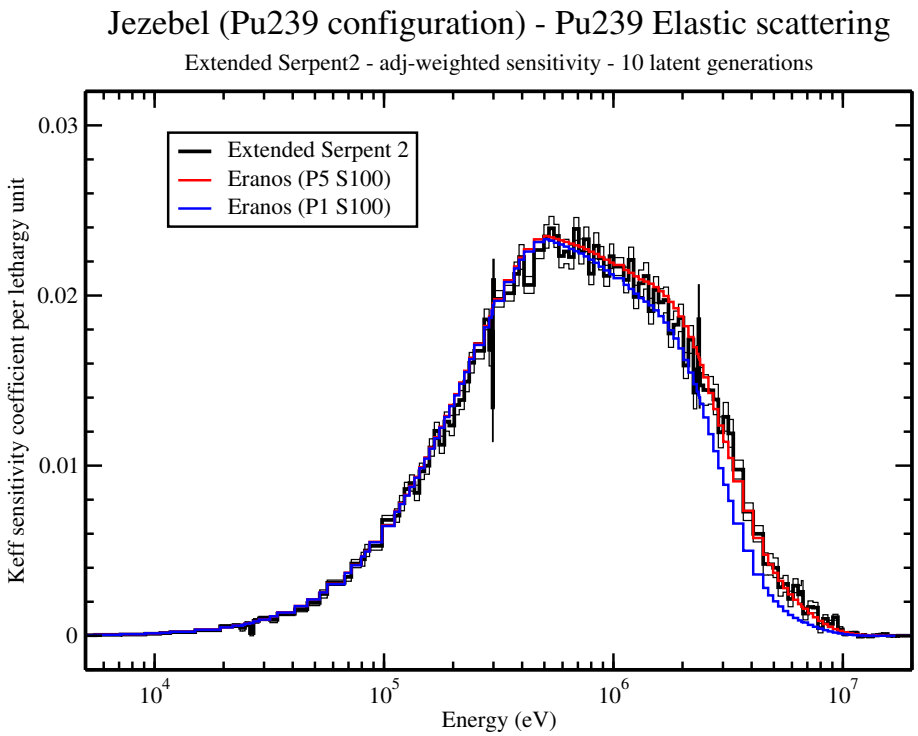

Figure A.13: *Adjoint-weighted k_{eff} sensitivity coefficients for the Jezebel critical assembly. ^{239}Pu elastic scattering cross-section.*

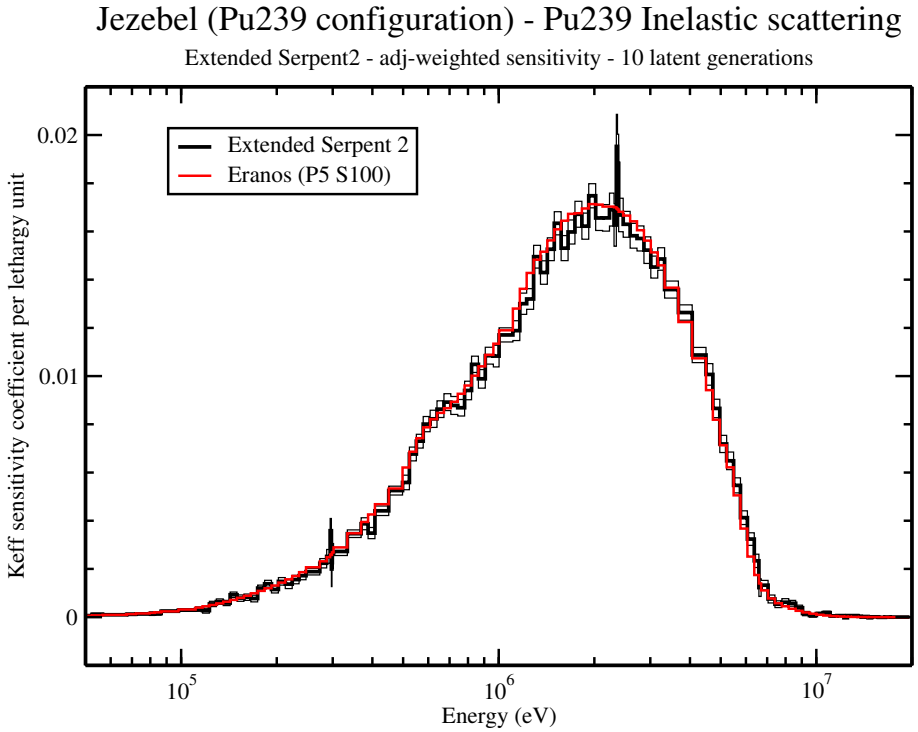

Figure A.14: *Adjoint-weighted k_{eff} sensitivity coefficients for the Jezebel critical assembly. ^{239}Pu inelastic scattering cross-section.*

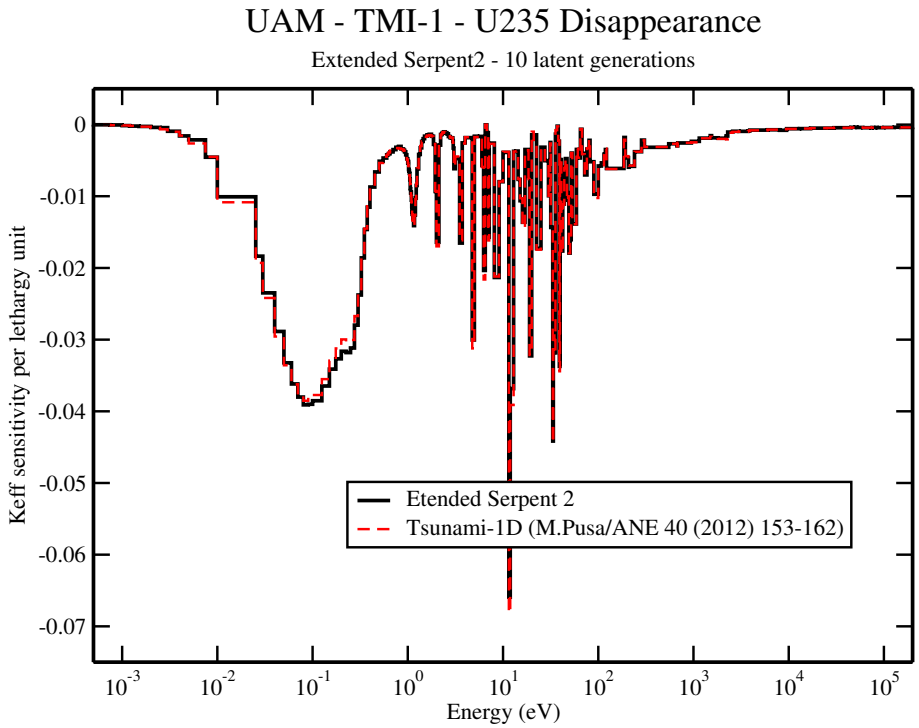

Figure A.15: *Adjoint-weighted k_{eff} sensitivity coefficients for the UAM TMI-1 PWR pin cell. ^{235}U capture cross-section.*

(2012). For these comparisons, the Scale 238 group energy structure and the ENDF/B-VI.8 library were adopted. Fair agreement is observed for the considered reactions. Appreciable differences can be found in the narrow resonances of the ^{238}U capture cross-section (Figure A.17).

A.4 Neutron transport tools for multiphysics applications

In Chapters 2 and 3, one-speed and multi-group neutron diffusion has been adopted in the development of the OpenFOAM solvers. These approximations proved to be fairly accurate in the MSFR considered case studies. Nonetheless, more accurate neutronics tools are desirable for specific multiphysics applications. In this direction, the development of neutron transport (deterministic and Monte Carlo-based) tools is being investigated. In this Sub-Section, a brief description of these activities is reported.

Discrete Ordinates solver in OpenFOAM

A simple Discrete Ordinates eigenvalue solver has been developed adopting the Finite-Volume library OpenFOAM. The Discrete Ordinates method involves the discretization of the neutron transport equation in n energy groups and m angular directions[6]. The balance equations of each angle-energy group i, j are solved iteratively in the spatial domain:

$$\nabla \cdot (\mathbf{\Omega}_j \cdot \varphi_{i,j}) + \Sigma_{t,i} = \text{Isotropic Source}_{i,j} + \text{Anisotropic Source}_{i,j} \tag{A.13}$$

[6] A detailed description of the Discrete Ordinates method is not given here. It can be found in several reactor physics textbooks (e.g., see Stacey, 2007).

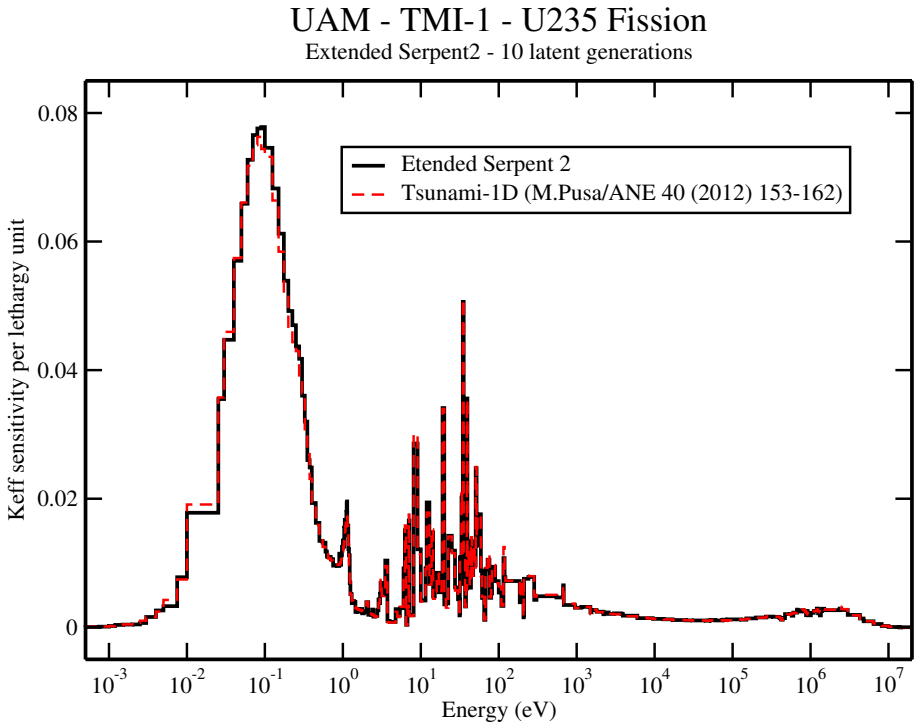

Figure A.16: *Adjoint-weighted k_{eff} sensitivity coefficients for the UAM TMI-1 PWR pin cell. ^{235}U fission cross-section.*

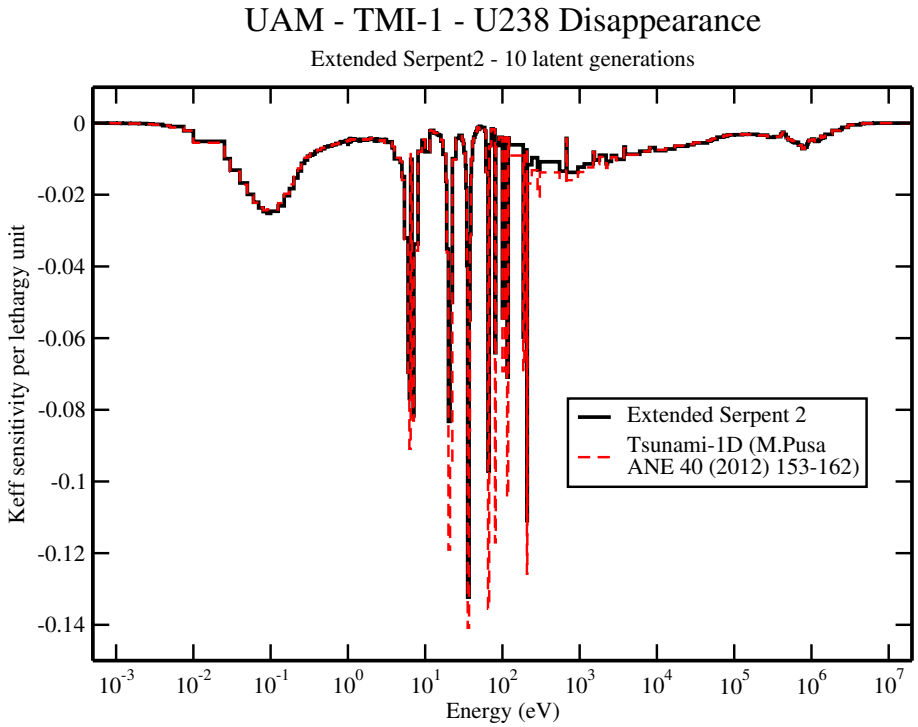

Figure A.17: *Adjoint-weighted k_{eff} sensitivity coefficients for the UAM TMI-1 PWR pin cell. ^{238}U capture cross-section.*

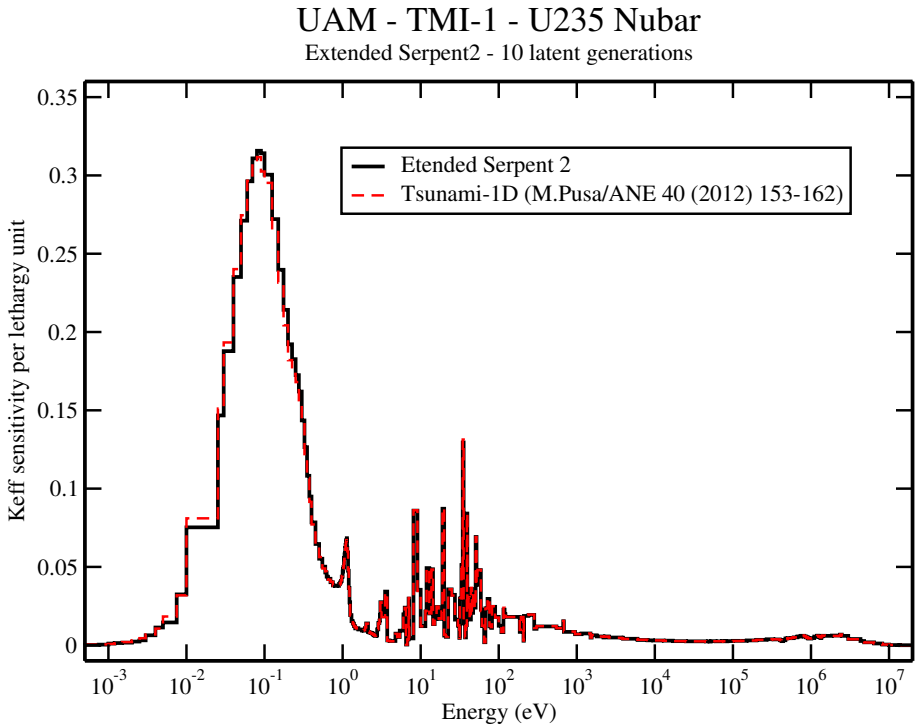

Figure A.18: *Adjoint-weighted k_{eff} sensitivity coefficients for the UAM TMI-1 PWR pin cell. ^{235}U total nubar ($\bar{\nu}$).*

where $\mathbf{\Omega}_j$ is the unit vector of the angular direction j, $\Sigma_{t,i}$ is the total cross-section of the energy group i, and the Isotropic Source$_{i,j}$ is defined as follows:

$$\text{Isotropic Source}_{i,j} = \sum_{i'=0}^{n}\sum_{j'=0}^{m} \omega_{j'} \cdot \varphi_{i',j'} \left(\frac{1}{k_{eff}} \nu\Sigma_{f,i'}\chi_i + \Sigma_{s,i\leftarrow i'} \right) \tag{A.14}$$

where the sums are performed over all the energy groups and discrete directions, $\nu\Sigma_{f,i'}$ is the fission neutron production cross-sections of the energy group i', χ_i is the fraction of fission neutrons emitted in the energy group i and $\Sigma_{s,i\leftarrow i'}$ is the scattering cross section from energy $E_{i'}$ to energy E_i. $\omega_{j'}$ is the normalized quadrature weight associated to the direction $\mathbf{\Omega}_{j'}$.

The anisotropic scattering terms are considered adopting a p^{th} order Legendre polynomial expansion of the scattering cosine $(\mathbf{\Omega}_j \cdot \mathbf{\Omega}_{j'})$:

$$\text{Anisotropic Source}_{i,j} = \sum_{i'=0}^{n}\sum_{j'=0}^{m} \omega_{j'} \cdot \varphi_{i',j'} \cdot \Sigma_{s,i\leftarrow i'} \left(\sum_{l=1}^{p} s^l_{i\leftarrow i'} \cdot P_l(\mathbf{\Omega}_j \cdot \mathbf{\Omega}_{j'}) \frac{2l+1}{2} \right) \tag{A.15}$$

where P_l is the l^{th} Legendre polynomial and $s^l_{i\leftarrow i'}$ is the l^{th} Legendre coefficient of the scattering cross-section $\Sigma_{s,i\leftarrow i'}$.

All the balance equations are spanned iteratively. Equation A.13 is solved implicitly for the LHS (Left Hand Side), while the RHS (Equations A.14 and A.15) are introduced as explicit source terms. The spatial discretization of the ∇ operator is based on the standard schemes available in OpenFOAM. The solution of the eigenvalue problem is achieved adopting the traditional Source Iteration – Power Iteration method.

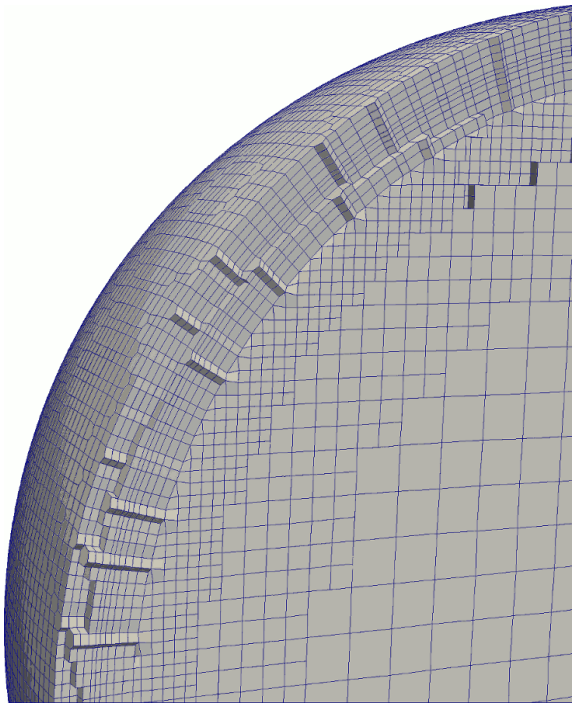

Figure A.19: *Spatial mesh adopted in the OpenFOAM Discrete Ordinates solver for the Godiva test case.*

The solver has been preliminary verified against SERPENT and ERANOS results, adopting the Godiva critical assembly as test case. The benchmark model (NEA Nuclear Science Committe, 2011) consists in a homogeneous sphere of highly enriched uranium ($\sim$94%) with a nominal radius of 8.74 cm. The ERANOS reference results have been obtained via 1-D calculations (performed by Sandro Pelloni). In OpenFOAM, the full 3-D sphere has been simulated, adopting a spatial mesh with progressive refinement close to the boundary (Figure A.19), along with the *linearUpwind* interpolation scheme.

The SERPENT code has been adopted to generate all the group constants for the OpenFOAM model, namely: the total cross-sections ($\Sigma_{t,i}$), the fission neutron production cross-sections ($\nu\Sigma_{f,i}$), the fission spectrum (χ_i), the scattering matrices ($\Sigma_{s,i\leftarrow i'}$) and the Legendre coefficients ($s^l_{i\leftarrow i'}$). (n, xn) reactions have been taken into account in the scattering terms. A 28 energy group structure has been adopted. The energy boundaries have been taken from the Ecco 33 group structure with refinement at high energy, and are reported in Table A.1. In the ERANOS simulations, the 175 groups Vitamin-J structure has been employed.

The LDFE-SA-2 quadrature set from Jarell and Adams (2011) has been adopted for the angular discretization, which consists in a total number of 128 directions (16 per octant). In ERANOS, 1-D S_{16} quadrature has been adopted. P_3 approximation has been adopted for the anisotropic scattering in both ERANOS and OpenFOAM. In Table A.2, the results obtained with the 3 codes adopting the JEFF-3.1 library are presented.

Considering the "challenging" test case, which is dominated by leakage, the OpenFOAM results appear in good agreement with both SERPENT and ERANOS. As a further verification of the fully convergence of the results, the effects of the P_n approximation on k_{eff} in ERANOS and OpenFOAM is compared in Figure A.20. The two codes show a very similar behaviour.

Table A.1: *Energy structure adopted in the OpenFOAM Discrete Ordinates solver for the Godiva test case.*

Group #	Upper boundary (MeV)	Group #	Upper boundary (MeV)
1	1.37e-05	15	6.73e-02
2	6.79e-05	16	1.11e-01
3	1.48e-04	17	1.83e-01
4	3.04e-04	18	3.01e-01
5	4.54e-04	19	4.97e-01
6	7.48e-04	20	8.20e-01
7	1.23e-03	21	1.35
8	2.03e-03	22	2.23
9	3.35e-03	23	3.67
10	5.53e-03	24	6.06
11	9.11e-03	25	7.78
12	1.50e-02	26	10.00
13	2.47e-02	27	13.84
14	4.08e-02	28	20.00

Table A.2: *Transport solver. Comparison between OpenFOAM, ERANOS and SERPENT. Godiva test case.*

Code	Energy discretization	Spatial discretization	Angular discretization	k_{eff}	$k_{eff} - k_{eff}^{S}$
OpenFOAM	28 groups	Finite Volume (3D) $\sim 1.1 \cdot 10^6$ cells	LDFE-SA-2 (128 directions)	0.99613	-21 pcm
ERANOS	175 groups	Finite Difference (1D)	S_{16}	0.99651	+ 17 pcm
SERPENT	–	–	–	0.99634 $\pm$ 2 pcm	–

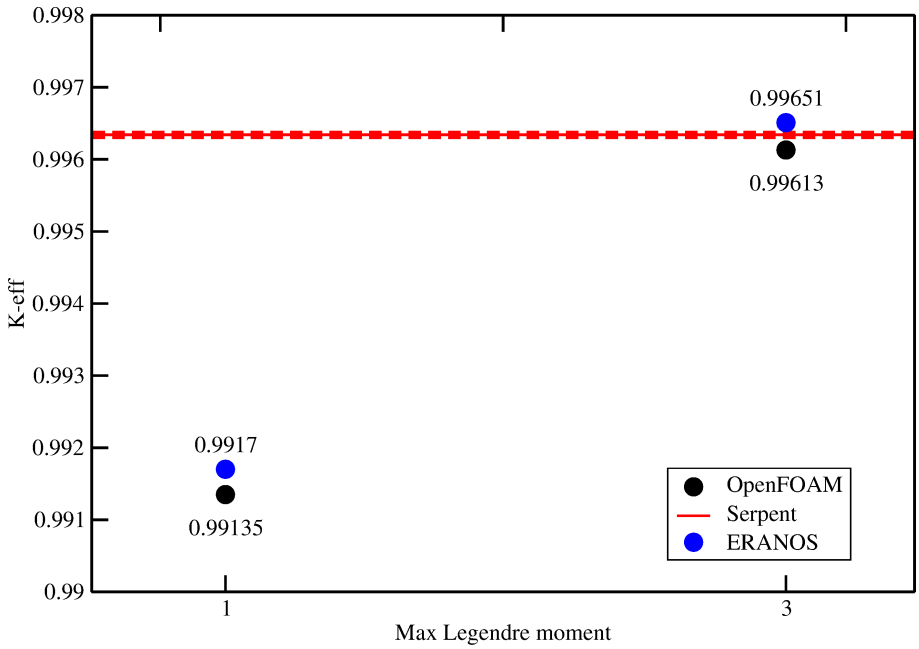

Figure A.20: *Comparison between P_1 and P_3 results obtained with ERANOS and OpenFOAM. Godiva test case.*

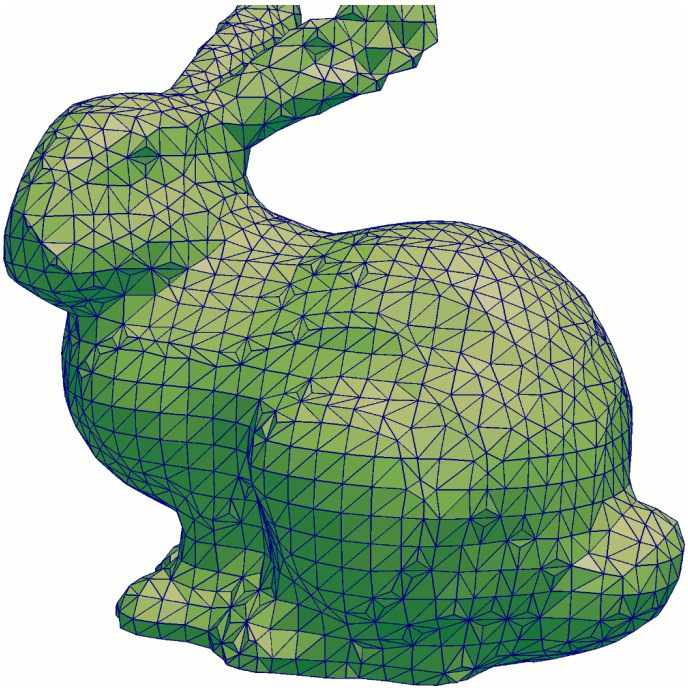

Figure A.21: *Example of unstructured mesh adopted in the SERPENT–OpenFOAM coupling (Stanford bunny – 12000 cells).*

The availability of an accurate neutron transport solver in OpenFOAM might ensure high flexibility in both physics coupling (e.g., with CFD) and spatial discretization (i.e., adoption of differentiation schemes, unstructured and moving meshes). Nonetheless, effective convergence acceleration techniques would be required for an useful exploitation of any OpenFOAM-based 3D neutron transport solvers.

SERPENT–OpenFOAM coupling at source code level

In this Sub-Section, the investigation of the possible tight coupling of the Monte Carlo code SERPENT and the Finite-Volume multi-physics toolkit OpenFOAM is briefly presented.

The OpenFOAM libraries for spatial mesh handling, equation discretization and matrices manipulation have been dynamically linked to the SERPENT code at source code level. The first step of the coupling involves the transport of neutrons over an OpenFOAM mesh, which is adopted as geometrical description of the computational domain. Briefly, at each collision, the SERPENT tracking routines "ask" to the OpenFOAM libraries the material properties at the collision position $\mathbf{r}$. OpenFOAM mesh search classes take care of finding the cell containing the point $\mathbf{r}$, and returning to SERPENT the required information (e.g., material density). The mesh search is a delicate and computationally expensive task. Octree-based algorithms available in OpenFOAM revealed to be both efficient and reliable in the tested geometries.

This approach allows the adoption of arbitrary complex geometries, that are handled with difficulties in common deterministic and Monte Carlo codes. In Figure A.21, an example of unstructured mesh adopted in the SERPENT–OpenFOAM coupling is shown, representing the Stanford bunny (Turk and Levoy, 2005) 3D model, described with ap-

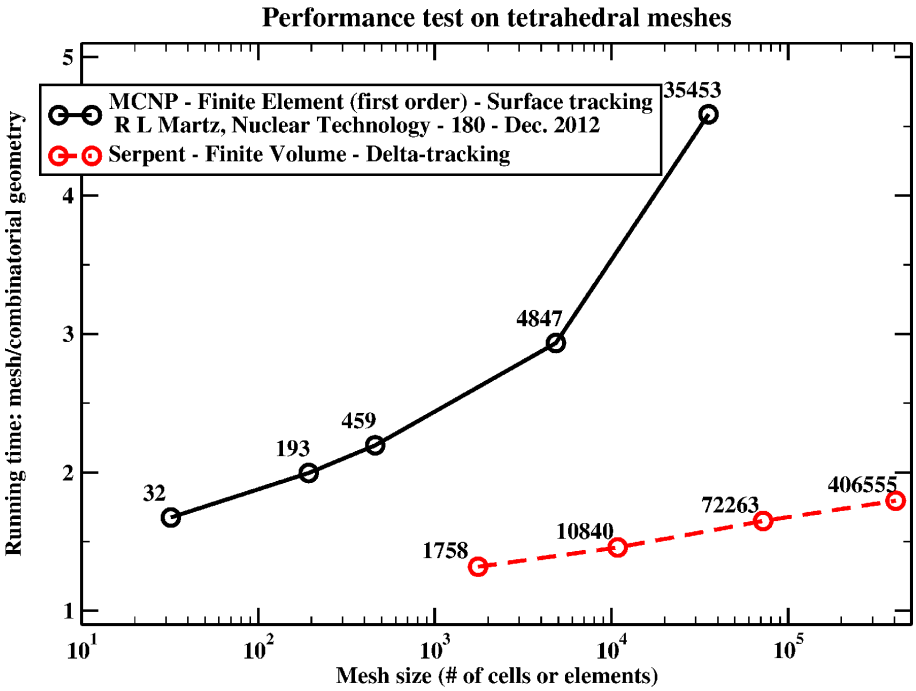

Figure A.22: *Running times for different mesh sizes. Comparison between SERPENT-OpenFOAM and MCNP.*

proximately 12000 cells. The run-time performances of the extended SERPENT code have been studied for the simple Godiva case study. The spherical geometry has been meshed with a growing number of cells, leading to an increase of the CPU time required for the tracking of a given number of neutron histories. The relative increase of CPU-time due to the mesh search operations has been compared to recent published results from Martz (2012), related to the adoption of MCNP in combination with a Finite-Element mesh. In Figure A.22, the CPU-time comparison between MCNP and SERPENT–OpenFOAM is shown for the Godiva test case. Running times have been normalized to the neutron transport performance of the legacy combinatorial geometry description, in each code. In abscissa, the mesh size (number of cells or elements) is given in logarithmic scale. In ordinate, the normalized CPU-time is shown. In SERPENT, the CPU-time overhead as function of the total cells number (N) shows a stable $\sim log(N)$ trend.

The second step of the coupling strategy consists in tallying useful quantities directly on the OpenFOAM mesh. In case of neutronics-CFD coupling, the main quantity to be exchanged is the power density distribution. At each neutron collision, an implicit estimation of the local fission energy deposition $(\phi \cdot \Sigma_f \cdot E_f)$ is computed and scored in the cell containing the collision point. At given intervals, the scored power density is normalized according to the volume of each cell and the domain-integrated power of the system. In Figure A.23, one of the meshes adopted in the Godiva test case and the distribution of fission energy deposition are shown.

The last step involves the solution of the equations describing the coupled problem in OpenFOAM. As a simple test case, the coupled neutronics/thermal-mechanics problem in the Stanford bunny (Turk and Levoy, 2005) geometry has been investigated. The simple solution scheme adopted is briefly described in the following:

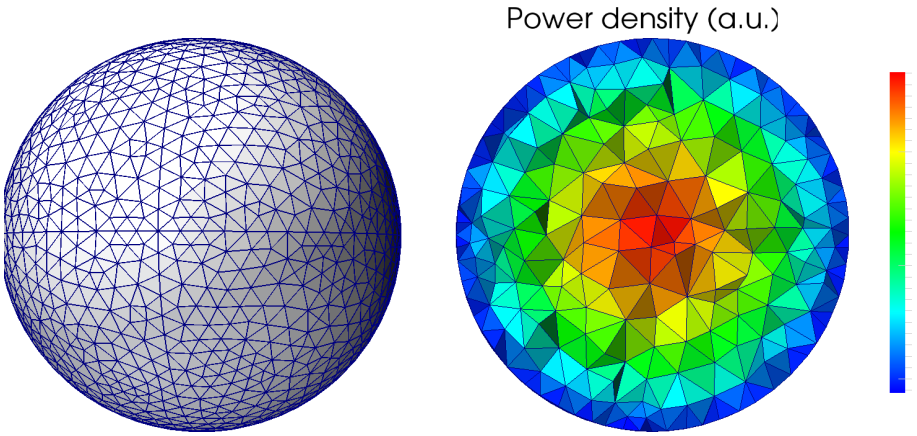

Figure A.23: *SERPENT–OpenFOAM coupling. Mesh and power density scoring for the Godiva test case (10840 cells).*

Table A.3: *Uranium thermo-mechanical properties adopted in the SERPENT–OpenFOAM coupling.*

Density (ρ)	18.74	$g \cdot cm^{-3}$
Poisson's ratio (ν)	0.23	–
Young's modulus (E)	208	GPa
Thermal conductivity (k)	27.5	$W \cdot m^{-1} \cdot K^{-1}$
Thermal expansion coeff. (α)	$1.39 \cdot 10^{-5}$	K^{-1}
Yield stress (σ_y)	250	MPa

(1) Transport neutrons on the "cold" (undeformed) bunny mesh
(2) Score fission energy deposition in each cell
(3) Normalize total power to a given value
(4) Solve the heat equation in the bunny, adopting the computed heat source distribution
(5) Solve the thermal-elasticity problem, adopting the computed temperature distribution
(6) Deform the mesh according to the computed displacement fields
(7) Update material density in each cell
(8) Transport neutrons on the deformed mesh
(9) Go back to **(2)** and loop until convergence
(10) Save the von Mises stresses and the multiplication factor of the converged solution

The same material isotopic composition of the Godiva critical assembly (highly enriched metallic uranium, NEA Nuclear Science Committe, 2011) has been used. The calculations have been performed adopting the JEFF-3.1 library, and the bunny geometry has been scaled, in order to get a system close to criticality. A simple "fixed temperature" condition has been adopted at the outer boundary of the bunny domain, along with the metallic uranium thermo-mechanical properties (assumed uniform and constant throughout the bunny) reported in Table A.3. It is worth nothing that a very simplified model has been here adopted with the main purpose of testing the numerical behaviour of the coupling scheme in presence of a moving mesh (more realistic thermo-mechanical analysis is out of the scope of this Appendix).

When fission heat is released in the bunny, the small thermal expansion increases the neutron leakages and leads to a negative temperature feedback on reactivity. In Figure A.24, the k_{eff} estimates from the SERPENT–OpenFOAM coupling for the bunny test cases are shown as function of the total system power. In Figure A.25, the temperature fields and von Misses stresses are shown for eigenvalue simulations at 2 kW and

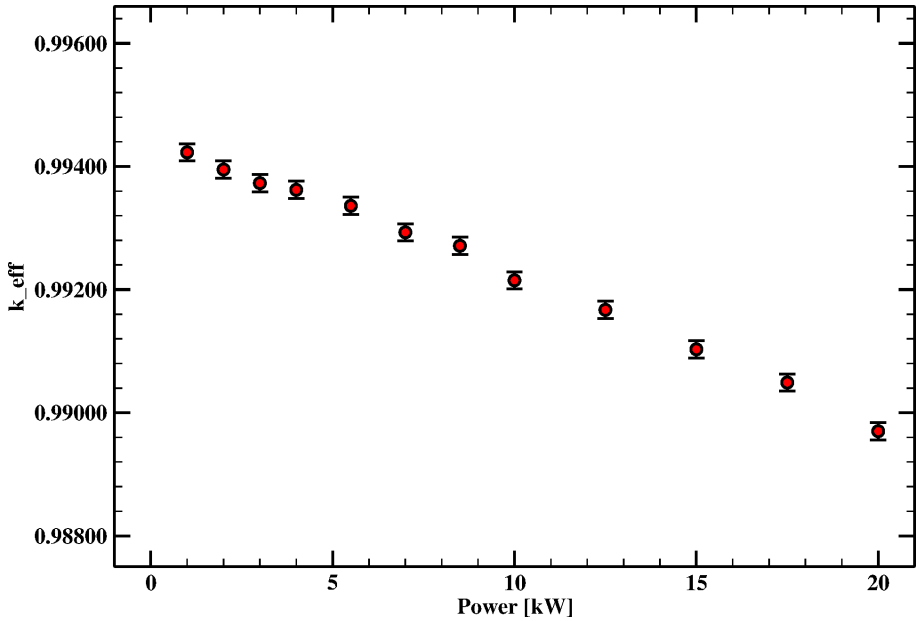

Figure A.24: *SERPENT–OpenFOAM coupling. k_{eff} in the bunny test case, as function of the total power.*

(a and c) and 5.5 kW (b and d). Red color represents zones of incipient yielding in the metallic uranium (equivalent stress ∼250 MPa).

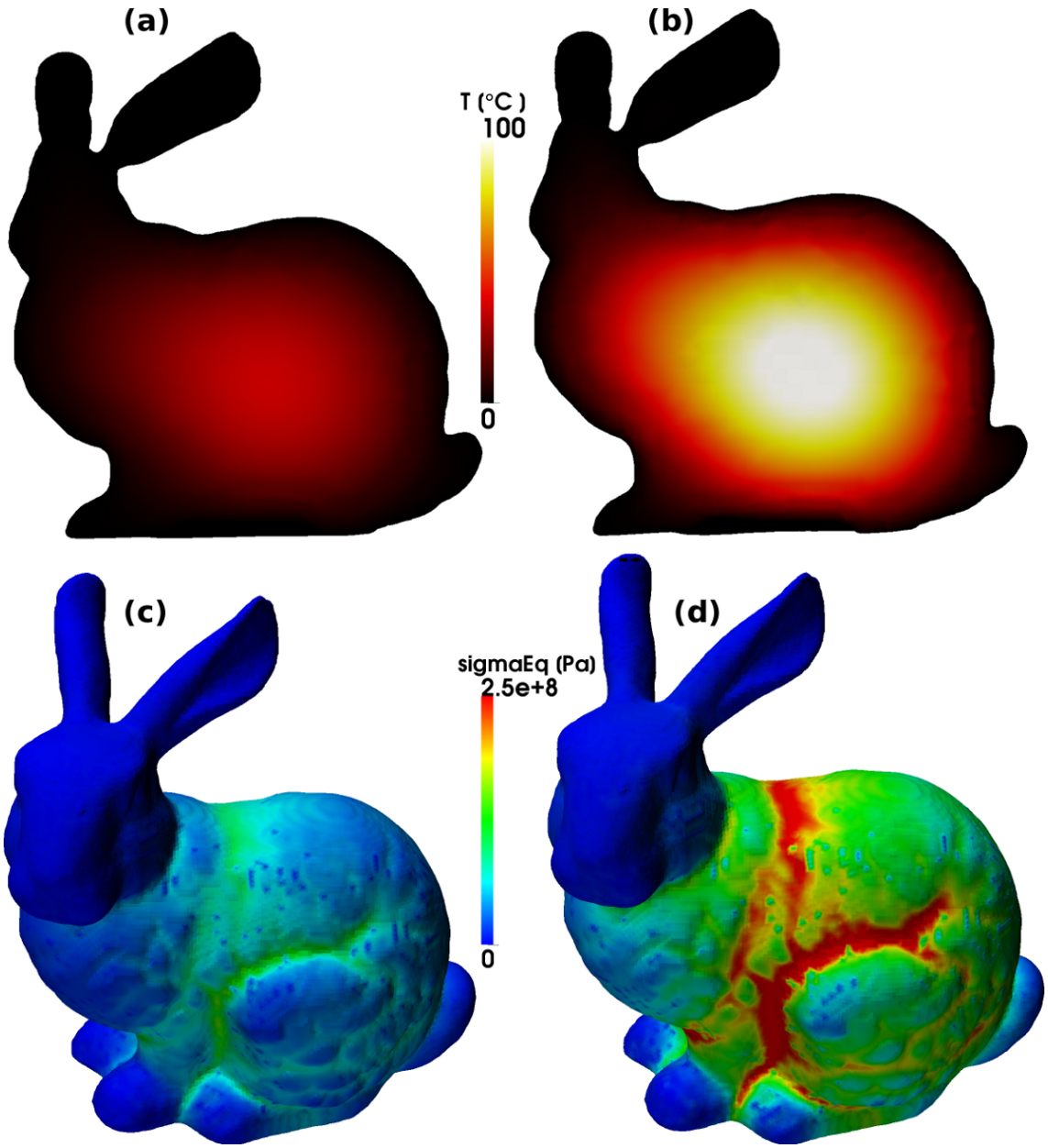

Figure A.25: *SERPENT–OpenFOAM coupling: bunny test case at 2 kW (a and c) and 5.5 kW (b and d). Temperature field in the longitudinal cross section (a and b) and von Mises stress at the external surface (c and d). Displacement magnification factor = 200.*

List of Figures

1 Schematic representation of the MSFR fuel loop (Brovchenko *et al.*, 2012). 13

1.1 Simplified axial symmetric geometry adopted in the Monte Carlo simulations. 19
1.2 Soluble (green) and insoluble (yellow) elements involved in the fuel cycle calculations. 21
1.3 Content of uranium isotopes in the fuel salt (TRU-started MSFR case study). Solid lines: EQL3D/ERANOS; dots: extended SERPENT-2. 22
1.4 Content of plutonium isotopes in the fuel salt (TRU-started MSFR case study). Solid lines: EQL3D/ERANOS; dots: extended SERPENT-2. 23
1.5 Simplified scheme of the reactivity control algorithm implemented in the extended SERPENT-2 version. Newly implemented features are marked in red. 24
1.6 Reactivity and uranium insertion rate (TRU-started MSFR). 26
1.7 Algorithm for the equilibrium search. 27
1.8 Equilibrium search from ^{233}U-started MSFR. Convergence test. 28
1.9 Cumulative uranium production from fuel and blanket in the first 50 years of operation (^{233}U-started MSFR case study). 29
1.10 Cumulative uranium production from fuel and blanket in the first 5 years of operation (^{233}U-started MSFR case study). 30
1.11 Conversion ratio at equilibrium as function of the daily fuel salt reprocessed amount (JEFF-3.1 library). 31
1.12 Molar concentration of trifluorides at equilibrium composition for different reprocessing rates. 32
1.13 In-core decay heat after reactor shutdown for different effective non soluble FP removal time constants at equilibrium. 32
1.14 Cumulative uranium production from fuel and blanket: comparison between JEFF-3.1 and ENDF/B-VII results. Solid lines: JEFF-3.1. Dashed lines: ENDF/B-VII (TRU-started case study). 33
1.15 Fission-to-capture ratio of ^{233}U as function of the incident neutron energy. . 34

1.16 Conversion ratio at equilibrium as function of the daily fuel salt reprocessed amount: comparison between JEFF-3.1 and ENDF/B-VII. 35
1.17 Specific decay heat in the fuel salt after extraction. 36
1.18 High energy gamma emission in the fuel salt after extraction. 37
1.19 Neutron emission in the fuel salt after extraction. 37
1.20 Specific ingestion radiotoxicity generation at equilibrium (nominal conditions). 38
1.21 (n, α) reaction cross-section for ^{58}Ni and ^{59}Ni (JEFF-3.1). 40
1.22 Cumulative helium production in the primary salt container material at core mid-line. 40
1.23 Helium production rate in the primary salt container material at core mid-line. 41
1.24 Atomic fraction of tungsten, rhenium and osmium in the primary salt container material, as funcion of the time. 42

2.1 Spatial mesh adopted for the modelling of the MSFR fuel circuit. 50
2.2 Head loss and heat exchange coefficient in the heat exchanger as function of the primary salt flow rate (intermediate salt at nominal flow rate). 52
2.3 Neutron flux as function of the axial (a) and radial (b) coordinates, as predicted by the OpenFOAM model and by the Monte Carlo code SERPENT. . 53
2.4 Decay heat as function of time. ^{233}U-started MSFR after long operation. SERPENT burn-up calculations and 3 terms exponential interpolation. . . . 55
2.5 150 pcm reactivity insertion. Comparison between implicit and explicit coupling strategies. 56
2.6 Coupling and time integration scheme. 58
2.7 Example of decomposed domain for parallel computing. Each zone is assigned to a different processor core. 59
2.8 Fuel temperature field at nominal conditions. Comparison between OpenFOAM, COMSOL and TUDelft model. Simplified 2D, axial-symmetric MSFR test case. 60
2.9 Power excursion after step-wise insertion of 200 pcm of reactivity. Comparison between OpenFOAM, COMSOL and TUDelft model. Simplified 2D, axial-symmetric MSFR test case. 61
2.10 Average core temperature after step-wise insertion of 200 pcm of reactivity. Comparison between OpenFOAM, COMSOL and TUDelft model. Simplified 2D, axial-symmetric MSFR test case. 61
2.11 Single pump failure unprotected scenario. Temperatures, flow rate and power. Solid lines refer to values relative to the broken pump loop. Dashed lines refer to reactor average values. 62
2.12 Temperature (top), velocity and power density (bottom) fields in the MSFR after the single pump failure accident. 63

3.1 Simplified axial symmetric (r, z) MSFR geometry. 70
3.2 Schematic representation of the reactor model adopted in the derivation of the analytical approach. 73
3.3 Stream lines and velocity fields of the 3 analysed cases: a) k-epsilon case study b) uniform velocity case study c) optimized geometry, 3D case study. 78

3.4 Comparison between IFP, "prompt" and Meulekamp methods (U235-started, k-epsilon case study; nominal flow rate). 81
3.5 Correction factor: comparison between analytical approach, SERPENT and OpenFOAM (uniform velocity case study). 82
3.6 Correction factor: comparison between analytical approach, SERPENT and OpenFOAM (k-epsilon case study). 83
3.7 Precursor concentration and importance for the k-epsilon case study for different values of the dimensionless parameter λT (OpenFOAM; arbitrary units). 84
3.8 Effective delayed neutron fraction as function of the turbulent Schmidt number Sc_T (U235-started, k-epsilon case study; nominal flow rate; OpenFOAM). 85
3.9 Effective delayed neutron fraction in the MSFR as function of the flow rate: comparison between analytical approach, SERPENT and OpenFOAM (U235-started, k-epsilon case study; no turbulent diffusion). 86
3.10 $\beta^c_{i,eff}/\beta^s_{i,eff}$ correction factors. Solid line: OpenFOAM; dots: SERPENT (U235-started, k-epsilon case study; no turbulent diffusion). 86
3.11 $\beta^c_{i,eff}/\beta^s_{i,eff}$ correction factors. Solid line: OpenFOAM; dots: SERPENT (U235-started, k-epsilon case study; no turbulent diffusion). 87
3.12 Delayed neutron fractions in the MSFR for different fuel compositions. . . 87
3.13 Spatial distribution of the delayed (left) and prompt (right) neutron sources at nominal flow rate (arbitrary unit; OpenFOAM; optimized geometry, 3D case study; nominal flow rate). 88

A.1 Normalized neutron flux in the MSFR. ^{233}U-started case study (from Brovchenko, 2013). 98
A.2 Reaction rates in the MSFR. ^{233}U-started case study. 99
A.3 Masses evolution in the MSFR fuel salt. TRU-started case study (from Brovchenko, 2013). 99
A.4 Decay heat at shutdown after long operation, normalized to the nominal reactor power (from Brovchenko, 2013). 100
A.5 β_{eff} as function of IFP generation in the Topsy case (from Leppänen *et al.*, 2014). 104
A.6 β_{eff} calculation in SERPENT-2: comparison between Meulekamp and van der Marck (2006) method, prompt method and the iterated fission probability. Godiva critical assembly (NEA Nuclear Science Committe, 2011). 105
A.7 β_{eff} calculation in SERPENT-2: comparison between Meulekamp and van der Marck (2006) method, prompt method and the iterated fission probability. Jezebel (^{239}Pu) critical assembly (NEA Nuclear Science Committe, 2011). 105
A.8 β_{eff} calculation in SERPENT-2: comparison between Meulekamp and van der Marck (2006) method, prompt method and the iterated fission probability. Flattop (^{235}U) critical assembly (NEA Nuclear Science Committe, 2011). 106

A.9 β_{eff} calculation in SERPENT-2: comparison between Meulekamp and van der Marck (2006) method, prompt method and the iterated fission probability. Flattop (^{239}Pu) critical assembly (NEA Nuclear Science Committe, 2011). 106
A.10Neutron weight change due to small cross-sections perturbation. 108
A.11Adjoint-weighted k$_{eff}$ sensitivity coefficients for the Jezebel critical assembly. ^{239}Pu capture cross-section. 109
A.12Adjoint-weighted k$_{eff}$ sensitivity coefficients for the Jezebel critical assembly. ^{239}Pu fission cross-section. 109
A.13Adjoint-weighted k$_{eff}$ sensitivity coefficients for the Jezebel critical assembly. ^{239}Pu elastic scattering cross-section. 110
A.14Adjoint-weighted k$_{eff}$ sensitivity coefficients for the Jezebel critical assembly. ^{239}Pu inelastic scattering cross-section. 110
A.15Adjoint-weighted k$_{eff}$ sensitivity coefficients for the UAM TMI-1 PWR pin cell. ^{235}U capture cross-section. 111
A.16Adjoint-weighted k$_{eff}$ sensitivity coefficients for the UAM TMI-1 PWR pin cell. ^{235}U fission cross-section. 112
A.17Adjoint-weighted k$_{eff}$ sensitivity coefficients for the UAM TMI-1 PWR pin cell. ^{238}U capture cross-section. 112
A.18Adjoint-weighted k$_{eff}$ sensitivity coefficients for the UAM TMI-1 PWR pin cell. ^{235}U total nubar ($\bar{\nu}$). 113
A.19Spatial mesh adopted in the OpenFOAM Discrete Ordinates solver for the Godiva test case. 114
A.20Comparison between P_1 and P_3 results obtained with ERANOS and OpenFOAM. Godiva test case. 115
A.21Example of unstructured mesh adopted in the SERPENT–OpenFOAM coupling (Stanford bunny – 12000 cells). 116
A.22Running times for different mesh sizes. Comparison between SERPENT-OpenFOAM and MCNP. 117
A.23SERPENT–OpenFOAM coupling. Mesh and power density scoring for the Godiva test case (10840 cells). 118
A.24SERPENT–OpenFOAM coupling. k_{eff} in the bunny test case, as function of the total power. 119
A.25SERPENT–OpenFOAM coupling: bunny test case at 2 kW (a and c) and 5.5 kW (b and d). Temperature field in the longitudinal cross section (a and b) and von Mises stress at the external surface (c and d). Displacement magnification factor = 200. 120

List of Tables

1 Nominal design parameters of the MSFR. 14

1.1 Comparison of recent works dealing with burn-up calculations in MSRs available in recent open literature. 18
1.2 Mass content in the fuel salt after 100 years for plutonium isotopes. Comparison between the extended version of SERPENT-2 and EQL3D/ERANOS. 24
1.3 Uranium production after 100 years of operation – JEFF-3.1 library (^{233}U-started MSFR case study). 29
1.4 Doubling time: comparison between JEFF-3.1 and ENDF/B-VII results. . . 34
1.5 Composition of the nickel-based alloy adopted in the SERPENT-2 simulations. 39
1.6 Cumulative helium production [at. ppm] in the axial reflector for increasing distance from the core reference line (see Figure 1.1). 42
1.7 Tungsten depletion [at. $\%$] in the axial reflector for increasing distance from the core reference line (see Figure 1.1). 43

2.1 Fuel salt thermophysical properties adopted in the present work (Deliverable EVOL D2.2, 2013). 50
2.2 Main specifications of the corrugated plate-type heat exchanger adopted in the present work. 51
2.3 Effective delayed neutron fractions and decay constants. 54
2.4 Butcher table of the adopted explicit, singly diagonally implicit Runge-Kutta integrator Kennedy and Carpenter (2003), with embedded error estimator. 55

3.1 Design parameters of the simplified axial symmetric (r, z) MSFR geometry. 69
3.2 6 energy-groups structure adopted in the deterministic approach. 77
3.3 Decay constants of delayed neutron precursors. Physical delayed neutron fractions of some isotopes are also reported, for incident neutron energy of 1 eV. JEFF-3.1 nuclear data library. 77
3.4 Butcher table of the adopted explicit Runge-Kutta integrator (Dormand and Prince, 1980), with embedded error estimator. 80

3.5 Effective delayed neutron fraction in the optimized geometry for different flow rates. Comparison between OpenFOAM and the analytical approach (U235-started, optimized geometry, 3D case study). 88

A.1 Energy structure adopted in the OpenFOAM Discrete Ordinates solver for the Godiva test case. 115
A.2 Transport solver. Comparison between OpenFOAM, ERANOS and SERPENT. Godiva test case. 115
A.3 Uranium thermo-mechanical properties adopted in the SERPENT–OpenFOAM coupling. 118

References

Angeliu, T., Ward, J., and Witter, J. (2007). Assessing the effects of radiation damage on Ni-base alloys for the Prometheus space reactor system. *Journal of Nuclear Materials*, **366**(1), 223–237.

Avramova, M. N. and Ivanov, K. N. (1997). Verification, validation and uncertainty quantification in multi-physics modeling for nuclear reactor design and safety analysis. *International Journal of Heat and Mass Transfer*, **40**, 4191–4196.

Barton, C., Bredig, M., Gilpatrick, L., and Fredricksen, J. (1970). Solubility of cerium trifluoride in molten mixtures of lithium, beryllium, and thorium fluorides. *Inorganic Chemistry*, **9**(2), 307–311.

Bauman, H., Cunningham I., G., Lucius, J., Kerr, H., and Craven Jr, C. (1971). Rod: A nuclear and fuel-cycle analysis code for circulating-fuel reactors. Technical Report, Oak Ridge National Laboratory, TN, USA.

Bell, G. I. and Glasstone, S. (1979). *Nuclear reactor theory*. RE Krieger Publishing Company.

Benes, O., Cabet, C., Delpech, S., Hosnedl, P., Ignatiev, V., Konings, R., Lecarpentier, D., Matal, O., Merle-Lucotte, E., Renault, C., *et al.* (2008). Review report on liquid salts for various applications, deliverable d50, assessment of liquid salts for innovative applications. *ALISIA project, Euratom 7th FWP*.

Brovchenko, M. (2013). *Études préliminaires de sûreté du réacteur à sels fondus MSFR*. Ph.D. thesis, Université de Grenoble.

Brovchenko, M., Heuer, D., Merle-Lucotte, E., Allibert, M., Capellan, N., Ghetta, V., and Laureau, A. (2012). Preliminary safety calculations to improve the design of Molten Salt Fast Reactor. In *Proceedings of PHYSOR 2012*, Knoxville, TN, USA, April 15–20, 2012.

Cammi, A., Di Marcello, V., Luzzi, L., Memoli, V., and Ricotti, M. E. (2011a). A multi-physics modelling approach to the dynamics of Molten Salt Reactors. *Annals of Nuclear Energy*, **38**, 1356–1372.

Cammi, A., Di Marcello, V., Guerrieri, C., and Luzzi, L. (2011b). Transfer function modeling of zero-power dynamics of circulating fuel reactors. *Journal of Engineering for Gas Turbines and Power*, **133**(5), 052916–1 – 052916–8.

Carta, M., Dulla, S., Peluso, V., Ravetto, P., and Bianchini, G. (2011). Calculation of the effective delayed neutron fraction by deterministic and Monte Carlo methods. *Science and Technology of Nuclear Installations*, **(vol. 2011)**, 8 pages.

Chadwick, M., Obložinskỳ, P., Herman, M., Greene, N., McKnight, R., Smith, D., Young, P., MacFarlane, R., Hale, G., Frankle, S., *et al.* (2006). ENDF/B-VII.0: Next generation evaluated nuclear data library for nuclear science and technology. *Nuclear Data Sheets*, **107**(12), 2931–3060.

Clifford, I. and Ivanov, K. (2010). PBMR 400MW benchmark calculations using the simplified P_3 approach. In *Proceedings of HTR2010, Prague, Czech Republic, October 18-20, 2010*.

References

Clifford, I. and Jasak, H. (2009). The application of a multi-physics toolkit to spatial reactor dynamics. In *2009 International Conference on Mathematics, Computational Methods & Reactor Physics (M&C 2009), Saratoga Springs, NY, USA, May 3-7, 2009*.

Dekoussar, V., Dyck, G., Galperin, A., Ganguly, C., Todosow, M., and Yamawaki, M. (2005). Thorium fuel cycle–potential benefits and challenges. Technical Report, IAEA-TECHDOC-1450, International Atomic Energy Agency, Vienna, Austria.

Deliverable EVOL D2.2 (2013). Optimization of the pre-conceptual design of the MSFR – Evaluation and Viability of Liquid Fuel Fast Reactor System (EVOL) Project. Brovchenko, M., Merle-Lucotte, E., Rouch, H., Alcaro, F., Aufiero, M., Cammi, A., Dulla, S., Feynberg, O., Frima, L., Geoffroy, O., Heuer, D., Ignatiev, V., Kloosterman, J.-L., Lathouwers, D., Laureau, A., Luzzi, L., Merk, B., Ravetto, P., Rineiski, A., Rubiolo, P., Rui, L., Szieberth, M., Wang, S., Yamaji, B., and et al.

Delpech, S., Merle-Lucotte, E., Auger, T., Doligez, X., Heuer, D., and Picard, G. (2009a). MSFR: Material issues and the effect of chemistry control. In *Proceedings of GIF Symposium*, Paris, France, September 9–10, 2009.

Delpech, S., Merle-Lucotte, E., Heuer, D., Allibert, M., Ghetta, V., Le-Brun, C., Doligez, X., and Picard, G. (2009b). Reactor physic and reprocessing scheme for innovative molten salt reactor system. *Journal of Fluorine Chemistry*, **130**(1), 11–17.

Delpech, S., Cabet, C., Slim, C., and Picard, G. (2010). Molten fluorides for nuclear applications. *Materials Today*, **13**(12), 34–41.

Dobson, A. (2008). GNEP Deployment Studies, Preliminary Conceptual Design Studies. *Report for the Nuclear Fuel Recycling Center and the Advanced Recycling Reactor*.

Doligez, X. (2010). *Influence du retraitement physico-chimique du sel combustible sur le comportement du MSFR et sur le dimensionnement de son unité de retraitement*. Ph.D. thesis, Institut National Polytechnique de Grenoble-INPG.

Dormand, J. R. and Prince, P. J. (1980). A family of embedded Runge-Kutta formulae. *Journal of computational and applied mathematics*, **6**(1), 19–26.

Duderstadt, J. J. and Hamilton, L. J. (1976). *Nuclear Reactor Analysis*. John Wiley and Sons, New York.

Dulla, S. (2005). *Models and methods in the neutronics of fluid fuel reactors*. Ph.D. thesis, Politecnico di Torino.

EVOL (2010–2013). Evaluation and Viability Of Liquid fuel fast reactor system. Available at: http://www.evol-project.org/.

Fiorina, C. (2013). *The Molten Salt Fast Reactor as a Fast-Spectrum Candidate for Thorium Implementation*. Ph.D. thesis, Politecnico di Milano.

Fiorina, C., Krepel, J., Cammi, A., Franceschini, F., Mikityuk, K., and Ricotti, M. E. (2013a). Analysis of thorium and uranium fuel cycles in an iso-breeder lead fast reactor using extended-EQL3D procedure. *Annals of Nuclear Energy*, **53**, 492–506.

Fiorina, C., Aufiero, M., Cammi, A., Franceschini, F., Krepel, J., Luzzi, L., Mikityuk, K., and Ricotti, M. E. (2013b). Investigation of the MSFR core physics and fuel cycle characteristics. *Progress in Nuclear Energy*, **68**, 153–168.

Fiorina, C., Lathouwers, D., Aufiero, M., Cammi, A., Guerrieri, C., Kloosterman, J. L., Luzzi, L., and Ricotti, M. E. (2014). Modelling and analysis of the {MSFR} transient behaviour. *Annals of Nuclear Energy*, **64**(0), 485 – 498.

Furukawa, K., Arakawa, K., Erbay, L. B., Ito, Y., Kato, Y., Kiyavitskaya, H., Lecocq, A., Mitachi, K., Moir, R., Numata, H., *et al.* (2008). A road map for the realization of global-scale thorium breeding fuel cycle by single molten-fluoride flow. *Energy Conversion and Management*, **49**(7), 1832–1848.

Geoffroy, O. and Aufiero, M. (2013). A few comments on the MSFR safety and design optimization. Presented at the EVOL WP2 Workshop + EVOL Meeting, Grenoble, France. Available at: http://indico.in2p3.fr/conferenceOtherViews.py?confId=8432.

GIF (2012). Generation IV International Forum, Annual Report. Available at: http://www.gen-4.org/gif/jcms/c_40359/2012-annual-report-gif-symposium-proceedings.

Guerrieri, C., Aufiero, M., Cammi, A., Fiorina, C., and Luzzi, L. (2012). A preliminary study of the MSFR dynamics. In *Proceedings of ICONE20*, Anaheim, CA, USA, July 30 – August 3, 2012.

Guerrieri, C., Cammi, A., and Luzzi, L. (2013). An approach to the MSR dynamics and stability analysis. *Progress in Nuclear Energy*, **67**(0), 56 – 73.

Ignatiev, V., Feynberg, O., Myasnikov, A., and Zakirov, R. (2003). Neutronic properties and possible fuel cycle of a molten salt transmuter. In *Proceedings of GLOBAL 2003, New Orleans, LA, USA, November 16–20, 2003*.

Isotalo, A. E. and Aarnio, P. A. (2011a). Comparison of depletion algorithms for large systems of nuclides. *Annals of Nuclear Energy*, **38**(2), 261–268.

Isotalo, A. E. and Aarnio, P. A. (2011b). Substep methods for burnup calculations with Bateman solutions. *Annals of Nuclear Energy*, **38**, 2509–2514.

Ivanov, K., Avramova, M., Kodeli, I. A., and Sartori, E. (2007). *Benchmark for uncertainty analysis in modeling (UAM) for design, operation and safety analysis of LWRs*. Citeseer.

Jarell, J. J. and Adams, M. L. (2011). Discrete-ordinates quadrature sets based on linear discontinuous finite elements. In *International conference on mathematics and computational methods applied to nuclear science and engineering*.

Jasak, H., Jemcov, A., and Tukovic, Z. (2007). OpenFOAM: A C++ library for complex physics simulations. In *International Workshop on Coupled Methods in Numerical Dynamics*, IUC, Dubrovnik, Croatia, September 19-21, 2007.

Kennedy, C. A. and Carpenter, M. H. (2003). Additive Runge–Kutta schemes for convection–diffusion–reaction equations. *Applied Numerical Mathematics*, **44**(1–2), 139–181.

Kiedrowski, B. C. (2012). Impact of delayed neutron precursor mobility infissile solution systems. In *Proceedings of PHYSOR 2012*, Knoxville, TN, USA, April 15–20, 2012.

Kiedrowski, B. C., Brown, F. B., and Wilson, P. P. (2011). Adjoint-weighted tallies for k-eigenvalue calculations with continuous-energy Monte Carlo. *Nuclear Science and Engineering*, **168**(3), 226–241.

Koning, A., Forrest, R., Kellett, M., Mills, R., Henriksson, H., and Rugama, Y. (2006). The JEFF-3.1 Nuclear Data Library. Technical Report. JEFF Report 21, NEA – OECD.

Kópházi, J., Szieberth, M., Fehér, S., Czifrus, S., and de Leege, P. F. (2004). Monte Carlo calculation of the effects of delayed neutron precursor transport in molten salt reactors. In *Proceedings of PHYSOR 2004*, Chicago, IL, USA, April 25–29, 2004.

Kópházi, J., Lathouwers, D., and Kloosterman, J. (2009). Development of a three-dimensional time-dependent calculation scheme for molten salt reactors and validation of the measurement data of the molten salt reactor experiment. *Nuclear science and engineering*, **163**(2), 118–131.

Křepel, J., Rohde, U., Grundmann, U., and Weiss, F.-P. (2007). DYN3D-MSR spatial dynamics code for molten salt reactors. *Annals of Nuclear Energy*, **34**(6), 449–462.

Krepel, J., Mikityuk, K., and Coddington, P. (2009). EQL3D: ERANOS based equilibrium fuel cycle procedure for fast reactors. *Annals of Nuclear Energy*, **36**, 550–561.

Lapenta, G., Mattioda, F., and Ravetto, P. (2001). Point kinetic model for fluid fuel systems. *Annals of Nuclear Energy*, **28**(17), 1759–1772.

LeBlanc, D. (2010). Molten salt reactors: A new beginning for an old idea. *Nuclear Engineering and design*, **240**(6), 1644–1656.

Lecarpentier, D. (2001). *Le concept AMSTER, aspects physiques et sûreté*. Ph.D. thesis, Conservatoire National des Arts et Métiers.

Leppänen, J., Aufiero, M., Fridman, E., Rachamin, R., and van der Marck, S. (2014). Calculation of effective point kinetics parameters in the serpent 2 monte carlo code. *Annals of Nuclear Energy*, **65**(0), 272 – 279.

Losa, M. (2013). *Multiphisics modelling of the Molten Salt Fast Reactor: comparison of three turbulence models.* M.Sc. thesis, Universidad Politécnica de Madrid / Politecnico di Milano.

References

Luzzi, L., Di Marcello, V., and Cammi, A. (2012). *Multi-physics Approach to the Modelling and Analysis of Molten Salt Reactors*. Nova Science Publishers, Inc., New York, NY.

MacPherson, H. (1985). The molten salt reactor adventure. *Nuclear Science and Engineering*, **90**, 374–380.

Mahadevan, V. S., Ragusa, J. C., and Mousseau, V. A. (2012). A verification exercise in multiphysics simulations for coupled reactor physics calculations. *Progress in Nuclear Energy*, **55**, 12–32.

Martz, R. L. (2012). Mcnp6 unstructured mesh initial validation and performance results. *Nuclear technology*, **180**(3), 316–335.

Mathieu, L. (2005). *Cycle thorium et réacteurs à sel fondu. Exploration du champ des paramètres et des contraintes définissant le Thorium Molten Salt Reactor*. Ph.D. thesis, Institut National Polytechnique de Grenoble.

Mattioda, F., Ravetto, P., and Ritter, G. (2000). Effective delayed neutron fraction for fluid-fuel systems. *Annals of Nuclear Energy*, **27**(16), 1523–1532.

Merle-Lucotte, E., Heuer, D., Allibert, M., Doligez, X., and Ghetta, V. (2009). Optimizing the Burning Efficiency and the Deployment Capacities of the Molten Salt Fast Reactor. In *Proceedings of GLOBAL 2009*, Paris, France, September 6–11, 2009.

Merle-Lucotte, E., Heuer, D., Allibert, M., Brovchenko, M., Capellan, N., and Ghetta, V. (2011). Launching the thorium fuel cycle with the Molten Salt Fast Reactor. In *Proceedings of ICAPP 2011*, Nice, France, May 2–6, 2011.

Merle-Lucotte, E., Heuer, D., Allibert, M., Brovchenko, M., Ghetta, V., Rubiolo, P., Laureau, A., *et al.* (2013). Recommandations for a demonstrator of Molten Salt Fast Reactor. In *International Conference on Fast Reactors and Related Fuel Cycles: Safe Technologies and Sustainable Scenarios (FR13)*, Paris, France, March 4-7 2013.

Meulekamp, R. K. and van der Marck, S. C. (2006). Calculating the effective delayed neutron fraction with Monte Carlo. *Nuclear Science and Engineering*, **152**(2), 142–148.

Nagaya, Y., Chiba, G., Mori, T., Irwanto, D., and Nakajima, K. (2010). Comparison of Monte Carlo calculation methods for effective delayed neutron fraction. *Annals of Nuclear Energy*, **37**(10), 1308 – 1315.

Nagy, K., Lathouwers, D., T'Joen, C., Kloosterman, J., and van der Hagen, T. (2014). Steady-state and dynamic behavior of a moderated molten salt reactor. *Annals of Nuclear Energy*, **64**(0), 365 – 379.

Nauchi, Y. and Kameyama, T. (2010). Development of calculation technique for iterated fission probability and reactor kinetic parameters using continuous-energy Monte Carlo method. *Journal of Nuclear Science and Technology*, **47**(11), 977–990.

NEA Nuclear Science Committe (2011). *International Handbook of Evaluated Criticality Safety Benchmarks Experiments*. OECD Nuclear Energy Agency.

Nuttin, A. (2002). *Potentialités du concept de réacteur à sels fondus pour une production durable d'énergie nucléaire basée sur le cycle thorium en spectre épithermique*. Ph.D. thesis, Université Joseph-Fourier-Grenoble I.

Nuttin, A., Heuer, D., Billebaud, A., Brissot, R., Le Brun, C., Liatard, E., Loiseaux, J., Mathieu, L., Meplan, O., Merle-Lucotte, E., Nifenecker, H., Perdu, F., and David, S. (2005). Potential of thorium molten salt reactors: detailed calculations and concept evolution with a view to large scale energy production. *Progress in Nuclear Energy*, **46**, 77–99.

OECD-NEA (2002). Accelerator-driven systems (ADS) and fast reactors (FR) in advanced nuclear fuel cycles - a comparative study. Technical Report. NEA-3109-ADS, OECD-NEA.

Olander, D. (1976). *Fundamental aspects of nuclear reactor fuel elements*. Technical Information Center – Energy Research and Development Administration, University of California, Berkeley, CA, USA.

Pusa, M. (2011). Rational approximations to the matrix exponential in burnup calculations. *Nuclear Science and Engineering*, **169**(2), 155–167.

Pusa, M. (2012). Incorporating sensitivity and uncertainty analysis to a lattice physics code with application to casmo-4. *Annals of Nuclear Energy*, **40**(1), 153 – 162.

Pusa, M. and Leppänen, J. (2010). Computing the matrix exponential in burnup calculations. *Nuclear Science and Engineering*, **164**(2), 140.

Ragusa, J. C. and Mahadevan, V. S. (2009). Consistent and accurate schemes for coupled neutronics thermal-hydraulics reactor analysis. *Nuclear Engineering and Design*, **239**(3), 566–579.

Renault, C. and Delpech, M. (2005). Review of molten salt reactor technology: Most final report. *European Commission, 5th Euratom Framework Programme (March, 2005)*.

Rollet, A.-L., Sarou-Kanian, V., and Bessada, C. (2010). Self-diffusion coefficient measurements at high temperature by PFG NMR. *Comptes Rendus Chimie*, **13**(4), 399 – 404.

Rouch, H. (2013). Thermal hydraulic benchmark. Presented at the EVOL WP2 Workshop + EVOL Meeting, Grenoble, France. Available at: http://indico.in2p3.fr/conferenceOtherViews.py?confId=8432.

Rouch, H., Geoffroy, O., Rubiolo, P., Laureau, A., Brovchenko, M., Heuer, D., and Merle-Lucotte, E. (2014). Preliminary thermal–hydraulic core design of the molten salt fast reactor (msfr). *Annals of Nuclear Energy*, **64**(0), 449 – 456.

Rudstam, G., Finck, P., Filip, A., D'Angelo, A., and McKnight, R. (2002). Delayed neutron data for the major actinides. *NEA0WPEC-6 Report*.

Sakurai, T., Okajima, S., Andoh, M., and Osugi, T. (1999). Experimental cores for benchmark experiments of effective delayed neutron fraction β_{eff} at FCA. *Progress in Nuclear Energy*, **35**(2), 131–156.

Salanne, M., Simon, C., Groult, H., Lantelme, F., Goto, T., and Barhoun, A. (2009). Transport in molten LiF–NaF–ZrF4 mixtures: A combined computational and experimental approach. *Journal of Fluorine Chemistry*, **130**(1), 61 – 66.

Salvatores, M., Chabert, C., Fazio, C., Hill, R., Peneliau, Y., Slessarev, I., and Yang, W. (2009). Fuel cycle analysis of TRU or MA burner fast reactors with variable conversion ratio using a new algorithm at equilibrium. *Nuclear Engineering and Design*, **239**(10), 2160–2168.

Serp, J., Allibert, M., Benes, O., Delpech, S., Feynberg, O., Ghetta, V., Heuer, D., Holcomb, D., Ignatiev, V., Kloosterman, J., Luzzi, L., Merle-Lucotte, E., Uhlír, J., Yoshioka, R., and Zhimin, D. (2014). The Molten Salt Reactor (MSR) in Generation IV: Overview and Perspectives. *Progress in Nuclear Energy (accepted for publication)*.

SERPENT (2011). PSG2 / Serpent Monte Carlo Reactor Physics Burnup Calculation Code. URL http://montecarlo.vtt.fi.

Sheu, R., Chang, C., Chao, C., and Liu, Y. (2013). Depletion analysis on long-term operation of the conceptual molten salt actinide recycler and transmuter (MOSART) by using a special sequence based on SCALE6/TRITON. *Annals of Nuclear Energy*, **53**, 1–8.

Shibata, K., Iwamoto, O., Nakagawa, T., Iwamoto, N., Ichihara, A., Kunieda, S., Chiba, S., Furutaka, K., Otuka, N., Ohasawa, T., Murata, T., Matsunobu, H., Zukeran, A., Kamada, S., and Katakura, J.-I. (2011). JENDL-4.0: A new library for nuclear science and engineering. *Journal of Nuclear Science and Technology*, **48**(1), 1–30.

Spriggs, G., Adams, K., and Parsons, D. (1997). On the definition of neutron lifetimes in multiplying and non-multiplying systems. Technical report, Los Alamos National Lab., NM (United States).

Stacey, W. M. (2007). *Nuclear reactor physics*. Wiley. com.

Tominaga, Y. and Stathopoulos, T. (2007). Turbulent schmidt numbers for CFD analysis with various types of flowfield. *Atmospheric Environment*, **41**(37), 8091 – 8099.

Turk, G. and Levoy, M. (2005). The stanford bunny. Stanford University Computer Graphics Laboratory, http://graphics.stanford.edu/data/3Dscanrep.

Uhlíř, J. (2007). Chemistry and technology of Molten Salt Reactors – history and perspectives. *Journal of Nuclear Materials*, **360**(1), 6–11.

Verboomen, B., Haeck, W., and Baeten, P. (2006). Monte carlo calculation of the effective neutron generation time. *Annals of nuclear energy*, **33**(10), 911–916.

References

Versteeg, H. K. (1995). *An introduction to computational fluid dynamics the finite volume method, 2/E*. Pearson Education India.

Weller, H. G., Tabor, G., Jasak, H., and Fureby, C. (1998). A tensorial approach to computational continuum mechanics using object-oriented techniques. *Computers in Physics*, **12**, 620 – 631.

Whatley, M., McNeese, L., Ferris, L., and Carter, W. (1968). Engineering development of MSBR fuel recycle. Technical Report, Oak Ridge National Laboratory, TN, USA.

Ringraziamenti

Il primo grazie va alla mia famiglia che mi ha sempre incoraggiato: grazie ai miei genitori, sul cui aiuto ho potuto contare ogni volta e a Giulia e Stefano, che ho sempre sentito vicini.
Grazie a Sara che (mi sopporta ancora e) in tutti questi anni insieme ha cercato di insegnarmi che a partire dalle piccole cose si può cambiare il mondo. Piccole cose, come stampare la tesi sulla sua carta riciclata (e spegnere le centrali nucleari... aggiungerebbe lei).

Ringrazio i prof. Antonio Cammi e Lelio Luzzi, relatori e tutor di questa tesi. Hanno saputo guidarmi in questo percorso, insegnandomi quanto sia importante, nella ricerca scientifica, cercare nuove strade, da un lato, e curare la chiarezza e l'accuratezza del proprio lavoro, dall'altro. Grazie anche al prof. Marco Ricotti che ha accompagnato i miei primi passi nell'ingegneria nucleare, sin dalla stesura della tesi di laurea triennale (già lì si parlava di Torio).

Alla fine di questi lunghi anni al Poli, ripenso con piacere a tutti gli amici che hanno condiviso con me un pezzo di strada. Ringrazio Marco, Simo e gli altri compagni di Ingegneria Energetica che mi hanno regalato il corso di laurea più divertente che potessi immaginare (compreso il corso di "Tecnologie Meccaniche").

Grazie agli amici che mi hanno accompagnato negli anni della specialistica, passati lontano dalla cara Bovisa. Grazie ai compagni di Ingegneria Nucleare e a Chiara, Paolo, Igor, Lorenzo, Daniel, Miguel, Pedro e tutti gli altri amici di Maunoury, all'École Polytechnique.

Venendo a questi ultimi anni, ripenso alle giornate in aula tesisti con Mirko, Giorgio e gli altri "coinquilini". Ho solo ricordi piacevoli. Senza di loro, la "fuel performance" mi sarebbe risultata molto più pesante. Grazie a Ponci, con cui ho iniziato questa avventura nel 26 ciclo di dottorato. Non abbiamo lavorato spesso sulle stesse cose, ma ho sempre avuto il piacere di discutere con lui delle nostre attività. Mi ha regalato i consigli, i suggerimenti e le critiche di chi è capace di vedere le cose da un punto di vista diverso dal tuo. Talvolta, abbiamo avuto punti di vista piuttosto "interesanti", come quelli di Karlsruhe.

Grazie ai "vecchi" (Carlo, Claudia e Marco) e "giovani" (Jacopo, Alberto, Stefano e Matteo) dottorandi e ai tanti altri impiantisti. Con tutti ho avuto il piacere di discutere e confrontarmi, spesso su argomenti decisamente più interessanti del nucleare, e giocare memorabili partite di Briscola Chiamata.

Un grazie speciale va a Carlo, con cui ho passato ore a parlare in questi anni, ogni volta di qualche strana idea che ci passava per la testa. Salvo poche eccezioni, abbiamo puntualmente scoperto che le nostre "nuove" idee erano già "vecchie" negli anni '70. Grazie a Mario, capitato un po' per caso nel gruppo Impianti. È stato un piacere lavorare con lui.

Ho avuto la fortuna di trascorrere due splendidi periodi all'estero durante il dottorato. I mesi a Grenoble e al PSI sono stati divertenti e interessanti. Ringrazio di cuore Elsa, Daniel e Pablo per avermi accolto al LPSC, e Axel e Mariya per le lunghe discussioni sul MSFR e i piacevoli momenti passati insieme. Un grazie davvero speciale va ad Olivier, devo a lui quasi tutto quello che so sulla CFD e sulla cucina francese. Trovare un amico così, ha reso il lavoro a Villard-de-Lans una vera vacanza. Ringrazio Konstantin per i mesi al PSI, trascorsi con Carlo, Sara, Boris, Jiri e Matteo. Mesi passati tra Serpent e OpenFOAM, di giorno, e simpatiche mangiate (e attraversamenti improbabili del Reno), di sera. Grazie a Sandro, che è stato per me la "verità" sul trasporto.

Sono tante le persone senza il cui lavoro questa tesi non sarebbe così. Dopo aver rotto le scatole a Ivor via mail per le sue librerie OpenFOAM, trovarlo inaspettatamente in Svizzera è stata una bella sorpresa. Grazie a Jaakko: senza Serpent, questa tesi sarebbe stata molto molto diversa.

Forse è un po' strano, ma voglio ringraziare questo bel paese. Nonostante tutto, si permette ancora il lusso di offrire una delle migliori istruzioni al mondo. Gratuitamente e a tutti.

Il più grande grazie, però, va a tutti quei delinquenti dei miei amici, che mi richiamano ogni giorno al mondo "reale" che c'è al di fuori di questo strano e bel "lavoro". Mi è difficile immaginare la mia vita senza di loro, a partire da quel lontano giorno d'estate a Chacas, con Ichic e gli altri, in cui la monetina da un Sol cadde sul lato... giusto.